Finanziato dall'Unione europea NextGenerationEU | Ministero dell'Università e della Ricerca | Italiadomani PIANO NAZIONALE DI RIPRESA E RESILIENZA

multi-Risk sciEnce for resilienT commUnities undeR a changiNg climate

Codice progetto MUR: **PE00000005** – **I33C22006910006**

Deliverable title: Report about the sharing with the DS spoke: identification and selection of the enablers

Deliverable ID: 2.5.4

Due date: 30 November 2025

Submission date: 31 March 2026

AUTHORS

Marta Della Seta (UniRoma1); Michele Delchiaro (UniRoma1); Valeria Ruscitto (UniRoma1); Daniela Piacentini (UniRoma1); Francesco Troiani (UniRoma1); Matteo Ferrarotti (UniRoma1); Leonardo Maria Giannini (UniRoma1); Carlo Esposito (UniRoma1); Maria Vittoria Struglia (ENEA); Marco Borga (UniPD); Eleonora Dallan (UniPD); Claudio Puglisi (ENEA); Luca Maria Falconi (ENEA); Gaia Righini (ENEA); Samuele Segoni (UniFI); Marianna Pirone (UniNA); Rita Tufano (UniNA); Giacomo Pepe (UniGE); Roberta Narcisi (PoliTO); Federico Vagnon (PoliTO); Glenda Taddia (PoliTO); Paola Mazzoglio (PoliTO); Giulia La Porta (PoliTO); Marina Pirulli (PoliTO); Giuseppe Bausilio (UniNA); Isabella Serena Liso (UniBA); Giovanni Scardino (UniBA); Chiara Martinello (UniPA); Edoardo Rotigliano (UniPA); Valeria Lo Presti (UniPA)

1. Technical references

Project Acronym	RETURN
Project Title	multi-Risk sciEnce for resilienT commUnities undeR a changiNg climate
Project Coordinator	Domenico Calcaterra UNIVERSITA DEGLI STUDI DI NAPOLI FEDERICO II domcalca@unina.it
Project Duration	December 2022 – November 2025 (36 months)

Deliverable No.	DV2.5.4
Dissemination level*	CO
Work Package	WP 2.5- Outcomes for mitigation strategies
Task	T2.5.4 - Eco-sustainable mitigation of ground instability scenarios in a changing climate framework
Lead beneficiary	UniRoma1
Contributing beneficiary/ies	ENEA, UniPD, UniBA, UniFI, UniGE, PoliTO, UniPA, UniNA

PU = Public

PP = Restricted to other programme participants (including the Commission Services)

RE = Restricted to a group specified by the consortium (including the Commission Services)

* CO = Confidential, only for members of the consortium (including the Commission Services)

Document history

Version	Date	Lead contributor	Description
0.1	22.11.2025	Marta Della Seta (UniRoma1)	First draft
0.2	31.01.2026	Marta Della Seta (UniRoma1)	Second draft
0.3	27.03.2026	Marta Della Seta (UniRoma1)	Third draft
0.4	xx.yy.2026		Critical review and proofreading
0.5	xx.yy.2026		Edits for approval
1.0	xx.yy.2026		Final version

2. Table of contents

List of Tables

List of Figures and Tables

(~20%). The table summarizes the types of climatic and environmental parameters categorized by data domain (e.g., rainfall, temperature, permafrost, snow/glaciers, wind).

Figure 6.1: Future relative changes for 20yr return level based on results by Dallan et al. (2024b) on Great Alpine Area and North Italy, using an ensemble of CPMs (scenario RCP8.5, end of century changes). Grid-points in the area are grouped in equally populated elevation ranges.

Figure 6.2: Empirical Rainfall intensity-duration (I-D) thresholds for the initiation of landslides at global, regional and local scale. threshold. 1, Caine (1980); 2, Moser and Hohensinn (1983); 3, Cancelli and Nova (1985); 4, Cannon (1985); 5, Wieczorek (1987); 6, Jibson (1989); 7, Guadagno (1991); 8, Rodolfo and Arguden (1991); 9, Ceriani et al. (1992); 10, Larsen and Simon (1993); 11, Arboleda and Martinez (1996); 12, Clarizia et al. (1996); 13, Tungol and Regalado (1996); 14, Zimmermann et al. (1997); 15, Paronuzzi et al. (1998); 16, Calcaterra et al. (2000); 17, Montgomery et al. (2000); 18, Wieczorek et al. (2000); 19, Crosta and Frattini (2001); 20, Marchi et al. (2002); 21, Ahmad (2003); 22, Jakob and Weatherly (2003); 23, Aleotti (2004); 24, Floris et al. (2004); 25, Baum et al. (2005); 26, Cannon and Gartner (2005); 27, Chien-Yuan et al. (2005); 28, Corominas et al. (2005a); 29, Hong et al. (2005); 30, Zezere et al. (2005); 31-33, Guzzetti et al. (2008); 34, Dahal and Hasegawa (2008); 35, Kanungo and Sharma (2014); 36, Zhou and Tang (2014). Modified after Guzzetti et al. (2008).

Figure 6.3: Red symbols represent points obtained from numerical analyses, where circles and triangles correspond to winter-like (w) and spring-like (s) initial hydrological conditions, respectively. Purple symbols indicate past flow-like landslide events that occurred in the Lattari Mountains. These results are compared with regional rainfall thresholds reported in the literature, developed using both empirical and physically-based approaches (Guadagno, 1991; Calcaterra et al., 2000; Napolitano et al., 2016; Piciullo et al., 2017) (Adapted from Guglielmi et al., 2023).

Figure 6.4: Comparison between piezometric level and rainfall data of Papanice slow landslide with time series obtained with the CPT-TSC algorithm. The blue shaded column is for the rainy period between November 11, 2013, and December 4, 2013, corresponding to a rapid rise of piezometric level (modified from Confuorto et al., 2017).

Figure 6.5: General cross section of the landslides studied by Ronchetti et al. (2010). The section highlights the hydrological features and triggering mechanisms of the different sectors of the landslides. Modified from Ronchetti et al. (2010).

Figure 6.6: Evolution of a slope affected first by wildfire and subsequently by rainfall, leading to instability. (a) Pre-fire condition: slope covered by soil and vegetation. (b) Wildfire event with varying burn severity, causing alterations in soil and vegetation. (c) Post-fire rainfall triggering a shallow landslide, with consequent damage to the built environment.

Figure 6.7: (a) Illustration of principal mechanical and hydrological mechanisms provided by vegetation on a slope. (b) Temporal variation of root strength in forested hillslopes after tree logging (redrawn and modified after Sidle & Ochiai, 2006). (c) Relationships between land abandonment, landslide occurrence/magnitude and vegetation growth in terraced slopes.

Figure 6.8: Role of antecedent rainfall in the earthquake-triggered shallow landslides involving unsaturated slope covers.

Figure 7.1: Inventory of tools compiled for modeling rainfall-induced preparation and triggering of ground instabilities. (*) These tools also support seismic forcing, potentially enabling multi-hazard scenario assessment.

Figure 7.2: Landslide scenarios (Safety Factor FS <= 1) computed by running the VS2 toolchains with 1-hour precipitation extremes with a 50-year return period for both historical conditions and end-century climate projections, under the worst emission scenario (SSP5-8.5). The tables indicate the total extent of landslide areas in the two scenarios. The magenta box is the frame zoomed in Figure 7.3.

Figure 7.3: Landslide areas for the historical (yellow) and future scenarios (red, incremental areas). The table shows the very low amount if incremental landslide area for the whole study case.

Figure 7.4: Landslide scenarios (Safety Factor FS <= 1,3) for the Inland environment of RETURNLAND, computed by running the VS2 toolchains with 1-hour precipitation extremes with a 100-year return period for both historical conditions and end-century climate projections, under the worst emission scenario (SSP5-8.5). The tables indicate the total extent of landslide areas in the two scenarios. The magenta box is the frame zoomed in Figure 7.5.

Figure 7.5: Landslide scenarios (Safety Factor FS <= 1) or the Inland environment of RETURNLAND, computed by running the VS2 toolchains with 1-hour precipitation extremes with a 50-year return period for both historical conditions and end-century climate projections, under the worst emission scenario (SSP5-8.5). The tables indicate the total extent of landslide areas in the two scenarios.

Figure 7.6: Landslide scenarios (Safety Factor FS <= 1,3) for the Coastal environment of RETURNLAND, computed by running the VS2 toolchains with 1-hour precipitation extremes with a 100-year return period for both historical conditions and end-century climate projections, under the worst emission scenario (SSP5-8.5). The tables indicate the total extent of landslide areas in the two scenarios. The magenta box is the frame zoomed in Figure 7.7.

Figure 7.7: Landslide scenarios (Safety Factor FS <= 1) for the Coastal environment of RETURNLAND, computed by running the VS2 toolchains with 1-hour precipitation extremes with a 50-year return period for both historical conditions and end-century climate projections, under the worst emission scenario (SSP5-8.5). The tables indicate the total extent of landslide areas in the two scenarios.

Figure 7.8: Ensemble sinkhole susceptibility map during MIS 5, referring to the training dataset.

Figure 7.9: Ensemble sinkhole susceptibility map for 2050, 2100, 2150 and 2175, referring to the projected dataset.

Figure 7.10: Comparison between e-ITALICA rainfall thresholds for landslide initiation and duration/intensity precipitation extremes with a 10-year return period, calculated by applying a Gumbel distribution to a 30-year reference dataset, both for the present time and for the 2071-2100 projections, under the worst emission scenario (SSP5-8.5).

Figure 7.11: Landslide scenarios for the demonstrator case of Calabria coastal railway (Safety Factor FS <= 1) computed by running the VS2 toolchains with 1-hour precipitation extremes with a 5-year return period for both historical conditions and end-century climate projections, under the worst emission scenario (SSP5-8.5). Plots indicate the frequency distribution of FS values for both the historical and future landslide scenarios.

Figure 7.12: Landslide scenarios for the RETURNLAND Virtual Test Bed Inland area (Safety Factor FS <= 1) computed by running the VS2 toolchains with 1-hour precipitation extremes with a 5-year return periods for both historical conditions and end-century climate projections, under the worst emission scenario (SSP5-8.5). Plots indicate the frequency distribution of FS values for both the historical and future landslide scenarios.

Figure 7.13: Landslide scenarios for the RETURNLAND Virtual Test Bed Coastal area (Safety Factor FS <= 1) computed by running the VS2 toolchains with 1-hour precipitation extremes with a 5-year return periods for both historical conditions and end-century climate projections, under the worst emission scenario (SSP5-8.5). Plots indicate the frequency distribution of FS values for both the historical and future landslide scenarios.

3. Abstract

This document describes the main results of the interaction between the spokes VS2 (Ground Instabilities) and the DS (Science underpinning climate services for risk mitigation and adaptation) of the RETURN Project. This interaction was first focused on the identification of best practice experiences and forefront analyses on ground instabilities, considering the most common weather-climatic parameters affecting them (precipitation, temperature, snow and glacial data, wind, and marine data) as impact-oriented hazard indicators. The identification of climatic stressors responsible for ground instabilities has been carried out also benefiting from recent advances in geomorphological approaches on climate services.

A special effort has been dedicated to investigating the spatio-temporal variability of landslide occurrence as a climate change impact indicator, with a specific focus on the preparatory and triggering factors to better understand the role of rainfall in landslide dynamics. The analysis was primarily focused on shallow landslides, where the rainfall-induced dynamics of preparation and triggering are more direct and clearly linked to short-term hydro-meteorological conditions, rather than on deep-seated landslides, whose response to rainfall is more complex and delayed.

As part of the joint task within VS2 and DS Spokes of RETURN, the development and validation of operational toolchains have been implemented, as sequences of computational and analytical tools designed to produce scenarios of ground instability effects linked to specific types of preparation processes and triggering actions. Finally, some ground instability scenarios of effects under a changing climate have been computed as simulations both in the demonstrator case of Calabria coastal railway and in the RETURNLAND Virtual Test Bed.

4. Introduction

4.1 Overview of Task 2.5.4 and Deliverable 2.5.4.

In Italy, the effects of ongoing climate change have become increasingly evident in recent years. The years 2022 and 2023 were the warmest years since 1961, considering the mean and the maximum temperatures with an average anomaly of +1.14°C (SNPA Report 2023). These anomalies have strongly influenced the national water balance, especially in northern and central Italy, causing several extreme floods and prolonged droughts. For example, extreme rainfall events occurred in Emilia Romagna (326 mm/day; Schilirò et al., 2025) and Tuscany regions (200 mm in 3 hours; Biondi et al., 2024) in May and October 2023, and November 2023, respectively, although the cumulative rainfall in Italy during 2023 was overall lower than climatological average of about 4% (SNPA Report 2023). During May 2023 Emilia-Romagna event more than 80000 rainfall-induced landslides (mostly first-failure) occurred over an area of more 6000 km2, with density reaching as high as 200 landslides per square kilometer (Berti et al., 2025). Moreover, prolonged dry periods occurred in Piedmont, Liguria, Emilia Romagna, Apulia, Sicily and Sardinia regions with more than 330 dry days. Even so, in the autumn of 2024 some exceptional events occurred: on 19th and 20th October the municipal area of Bologna registered the absolute record of daily rainfall since 1900 (ARPAE, 2024).

Also in the Mediterranean area waterspouts, cyclones, floods and storm surges increase their frequency and intensity (Flaounas et al., 2022; Makris et al., 2023; Bloomfield et al., 2023), like Ciarán and Domingos Storms in November 2023. During these events, along the Ligurian coast the wind speed reached 100 km/h (classified as a violent storm in the Beaufort Wind Force Scale), locally exceeding 200 km/h (hurricane), and causing severe storm surges comparable to Vaia Storm occurred in North-East of Italy in October 2018 (ARPAL, 2023). Exceptional high tides were recorded in the Northern Adriatic Sea, reaching the third highest value since 1869 (110 cm Punta della Salute zero tide gauge in Venice) at the end of October - beginning of November 2023 (ARPA FVG, 2024).

The Task 2.5.4. of the VS2 spoke has been focused on the deep interaction with the DS spoke, in order to provide ground instability scenario effects in a changing climate framework and the Deliverable 2.5.4 reports about the sharing with the DS spoke.

Dedicated VS2 work packages (WPs) were defined focusing on the predisposing (time-independent - WP2) conditions, preparatory processes (time-dependent - WP3) and triggering actions (impulsive and transitory - WP4) in subaerial and submarine environments. Excluding the predisposing conditions like the geo-structural and lithological ones (Sharma et al., 2024; Delchiaro et al., 2024a) that are poorly or at all influenced by climate change, the preparatory processes and triggering actions

related to temperatures and rainfall are strongly controlled by climate regime. In this perspective, the identification of climatic stressors for ground instabilities has been carried out by three specific Tasks of VS2 (one for learning and training through field laboratories, and another two for generating scenarios of effects through machine and deep learning), also benefitting from recent advances in geomorphological approaches on climate services (Delchiaro et al., 2024b; Delchiaro et al., 2025; Iacobucci et al., 2025).

To delineate specific climate- and weather-related hazards, the DS spoke has identified and defined specific impact-oriented hazard indicators for each natural sector (SNPA Report 2021).

Furthermore, thanks to the refining of climate modelling performed within the DS spoke, the latest historical and future climate projections, both in terms of cumulative rainfalls and sea-level changes, have been provided to VS2 to run specific tools for generating ground instability scenarios of effects under a changing climate.

4.2 Available climate datasets and models

Model studies indicate the Mediterranean region as a climate change hotspot, prone to the impacts of local scale and severe weather (Giorgi, 2006; Ducrocq et al., 2014). Because of the complex morphology (semi-closed basin with high and complex surroundings), the Mediterranean region and the Italian territory need to rely on high-resolution information to deal and manage the impacts of weather extremes, both for current and future climate.

Table 4.1 summarizes a set of databases and research groups currently providing up to date and ready-to-use climate scenarios and benchmark products (for more details see also the DS Deliverable 8.4.1). The table reports both observational products that refer to time series of in situ measurements, as well as interpolated products on regular grids. In the latter case, the nominal resolution depends greatly on the spatial extent of the database and the number of stations used. A detailed evaluation of the characteristics of individual products is beyond the scope of this discussion, and readers are referred to the relevant literature for further information.

In the table, products are differentiated according to their type: observational (OBS), remote sensing data (RS), and climate models. Among the latter there are: Reanalyses (RE), hindcast simulation (HI), climate simulation (CS). The table also contains the name of the product, the institution that developed/maintains it, whether data-assimilation has been used or not, whether CP scheme is active or not, the Horizontal Resolution in km or degrees (HR), the time resolution (m-monthly, d-daily, h-hourly), the domain covered, and the reference paper if any. In case the information was not available or not easily identifiable for the whole dataset, we leave a blank entry.

All the datasets listed in Table 4.1 refer to atmospheric variables except ERA5-Land which is a reanalysis achieved through global high-resolution numerical integrations of the ECMWF land surface model driven by the downscaled meteorological forcing from the ERA5 climate reanalysis and contains land and soil variables.

Beside the specific products listed in the table it is worth to mention also the dataset stemming from intercomparison experiments, such as CORDEX (https://cordex.org/) which covers the European domain both with the EURO-CORDEX and the MED-CORDEX initiative.

In particular, we report that the CORDEX initiative dedicated a Flagship Pilot Study to convection (CORDEX-FPSCONV) whose major protocol and potentiality are described in Coppola et al., 2018, while preliminary results over climate scale for precipitation are presented in Ban et al. (2021) and Pichelli et al. (2021).

In the framework of the RETURN project, several activities have generated new convection-permitting scales climate model runs. The ensemble runs from CORDEX Flagship Pilot Study on Convective Phenomena over Europe and the Mediterranean have been remapped to a common resolution and benchmarked in some areas using ground-observed extremes (Dallan et al., 2024b). A national scale benchmark based on observed extremes is being produced using a regionalized formulation of the Metastatistical Extreme Value Distribution (Devò et al., 2025). New convection-permitting model runs have been completed over Italy (and including most of Europe) at 3 km and 1 h scale by ICTP-Trieste, forced by EC-Earth3-Veg GCM, according to CMIP6 scenarios (see Table 2). A regional downscaling of CMIP6 global climate projections to local scales for the Mediterranean and Italian regions has been performed, aiming to produce high-resolution climate information for the assessment of climate change signals, with a focus on precipitation extreme events (also reported in Table 2). The experiments cover hindcast (i.e. ERA5-driven) and historical simulations (driven by the MPI-ESM1-2-HR model) to simulate the present (1980-2014) and future (2015-2100) climate under three different emission scenarios (SSP1-2.6, SSP2-4.5, SSP5-8.5). Based on a double-nesting approach the experiments were conducted at two different resolutions, 15 km and 5 km. Although the highest resolution falls in the so called “gray zone” where the convection parameterization cannot be switched off leading to convection permitting simulations, it has been proved that the use of “scale-aware” parameterization leads to results analogous to those of a CPM (Struglia et al, 2025).

Table 4.1

Acronym	Institution	Product	start Date	end date	data assim	CP	H R	TR	Domain	Paper
E-Obs	COPERNICUS	OBS	1950	2024			0.1°	d	Europe	Cornes et al. 2018
CRU	East Anglia U	OBS	1901	2018			0.5°	m	global	Harris et al., 2020

GRIPHO	ICTP	OBS	2001	2016			3 km	h	Italy	Fantini, 2019, tesi
ARCIS	ARPAs	OBS	1961	2015			5 km	d	C-N Italy	Pavan et al. 2019
SCIA	ISPRA	OBS							Italy	Desiato et al.,2011
EURO4M		OBS	1971	2019			5 km	d	Alps	Isotta et al., 2014
ESA - CCI	ESA	RS data					0.25°	d, m	global	Waliser et al.2020
ERA5	ECMWF	RE	1940	2022	yes	no	31 km	h	global	Soci et al., 2024
ERA5-Land	ECMWF	RE	1950	present	indirect	NA	0.1°	h	global	Muñoz-Sabater et al., 2021
UERRA	COPERNICUS	RE	1961	2019	yes	no	11,1	6h	Europe	UERRA home page
SPHERA	ARPAE	RE	1995	2020	yes	yes	2.2 km	h	Italy	Giordani et al., 2023:
MERIDA	RSE	RE			yes	no	7 km	h	Italy	Bonanno et al., 2019)
MERIDA-HRES	RSE	RE			yes	yes	4 km	h	Italy	Viterbo et al., 2024
VHR-REA_IT	CMCC	HI	1989	2020	no	yes	2.2km	h	Italy	Raffa et al 2021:
COSMO-REA6	DWD	RE	2008	2018	no	no	6 km		Europe	Wahl et al. 2017
COSMO-REA2	DWD	RE	2008	2018	yes	yes	2 km		Central Europe	Wahl et al. 2017
CERRA	COPERNICUS	RE	1984	2021	yes	no	5 km		Europe	Ridal et al. 2024
MERRA2	NASA	RE	1980	2024	yes	no	0.5°	3h	global	Gelaro et al. 2017
CHAPTER	CIMA	HI	1981	2020	no	yes	3 km		Europe	Bernini et al., submitted
VHR-PRO_IT	CMCC	CS	2006	2070	no	yes	2.2 km	h	Italy	Raffa et al., 2023
ENEA-5km	ENEA	HI CS	1980 2015	2023 2100	no	no	5 km	h	Italy and West Med	Struglia et al., 2025
ICTP-Reg_CM5	ICTP	CS	1995 2021 2048 2067	2021 2042 2067 2086	no	yes	3 km	h	Europe	-
FPS Convection	CORDEX Team	CS	1996 2041 2090	2005 2050 2099	no	yes	3 km	h	ALP-3	Fosser et al., 2024

5. Climate change impact indicators related to ground instabilities

5.1 Impact of climate change on ground instabilities in different natural sectors

Climate change can be defined as a long-term change in the statistical distribution of weather variables. These variations may result from both natural processes (Hays et al., 1976), including volcanic activity, solar radiation fluctuations, and internal climate variability, and from anthropogenic influences (Lynas et al., 2021), primarily the increase in greenhouse gas concentrations linked to human activities such as fossil fuel combustion, deforestation, and land-use changes (IPCC, 2023).

These alterations in the Earth's energy balance are leading to direct consequences on the frequency, duration, and magnitude of extreme meteorological events (Held and Soden, 2006). Observational and modeling evidence indicates that episodes of intense precipitation, heatwaves, droughts, and windstorms have become more frequent and severe over recent decades, globally influencing ecosystems, people, settlements and infrastructures (Figure 5.1).

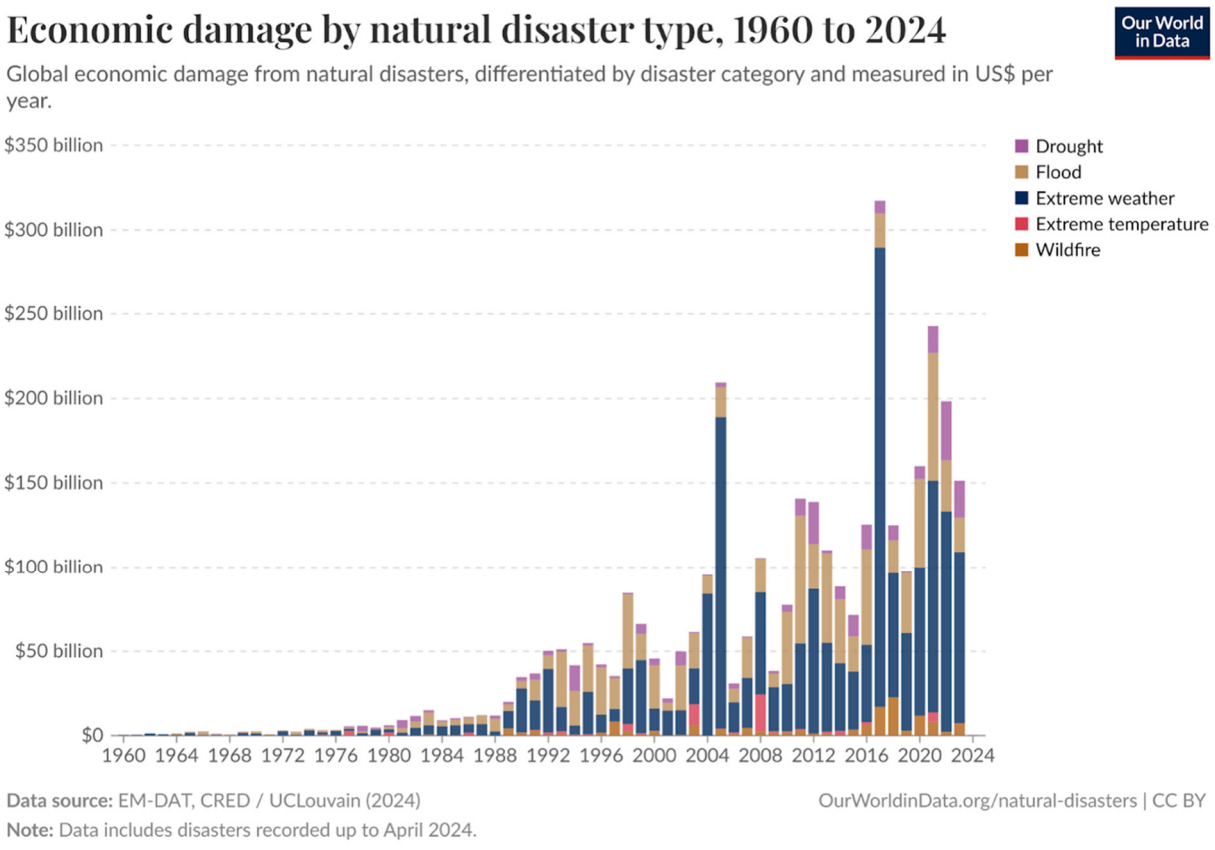

Figure 5.1: Global economic damage by natural disaster from 1960 to 2024. The amount of damage to property, crops, and livestock is given in US$ (EM-DAT, CRED/UCLouvain, 2024). Data includes disasters recorded up to April 2024.

According to the IPCC (2023), climate change parameters refer to the fundamental variables that describe the state and evolution of the climate system, such as temperature, precipitation, wind speed, or snow cover. They quantify how the climate itself is changing over time. Conversely, climate change impact indicators (SNPA Report 2021) capture the effects of these changes on natural (Figure 5.2) and socio-economic (Figure 5.3) systems, representing measurable responses to climatic variability. Examples of climate change impact indicators include variations in landslide frequency, flood occurrence, glacier retreat, or drought severity. In essence, while climate change parameters act as drivers of environmental change, impact indicators reflect the consequences of these changes on ecosystems, hazards, and socio-economic processes.

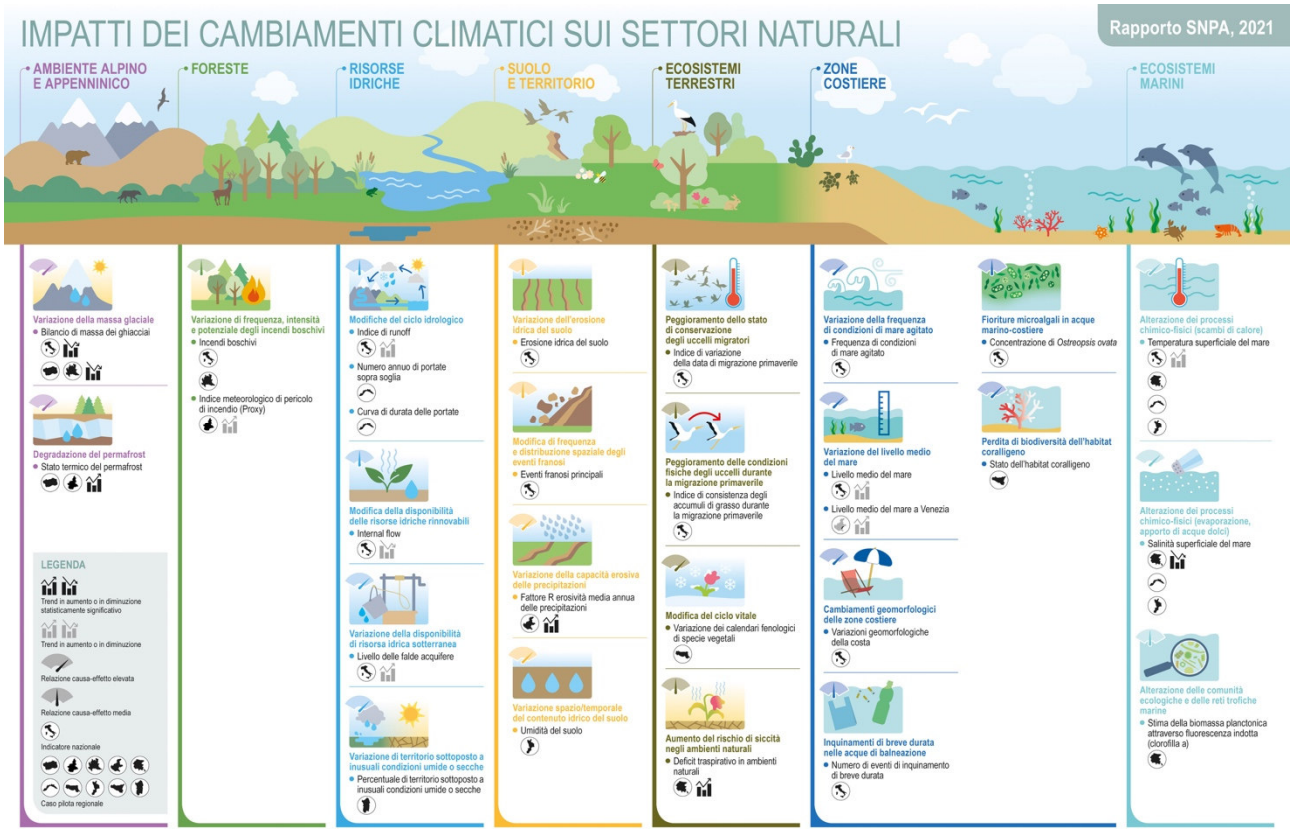

Figure 5.2: Climate change impact indicators on natural sectors (SNPA Report 2021)

Figure 5.3: Climate change impact indicators on socio-economic sectors (SNPA Report 2021)

The DS spoke examined the recent literature on hazard climate-related indicators. Besides the SNPA Report 2021, the DS spoke took into account also the UN Global Set of Climate Indicators (UN, 2022), which was adopted by the UN Statistical Commission in 2022. A hierarchical structure was adopted here, inspired by the UN approach, to qualify indicators according to 15 impact sectors (see also DS Deliverable 8.2.1). The structure adopted for climate change of the RETURN Project was thus devised to be consistent with the above two important frameworks, at an international and national level. Once the structure of the indicator set was defined, extensive interactions with all the other spoke Ambassadors spoke were carried out. In particular, a list devised by TS8.2.1 Leaders, which contained more than 200 indicators, was circulated to stimulate suggestions, integrations, and revisions in general. Furthermore, researchers from all Spokes were invited to take ownership of indicators of interest to their work and spoke. This process ensured a large participation by the entire RETURN partnership. Such an initiative was called *"Adopt an Indicator"* and the interactions between VS2 and DS will be detailed below.

According to the VS2 Deliverable 2.2.3, the ground instabilities are distinguished among landslides, sinkholes, subsidence, and liquefaction (Table 5.1) and most of them are affected by climate change parameters that describe the state and evolution of the climate system, such as temperature, precipitation, wind speed, or snow cover.

Table 5.1. Categories of ground instabilities as conceptualized in the Extended Partnership RETURN. In bold the kinematics and typologies considered in the present work.

Ground Instabilities	**Subaerial Landslides**	**Subaerial Slow Landslides Typologies**	**Slow Flows (Earthflows)**
			Slow Slides (Rotational and Planar Slides, Soil slips)
			Slow Spread & Slow Slope Deformations (Spread (except Liquefaction), Rock/Soil Slope Deformations, Creep, Deep-Seated Gravitational Slope Deformation)
		Subaerial Rapid Landslides Typologies	**Rapid Flows (Debris flows, Mudflows)**
			Rapid Slides (Rock Slides, Rock Avalanches)
			Falls & Topples (Rock Falls, Rock Topples)
	Submarine Landslides	Submarine Landslides Typologies	Slow Submarine Landslides (Creep, Deep-seated Gravitational Slope Deformation)
			Rapid Submarine Landslides (Flows, Avalanches, Slides)
	Sinkholes	Slow Sinkholes Typologies	Slow Sinkholes (Suffosion Sinkholes, Solution Sinkholes)
		Rapid Sinkholes Typologies	Rapid Sinkholes (Collapse Sinkholes, Cover-collapse Sinkholes)
	Subsidence	Subsidence Typologies	Subsidence (all types)
	Liquefaction	Liquefaction Typologies	Liquefaction (all types)

5.2 Joint initiative VS2-DS: *"Adopt an Indicator"*

The interaction between VS2 and DS in the frame of the initiative *"Adopt an Indicator"* was first focused on the study of the state of the art grounded on the identification of a series of case studies on ground instabilities (defined as Learning Examples; see also the VS2 Deliverable 2.2.2) which represent best practice experiences and forefront analyses. From a hundred Learning Examples proposed by VS2, a total of 38 impact-oriented hazard indicators were selected, considering the most

common weather-climatic parameters like precipitation, temperature, snow and glacial data, wind, and marine data (Figure 5.4).

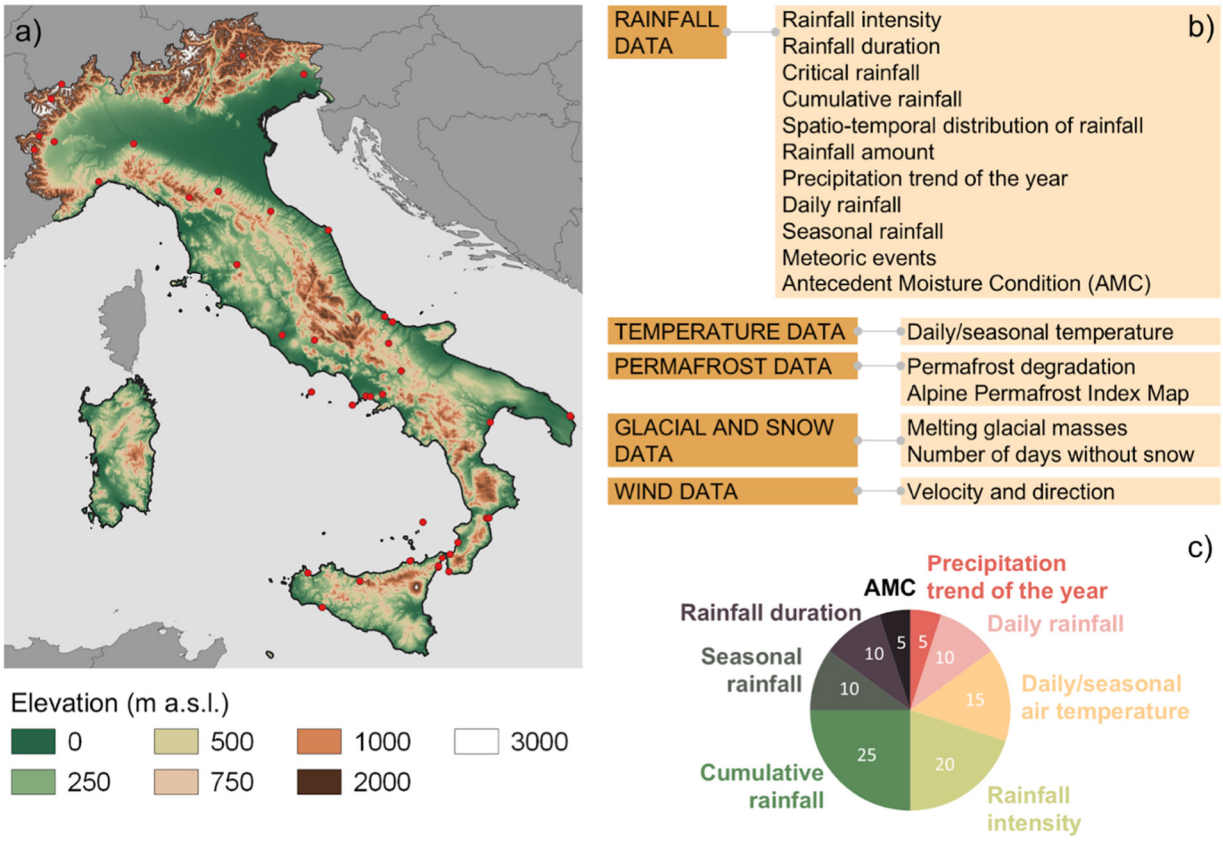

Figure 5.4: Localization of the 38 Learning Examples (LEs) selected within the RETURN project across the Italian territory (a) that account for the main meteo-climatic parameters (right) affecting the occurrence of ground instability, and classification of the associated climate indicators (b, c). The pie chart in panel c) displays the relative frequency of indicators used to assess landslide preparatory and triggering conditions, highlighting the predominance of rainfall-related variables, particularly cumulative rainfall (~25%) and rainfall intensity (~20%). Panel b summarizes the types of climatic and environmental indicators categorized by data domain (e.g., rainfall, temperature, permafrost, snow/glaciers, wind).

As a result of this VS2-DS joint initiative the most significant impacts of the climate variations among the ground intabilities listed above are landslides and sinkholes, mostly affected by rainfall regime variability and sea-level change, respectively.

Several studies (e.g., Benz and Blum, 2019; Emberson et al., 2021; Brunetti et al., 2025; Gariano and Rianna, 2025) have demonstrated how landslides are particularly susceptible to climate variability causing damages for over 6 billion euros per year in the industrialized countries of the world and several injuries every year. Emberson et al. (2021) demonstrated that the greater the intensity of El Niño, the greater implication for rainfall-induced landslides in parts of South-Asia and Latin America;

similarly, Rutllant et al. (2023) show how the atmospheric rivers (i.e., the narrow corridors where the vapor transport is enhanced and associated with extratropical cyclones, Zhu and Newell, 1998) play a key role in all landslide-producing storms observed between 1957 and 2017 in subtropical Andes; Zhao et al. (2022) investigate the role of random rainfall patterns in the time evolution of triggered landslides and in defining the cumulative landslide area. However, it must be considered that rising temperatures and increasing frequency of extreme precipitation events exert a multifaceted influence on vegetation dynamics, leading in some cases to degradation while in others to excessive growth (Chelli et al., 2017), which may locally counteract slope instability (Löbmann et al., 2020).

Successively, The VS2-DS interaction deepened the investigation of the spatio-temporal variability of landslide occurrence as an indicator of climate change impact, with a specific focus on the preparatory and triggering factors to better understand the role of rainfall in landslide dynamics. Examining the current state of knowledge research, areas where further research is needed have been identified. Moreover, a national-scale procedural framework with standardized toolchains assessing and integrating systematically the impacts of climate on landslide dynamics has been defined.

6. The role of rainfall regime in landslide dynamics

The RETURN project and the joint initiative called *"Adopt an Indicator"* have been essential for identifying landslides as key indicators of climate change impacts, with a specific focus on understanding their preparation and triggering processes in mountainous, hilly, and coastal areas.

Landslides, whose spatio-temporal variability has been recognized as an indicator of climate change impact, are influenced by a complex interaction of static (predisposing) and dynamic (preparatory and triggering) factors. While static factors define the inherent susceptibility of a slope to failure (Sharma et al., 2023; Delchiaro et al., 2024a), only dynamic factors allow for the assessment of climate change impacts on slope instability.

On one hand, the study of the predisposing static factors includes the analysis of landslide susceptibility (see also VS2 Deliverables 2.2.5 and 2.2.6), which can be carried out using qualitative (heuristic, descriptive) or quantitative (numerical, probabilistic) methods (e.g., Reichenbach et al., 2018; Conte et al., 2022; Mondini et al., 2023; Guzzetti et al., 2025; Brunetti et al., 2025).

On the other, the study of dynamic factors, encompassing both preparatory and triggering phases, focuses on the time-dependent processes that control slope instability. These factors respond directly to variations of meteorological and environmental conditions. Among these, rainfall, taken here as a representative variable, plays a dual role, both preparatory and a triggering. In general, intense and prolonged precipitation progressively reduces slope stability by altering soil moisture, increasing pore pressure, and consequently decreasing shear strength (Crosta & Frattini, 2003; Ran et al., 2018; Liu et al., 2021). The preparatory phase is further modulated by antecedent and cumulative rainfall, as well as seasonal trends (Mathew et al., 2014; Kim et al., 2021), which promote soil saturation, internal erosion, and progressive weakening (Bittelli et al., 2012; Bogaard & Greco, 2016; Wicki et al., 2020). However, the impacts of climatic forcing vary spatially due to differences in soil properties, vegetation cover, topography, and land use, and are further influenced by microclimatic variability and climate change, which is intensifying heavy rainfall events. Consequently, the response of landslides to evolving climatic patterns remains highly region-dependent (Crozier, 2010; Gariano & Guzzetti, 2016; Wong et al., 2022).

Despite the intensification of extreme rainfall events observed in recent decades due to climate change (IPCC, 2023), a comprehensive understanding of how climate influences the preparatory and triggering factors of landslides is still lacking. Moreover, although numerous site-specific studies in Italy have explored the preparatory and triggering role of rainfall in gravitational processes, these investigations remain fragmented and localized. Currently, there is no shared procedural framework or standardized toolchain at the national level to systematically assess and integrate the impacts of climate on landslide dynamics, a gap that RETURN aims at filling.

6.1 State of art of rainfall in Italy

6.1.1 Precipitation climatology

Italy's annual and extreme precipitation climatology is shaped by complex atmospheric and topographic influences (Avanzi et al., 2015; Mazzoglio et al., 2022, 2023). In northern Italy, precipitation is mainly generated by cyclonic systems originating from the North Atlantic or near the Iberian Peninsula (Buzzi et al. 1998; Rudari et al. 2005), which often intensify over the Gulf of Genoa which is also known as the "Genoa cyclogenesis" region (Trigo et al. 1999). Coupled with orographic uplift, this leads to high annual precipitation (in the range 1500–2500 mm) across northern windward regions such as Liguria, northern Tuscany, southern Alpine foothills, reaching 3000 mm in Friuli, the north-easternmost area (Brunetti et al. 2009; Crespi et al. 2018). Conversely, the whole Po River valley, leeward regions like the Adriatic coast, and the inner part of the Alps like South-Tyrol receives significantly less precipitation amounts (<1000 mm; Frei and Schär 1998). In southern Italy, precipitation is mainly driven by convective systems and cyclones over the Tyrrhenian and Ionian Seas (Trigo et al. 1999), especially in winter. The higher precipitation totals range from 1000–1300 mm on Sicily's northern and eastern coasts to 1200–1800 mm in the Calabrian Apennines (Cannarozzo et al. 2006), while much drier conditions are present in the rest of the central-southern Italy (<600 mm). More detailed information on the annual precipitation distribution over Italy is available in Crespi et al. (2018).

Strong spatial variability is also evident for extreme precipitation in Italy, particularly for short durations, as shown in Avanzi et al. (2015). They estimated the highest values of 1-h extreme precipitation events (e.g. 50-year return period quantiles, ranging from ~17–220 mm) along much of Italy's coastline, especially the southern coast of Friuli–Venezia Giulia, the western coast of central Italy, and the eastern coasts of Sicily, Calabria, and Sardinia, with values exceeding 200 mm. High values are also found inland, notably across the Po Valley, Venice lagoon, and mountainous Apennine regions, highlighting the widespread nature of convective storms in lowland and coastal areas. As the duration increases to 24 hours (50-yr quantiles in the range ~40–1010 mm), the highest values are concentrated in narrower regions like the northwestern Alps, the Italian western coast, eastern Sardinia, southern Calabria, and eastern Sicily. As discussed in Avanzi et al. (2015), this variability reflects the transition from convective systems (dominant at short durations) to stratiform precipitation (more common over longer durations) in combination to the Italian topography. Indeed, although convective storms (e.g., 1-hour events) are smaller in extent than stratiform systems, their presence is more widespread, especially over large plains like the Po Valley owing to strong vertical

instability. In contrast, extreme daily precipitation events are spatially confined where moist airflows are uplifted by the presence of relief.

6.1.2 Observed trends

In recent years, growing attention has been given to quantifying and understanding trends in precipitation amounts, particularly on extreme precipitation to establish empirical baselines for climate impact studies. On an annual scale, a review by Caporali et al. (2021) found a general consensus on the decreasing trend in the number of wet days across Italy, with only minor regional variations, and a less-pronounced decline in total precipitation, particularly during the winter months. A recent study by Vicente-Serrano et al. (2025) over the Mediterranean Region, spanning a period from 1871 to 2020, highlights the variability of detected trends on the considered period and region, while a long-term trend over the whole region is not emerging. They attribute the detected trend mostly to the variability of atmospheric circulation patterns, that is internal variability of climate. However, over most of Italy a tendency of decreasing annual precipitation is found from long-term analysis, while in the last decades they found increasing trends.

In the past 20 years many studies have been developed on trend in extreme precipitation over Italy at regional extent (e.g. Crisci et al., 2002, Bonaccorso et al., 2005, Arnone et al., 2013, Persiano et al., 2020, Avino et al., 2024, Treppiedi et al., 2021, Roseto et al., 2024). Most of them show a lack of statistical significance in the trends over large parts of the investigated areas, while significant trends could emerge over smaller regions. This clearly emerges from a couple of studies recently carried over the whole Italy by using long-term records of annual maxima at sub-daily durations (Libertino et al., 2019, Mazzoglio et al. 2025b). By using a quantile regression approach and analyzing data from 1960 to 2022, Mazzoglio et al. (2025b) provide a broader picture of trends in extreme precipitation. Their results suggest that rarer extremes (high quantiles) exhibit greater spatial and temporal variability than ordinary ones, and higher magnitude of the trend. Notably, 1-hour extremes show mostly increasing trends, especially in parts of northern Italy and Sardinia, and part of central Italy, while 24-hour extremes reveal both positive and negative trends depending on the region. For sub-hourly durations, the study of observed trend is much more limited due to the reduced availability of long records or good-quality weather radar data, even if it would be of great interest for impact study of precipitation-driven hazards such as debris flows and flash floods. Indeed, a few recent studies highlight a tendency for a much faster increasing trend at those short durations compared to hourly or higher durations (e.g. Ayat et al. 2022 nearby Sydney, Australia; Kendon at al. 2018 from climate projection in UK). Over Italy, just a few studies analyzed trends in sub-hourly rare extremes in the last 20-30 years, in the Eastern Alps (Dallan et al. 2022) and in Sicily Island (Treppiedi et al.

2021), both confirming a more significant increasing trend at sub-hourly durations with respect to hourly duration.

All these findings highlight Italy's high climatic variability and the need for spatially resolved, duration-specific analyses when evaluating the impacts of (climate) change on precipitation extremes.

6.1.3 Climate Change

Recent advances in climate modeling have significantly enhanced projections of future precipitation, particularly in climate-sensitive regions like the Mediterranean, which has been recognized as a primary hotspot of climate change (Giorgi, 2006). Global climate models (GCMs) have proven insufficient for the representation of intense precipitation at the regional and local scales, and downscaling methods have been developed to better resolve sub-grid processes (Giorgi et al., 2009; Maraun and Widmann, 2018). Among these, dynamic downscaling with regional climate models (RCMs) has played a key role, and the possibility of accounting for interactions between the atmosphere and the ocean first led to the development of coupled regional systems for the Mediterranean basin (Ruti et al., 2016) that are rapidly evolving into the development of Earth System Models. However, in the last decade the increasing availability of computational power has allowed the development of atmospheric convection-permitting models (CPMs), which operate at grid spacings below 4 km. These models explicitly resolve convective processes, eliminating the need for parameterization schemes, and offer improved simulation of hourly precipitation characteristics, including diurnal cycles, spatial patterns, intensity distributions, and extremes (Prein et al., 2015; Lucas-Picher et al., 2021; Dallan et al.,2023). CPMs also allow for more accurate representation of land-surface heterogeneities, such as mountains, coastlines, and urban zones, and of land-atmosphere feedback that influence other climatic extremes like droughts and heatwaves. In the European context, within the CORDEX-FPS Convection project, Ban et al. (2021) and Pichelli et al. (2021) introduced the first 10-year CPM ensemble simulations at ~3 km resolution over the greater Alpine region. Ban et al. (2021) showed that CPMs driven by ERA-Interim reanalysis better reproduce observed daily and hourly precipitation extremes than coarser RCMs. Pichelli et al. (2021) extended this by evaluating CPMs driven by CMIP5 GCMs under the RCP8.5 scenario, finding that these high-resolution models not only refine the spatial detail of projected changes but can even alter the sign of projected intensity and extreme trends compared to RCMs. Over Italy, in summer, Pichelli et al. (2021) report a future intensification of heavy precipitation (here evaluated as high percentiles) across both hourly and daily timescales. Autumn projections reveal a north-south increase-decrease pattern in precipitation changes, although substantial inter-model variability limits certainty. Further analysis by Dallan et al. (2024a, b) assessed changes in extreme precipitation from sub-daily to daily durations

(Figure 6.1), with return periods up to 100 years. Their results show a general intensification of precipitation extremes across all durations, with the strongest increases found at the shorter durations and for rarer events (that is, higher future intensification at 100 year than at 20 year return period) and in the mountainous regions, particularly the Eastern Alps and Northern Apennines. These results point to a shift in the statistical distribution of precipitation toward heavier tails. The relation of the changes with elevation is summarized in Figure 3, showing the projected changes for the 20yr return level at sub-daily durations. At 1, 3, 6 h, it clearly emerges how the future increase is generally higher in both the more elevated areas and in lowlands, and how, in orographically complex terrains, it enhances with elevation.

This study suggests that the most intense events are becoming more dominant, especially in elevated areas potentially prone to ground instabilities, which may be critical information for hydro- and geomorphological risk management and climate adaptation.

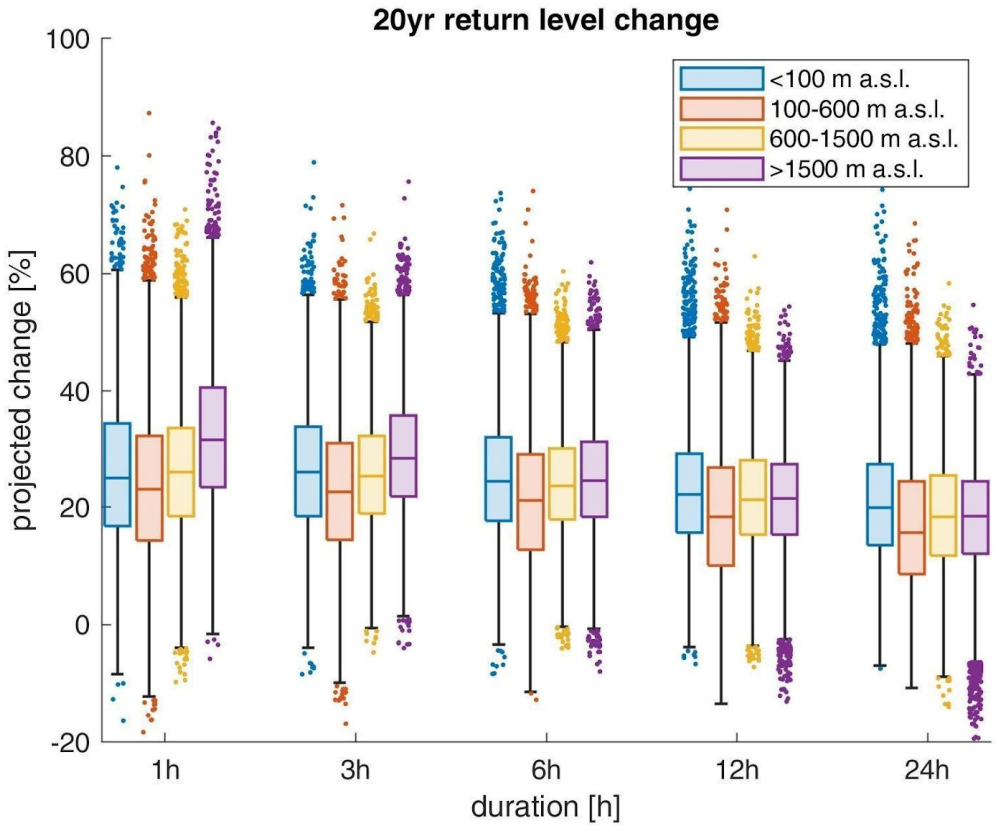

Figure 6.1: Future relative changes for 20yr return level based on results by Dallan et al. (2024b) on Great Alpine Area and North Italy, using an ensemble of CPMs (scenario RCP8.5, end of century changes). Grid-points in the area are grouped in equally populated elevation ranges.

A national-scale perspective over Italy is provided by the VHR-PRO_IT model (Raffa et al., 2023), which is, since recently, the only convection-permitting projection that covers the entire country and spans a 90-year simulation window (1981–2070) under both RCP4.5 and RCP8.5 scenarios. Results indicate a consistent increase in average precipitation intensity under both scenarios, with stronger increases under RCP8.5. In contrast, the frequency of precipitation events decreases, especially in complex terrain such as the Alpine region. These changes, higher average intensities but less frequent events, align with the multi-model findings of Pichelli et al. (2021). Notably, increases in heavy precipitation intensity (characterized here as high percentile of hourly values) are expected in the Alps, Po Valley, and Eastern Mediterranean, while decreases are projected for southern and insular regions like Sicily and Sardinia. The spatial distribution of these changes remains similar between scenarios, but with lower magnitudes under RCP4.5. Lompi et al. (2025) applied a non-stationary statistical frequency analysis to exploit the multi-decadal simulation and assessed the changes in extreme sub-daily precipitation characterized by high return periods. Their study confirms a general increase in extremes in a warmer climate, with larger areas of statistically significant change for shorter durations and higher return periods, but the heaviest increases for longer-duration extremes.

By the best of our knowledge, the aforementioned studies are the only studies based on CPM projections covering completely the Italian territory and refer to global scenarios produced in the CMIP5 context. Most recently, in the framework of the RETURN project, a regional downscaling of CMIP6 global climate projections has been performed, aiming to produce high-resolution (5 km) climate information for the assessment of climate change signals over the Italian regions. The experiments cover hindcast (i.e. ERA5-driven) and historical simulations (driven by the MPI-ESM1-2-HR model) to simulate the present (1980-2014) and future (2015-2100) climate under three different emission scenarios (SSP1-2.6, SSP2-4.5, SSP5-8.5) (Struglia et al, 2025). Although the resolution adopted does not allow us to switch off the convective parameterization, the authors show that, with the model configuration adopted, most of the precipitation, either large scale or convective, is explicitly resolved. This suggests that the model mimics a convection permitting model.

Doing so, Struglia et al. 2025 were able to cover a domain that includes all the italian territory and to perform scenario simulations long enough to speculate on the impacts of extreme events under climate change conditions. The authors analyzed the seasonal projections of precipitation change at the end of the century across the three scenario experiments finding only in the scenario SSP1-2.6 a significant increase of the mean precipitation over most of the Italian peninsula in winter and spring. The other two scenarios project a decrease in mean precipitation for all seasons that intensifies with the scenario severity. The only exception to this signal in SSP2-4.5 and SSP5-8.5 is the projected increase of precipitation in the alpine regions during winter and fall. On the other hand, the analysis

of change in extreme events highlights that at the end of the century, the SSP2-4.5 and SSP5-8.5 scenarios project higher probabilities for extreme events as well as events of unprecedented intensity with respect to the present climate simulations. Seasonal analysis of the difference between the values of the 99th percentile (P99) of daily rainfall during the period 2071–2100 and the corresponding values computed for the period 1985–2014 clearly shows that this intensification of extreme events is mostly concentrated in fall (SON) almost over all italian regions. It is worth noting that in Struglia et al. 2025 is also presented an intercomparison through different datasets (observations, reanalysis and the newly produced hindcast simulations) of the current spatial distribution of extreme precipitation events in Italy (P95, P97 and P99 values) which show that the most affected regions are Liguria and north of Tuscany, as well alpine regions and the Appennines in central and southern Italy and northern part of Sicily. For all these regions, an increase in the intensity and frequency of extreme events is expected, especially in the autumn season. With a view to analysing the spatial and temporal variability of landslide phenomena as indicators of climate change impact, considering that precipitation is one of the main drivers of these phenomena, we can therefore conclude that, under the most severe scenario, the spatial variability of these phenomena is expected to be altered in a non-obvious way by the combination of a trend towards a reduction in average precipitation with a consequent increase in drought periods and an increase in extreme events.

Based on this review about extreme precipitation projections over Italy, it emerges that only a limited number of studies have used CPM ensembles to investigate rare-event statistics such as annual exceedance probabilities or long return periods (Ban et al., 2020; Dallan et al., 2024 a,b), which are critical for engineering and hydrological planning and impact studies. Further developments are thus needed in the context of climate models, for increasing availability of multi-model long simulations at CPM resolution. Equally important is the validation of such high-resolution simulations against dense observational datasets, which remains a key challenge for ensuring their reliability in reproducing extremes at different sub-daily durations and supporting their operational use (Mazzoglio et al., 2025a). Many of these studies focus on fixed-time-window rainfall durations, and caution should be taken in transferring their findings in the context of landslide triggering. Recent studies emphasize that intensity–duration (ID) thresholds for landslide initiation and intensity–duration–frequency (IDF) curves for rainfall probability represent fundamentally different concepts and conflating them can lead to significant misinterpretations of landslide-triggering probabilities (Marra et al., 2025). ID thresholds are empirical relations between average rainfall intensity and event duration that separate landslide-triggering events from non-triggering ones, while IDF curves relate rainfall intensity to duration and frequency (often expressed as return period or annual exceedance probability) for a gauge, assuming a long record and a specific statistical model of extremes.

Consequently, in ID thresholds, "duration" is the length of a user-defined triggering rainfall event, i.e., the contiguous wet period that led to landslides (often variable and event-based), while in IDF curves, "duration" is the length of an arbitrary, fixed window used in the frequency analysis (1 h, 3 h, 24 h, etc.), independent of event structure and landslide timing.

A common but incorrect practice is to take the intensity value on an ID threshold for a given duration and read its return period directly from an IDF curve, implicitly treating the threshold intensity as if it were one of the IDF design intensities. This assumes (wrongly) that the probability of exceeding the ID threshold is the same as the probability that a random fixed-window block exceeds that intensity, ignoring that landslides occur during specific, event-based sequences and under particular antecedent conditions.

6.2 Rainfall as preparatory factor in rapid landslides

Numerous studies analyzed how climate change in terms of variations in precipitation and temperature affect hydrological regimes and, consequently, the intensity of shallow landslide phenomena (Collison et al., 2000; Dehn et al., 2000; Dixon & Brook, 2007; Gariano & Guzzetti, 2016; Jakob & Lambert, 2009; Jakob & Owen, 2021; Jomelli et al., 2009; Schmidt & Glade, 2003; Stoffel et al., 2014; Zêzere et al., 2005).

In this regard, rainfall is widely recognized as a primary triggering factor for shallow and rapid landslides. However, the rainfall preparatory role has historically received less attention, and the effects of climate change remain controversial and are not easily generalizable.

6.2.1 Empirical Thresholds and Antecedent Rainfall Indicators

Traditionally, shallow and rapid landslides have been considered influenced mainly by intense rainfall which is considered to play a crucial role as a triggering factor (Caine, 1980; Guzzetti et al., 2008). The preparatory role of rainfall was considered of secondary importance or even negligible, depending on the hydrological characteristics of the material involved (the coarser and permeable the material, the less relevant the role of antecedent rainfall in preparing the ground instability). This was clearly reflected in empirical approaches, in which the triggering process is modeled through statistical correlations between a few key parameters, completely neglecting any preparatory role (Guzzetti et al., 2007; Segoni et al., 2018).

However, a relevant number of works have been published where triggering thresholds were defined using rainfall indicators based on antecedent rainfall (Guzzetti et al., 2008; Segoni et al., 2018). Besides the technical advantage that antecedent rainfall indexes do not require rainfall measurements acquired at high temporal resolution (Gariano et al., 2020; Abraham et al., 2020), many studies

observed that antecedent rainfall better captures the preparatory role of precipitation, in addition (or in alternative, depending on the models) to the triggering role. Indeed, antecedent rainfall has been taken into account in a wide variety of ways: Tien Bui et al. (2013) combined daily rainfall (considered as triggering process) and 15-day antecedent rainfall (as a preparatory role), Saadatkhah et al. (2015) considered 3- and 30-day antecedent rainfall, Lee et al. (2015) used daily and 3-day cumulated rainfall. Moreover, some authors do not use directly the rainfall measures, but process them to calculate weighted antecedent rainfall indexes, trying to better account for the preparatory role of antecedent rainfall in influencing the degree of saturation of the terrain (Jaiswal and van Westen 2009; Lee et al. 2014; Ma et al. 2014; Kanjanakul et al. 2016; Liu et al., 2024; Liang et al., 2025). Martelloni et al. (2012) introduced the use of the standard deviation from the mean rainfall amount accumulated during progressively increasing time steps (up to the whole duration of the wet season). Greco et al. (2013) used a mobility function defined as the convolution integral of rainfall intensity with an empirical transfer function.

However, in the same research topic (empirical rainfall thresholds) recent advances proposed a more complete integration of preparatory and triggering rainfall indicators. Nocentini et al. (2024a) merged the classical I-D (intensity-duration) approach with a third rainfall parameter based on the average antecedent rainfall. While the first couple of parameters accounts for the triggering effect of the peak rainfall intensity, the third parameter accounts for the preparatory role played by antecedent rainfall, identifying a third dimension of the threshold (which is thus constituted by a plane in 3D rather than a line in 2D). Accounting for the preparatory role of antecedent rainfall by means of the third parameter allows identifying uninfluential rainstorms and filters off many false alarms usually committed by traditional I-D approaches.

Moving forward on the same conceptual line, another series of approaches tried to directly include soil moisture (Marino et al., 2020; Halter et al., 2024), soil saturation (Mirus et al., 2018) or soil volumetric water content (Conrad et al., 2021; Palau et al., 2023) in the models, thus defining hydro-meteorological thresholds, where the preparatory role of rainfall is directly accounted by indicators quantifying its hydrological effects in the soil.

6.2.2 Data-Driven and Machine Learning Approaches

Building on the increasing effectiveness of available technology and on the hybridization of different approaches, a recent trend in empirical landslide forecasting is the use of machine learning to handle a more complete set of input parameters, including a wide range of rainfall indexes to be used simultaneously (overcoming the traditional limitation of selecting only two or three of them). This approach allows testing and including in the modelling several indicators to account for the

preparatory role of rainfall. For instance, Ng et al. (2021) apply several machine learning models only for a rainstorm-based landslide inventory with related short and antecedent rainfall. Similarly, Liu et al. (2021) uses a landslide inventory related to the same rainstorm triggering event for the application of various machine learning models. Stanley et al. (2021) added snow water equivalent and soil moisture content data as dynamic input parameters for an eXtreme Gradient Boosting model, representing the non-occurrence of landslide cells by selecting them across space and time. Distefano et al. (2022) used Artificial Neural Networks to automatically identify the intensity-duration rainfall thresholds with higher predictive power. Nocentini et al (2023; 2024b), working in two very different test sites (in Italy and in Norway) included rainfall amounts recorded over durations from 1 day to 30 days, discovering that this approach allows accounting for the preparatory effect of antecedent rainfall. In addition, and surprisingly, they discovered that a simple categorical variable consisting in the month of the year had a good predictive capability if used together with the others. Although the spatio-temporal prediction of landslides combining static and dynamic parameters in machine learning algorithms is still in a preliminary phase (Distefano et al., 2022; Tehrani et al., 2022; Jin et al., 2024), the cited series of studies clearly shows that even for shallow rapid landslides the preparatory role of rainfall can be relevant, and can be better considered with complex data-driven models.

Also in landslide susceptibility studies, which traditionally are based on the study of predisposing factors, indicators based on rainfall have been recently included in a growing number of works (Cantonati et al., 2025; Vianello et al., 2023). This recent advance aims at implicitly or explicitly accounting for the preparatory role of rainfall, which has been considered to characterize the general climate or peculiar micro-climates of the studied area. Traditionally, the preparatory role of rainfall has never been explicitly accounted for in susceptibility studies. At best, it can be considered somehow implicitly included in some hydrological indexes which quantify the propensity of each spatial unit to retain water into soil. Among these indexes, the most used are the Topographic Wetness Index, the upslope drained area, and planform curvature (indicating convergence or divergence of surface and subsurface flow) (Reichenbach et al., 2018; Segoni et al., 2024). It is worth noting that in most of the works where the shallow landslide susceptibility assessment is completed by a quantitative evaluation of the importance of each input parameter, the aforementioned hydrological factors are ranked among the most important ones. This outcome clearly indicates that terrain features, combined with rainfall, play a key role in preparing shallow landslides. Some studies, instead, use the mean annual precipitation to characterize the climate of the study area (Pourghasemi et al., 2018). Spatial variations in this index highlight micro-climatic differences that may be correlated with the preparatory effect of new rainfall. However, in the framework of the ongoing

global warming and changing precipitation trends, several authors identified a shift in landslide activities, thus highlighting the necessity of considering rainfall anomalies rather than rainfall regimes characterized with data pertaining to decades ago.

For this reason, more recently, an increasing number of researchers are using compound rainfall indicators to characterize rainfall anomalies rather than rainfall amounts sensu strictu. For instance, Catani et al (2013) used the return period of rainfall at varying duration and intensity, using in particular combinations of short durations and high intensities to account for the effect on shallow rapid movements and combinations of long durations and low intensities for deep seated landslides; they also found that these factors held a high predictive power. Marc et al. (2019) used the 10-years return time rainfall anomaly to characterize the spatial pattern of storm-induced landslides. More recently, Caleca et al. (2024) used a rainfall anomaly index (defined as the ratio between the event rainfall and the mean annual precipitation) demonstrating that spatial variations of this index have a strong influence on landslide susceptibility.

6.2.3 Physically based methods: Soil Moisture monitoring

There is a close relationship between soil moisture and intense rainfall (Caine, 1980; Guzzetti et al., 2008; Wieczorek & Glade, 2005).

For instance, while an increase in average temperatures and a decrease in precipitation could lead to a reduction in the average volumetric water content (VWC), an increase in rainfall intensity could result in a higher frequency of sudden VWC increases. Notably, the effects of extreme temperatures and reduced precipitation on the ground can also lead to opposing outcomes. Prolonged drought periods may result in the formation of a low-permeability surface crust, which increases runoff and reduces effective infiltration, making it harder to reach critical soil moisture levels. Conversely, drought events may also cause soil fractures, which can enhance effective infiltration.

A rapid, shallow landslide typically occurs when a thin, granular, partially saturated layer resting on steep bedrock increases its degree of saturation due to changes in moisture content caused by the vertical infiltration of water following rainfall events or snowmelt. As soil moisture increases, the suction decreases, leading to a reduction in cohesion and shear strength. When the soil becomes saturated, a temporary water table within the debris cover is generated, supported by the less permeable underlying layer, increasing pore pressures, weakening the soil structure and destabilizing the slope. Critical soil moisture can be reached through either intense or prolonged rainfall, depending on the antecedent rainfall, infiltration rate and soil's pre-existing moisture condition (Schmidt & Glade, 2003). If the shear forces exceed the shear strenght, (Lann et al., 2024), a failure plane forms within the soil layer or on the bedrock-soil interface, causing it to slide downslope.

The importance of hillslope hydrology in rainfall-induced landslides has gained attention, leading to the replacement of antecedent rainfall with average soil saturation measured over the same period. Ponziani et al. (2012) identified an inverse linear relationship between rainfall thresholds and initial soil moisture conditions, with correlation coefficients reaching up to 0.60. Their study proposed a procedure for landslide warning by integrating rainfall thresholds with soil moisture estimates derived from a calibrated and locally tested soil water balance model. Mirus et al. (2018) demonstrated the advantages of incorporating soil saturation data into landslide prediction models. For the Seattle area in Washington, USA, they found that replacing 15-day antecedent rainfall data with average soil saturation significantly improved the accuracy of established rainfall-only thresholds, which also used 3-day recent rainfall data. Similarly, Marino et al. (2020) emphasized the potential of incorporating soil moisture information into hydro-meteorological thresholds, noting that such data is increasingly accessible through remote sensing and sensor networks. In fact, soil moisture can be measured locally using various on-site techniques or remotely through satellites and airborne systems. Alternatively, hydrological models, such as those discussed by Abraham et al. (2020), are being employed to predict moisture content over larger areas. These measurements, whether direct or modelled, can complement empirical and statistical landslide-triggering thresholds, which are often formulated in terms of rainfall intensity and duration (Kirschbaum et al., 2009; 2012).

Soil moisture data is increasingly available through a variety of monitoring systems, ranging from ground-based monitoring to remote sensing technologies (Fares et al., 2013; Gemitzi et al., 2024; Peng & Loew, 2017; Petropoulos et al., 2015). In-situ monitoring involves installing sensors directly in the ground to measure Volumetric Water Content (VWC) or matric suction at various depths. Although such systems are expensive and have limited spatial coverage, they provide continuous, real-time data that is invaluable for understanding localized moisture dynamics. Remote sensing technologies, such as satellite-based systems (e.g., SMAP, Sentinel-1), offer broader spatial coverage and can estimate surface soil moisture over large areas. These systems use microwave radiometry and radar to detect soil moisture at shallow depths, typically up to 5 cm.

Remote sensing provides valuable regional data, but challenges with data resolution and accuracy at deeper soil layers persist. Ground-based monitoring offers greater precision and is often used to calibrate remote sensing data. Integrated monitoring networks that combine both approaches, along with hydrological models, can offer more comprehensive soil moisture spatial data (Dai & Cheng, 2022; Galvincio et al., 2024) useful to improve landslide early warning systems as well as long-term hazard scenarios.

6.3 Rainfall as triggering factor in rapid landslides

Rainfall is widely recognized as the most common cause of landslides. High-intensity short duration rainfall mainly triggers shallow soil slips and flow-like landslides. Shallow landslides are often initiated during intense rainfall events due to a rapid increase in pore pressure or the loss of apparent cohesion caused by partial saturation. Factors influencing the occurrence and distribution of shallow landslides can be broadly divided into two categories: almost-static variables and dynamic variables. Almost-static variables include soil properties, seepage in the bedrock, and topographic features, which define the inherent predisposition of slopes to failure and determine the spatial distribution of landslide susceptibility. In contrast, dynamic or transitory variables, such as the degree of soil saturation and cohesion influenced by root systems or partial saturation, primarily control the initiation of landslides on predisposed slopes. Both predisposing and preparatory factors have already been discussed in the previous sections; here, the role of the triggering factor is addressed.
Approaches to comprehend rainfall-triggered landslides can be categorized as empirical (historical, statistical) and physically based (simplified or advanced) (Segoni et al., 2018).

6.3.1 Empirical methods

The empirical relationship between rainfall intensity, rainfall duration and slope instability has been extensively documented. Empirical rainfall thresholds are defined by studying rainfall events that have triggered landslides (Calcaterra et al., 2000). Rainfall intensity refers to the amount or rate of precipitation over a specific period, typically measured in millimeters (or inches) per hour. These thresholds are often established by plotting the rainfall conditions leading to landslides on Cartesian, semilogarithmic, or logarithmic scales and drawing lower-bound lines. Depending on the area investigated, empirical thresholds for the initiation of landslides can be loosely defined as global (Caine, 1980), national (Mathew et al., 2014, Ma et al., 2014) or regional (Rosi et al., 2012; Hariral et al., 2019). A global threshold attempts to establish a general (‘‘universal’’) minimum level below which landslides do not occur, independently of local morphological, lithological and land-use conditions and of local or regional rainfall pattern and history. For example, based on 73 events across diverse geological and climatic settings, Caine (1980) first proposed a global threshold applicable for time periods ranging from 10 minutes to 10 days. Subsequently, many Authors developed empirical thresholds working at different scales and based on combinations of precipitation measurements obtained from individual or multiple rainfall events that resulted (or did not result) in landslides (i) intensity-duration (I-D) thresholds, (ii) thresholds based on the total event rainfall, (iii) rainfall event-duration (E-D) thresholds, and (iv) rainfall event-intensity (E-I) thresholds. Among these, the most common type are the intensity-duration thresholds (Figure 6.2).

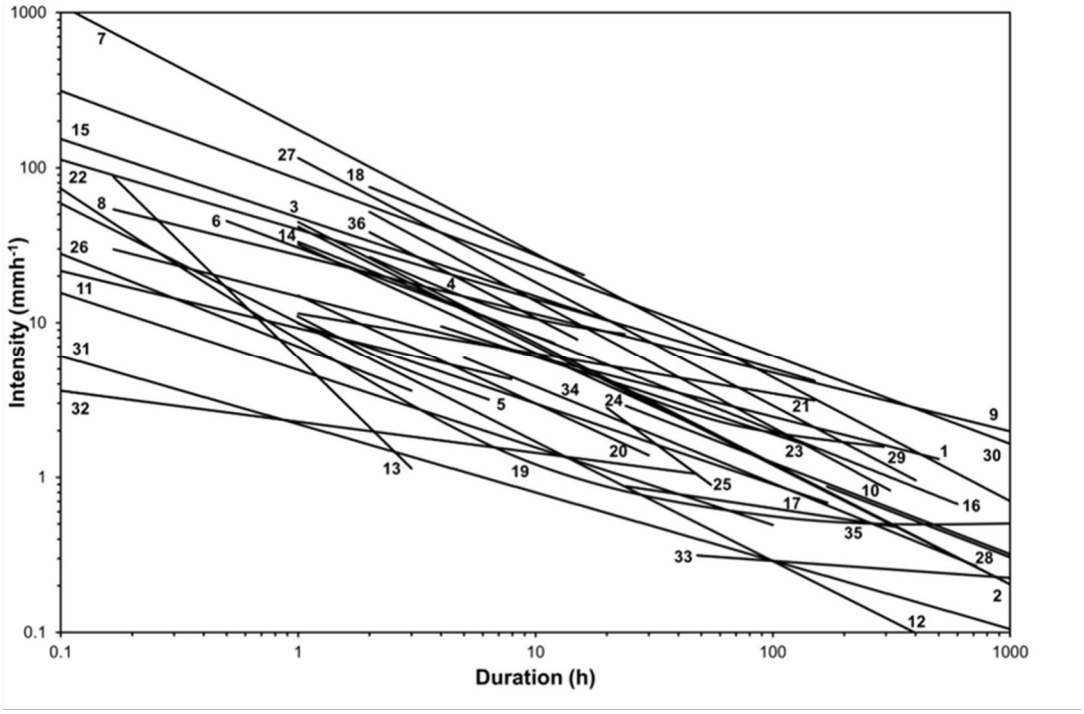

Figure 6.2: Empirical Rainfall intensity-duration (I-D) thresholds for the initiation of landslides at global, regional and local scale. threshold. 1, Caine (1980); 2, Moser and Hohensinn (1983); 3, Cancelli and Nova (1985); 4, Cannon (1985); 5, Wieczorek (1987); 6, Jibson (1989); 7, Guadagno (1991); 8, Rodolfo and Arguden (1991); 9, Ceriani et al. (1992); 10, Larsen and Simon (1993); 11, Arboleda and Martinez (1996); 12, Clarizia et al. (1996); 13, Tungol and Regalado (1996); 14, Zimmermann et al. (1997); 15, Paronuzzi et al. (1998); 16, Calcaterra et al. (2000); 17, Montgomery et al. (2000); 18, Wieczorek et al. (2000); 19, Crosta and Frattini (2001); 20, Marchi et al. (2002); 21, Ahmad (2003); 22, Jakob and Weatherly (2003); 23, Aleotti (2004); 24, Floris et al. (2004); 25, Baum et al. (2005); 26, Cannon and Gartner (2005); 27, Chien-Yuan et al. (2005); 28, Corominas et al. (2005a); 29, Hong et al. (2005); 30, Zezere et al. (2005); 31-33, Guzzetti et al. (2008); 34, Dahal and Hasegawa (2008); 35, Kanungo and Sharma (2014); 36, Zhou and Tang (2014). Modified after Guzzetti et al. (2008).

Statistical methods have also been used to define empirical rainfall thresholds at national (Hong et al., 2018) and regional levels (Martelloni et al., 2012; Piciullo et al., 2017). For example, Brunetti et al. (2010) proposed new national thresholds for Italy and regional thresholds for the Abruzzo Region by employing two independent statistical approaches: a Bayesian inference method and a Frequentist approach. Martelloni et al. (2012) defined statistical rainfall thresholds using a single parameter (cumulative rainfall) for the Emilia Romagna region of Italy. Gariano et al. (2015) analyzed a catalogue of 200 rainfall events linked to 223 shallow landslides in Sicily, southern Italy, over an 11-

year period (2002–2011). They determined regional event duration–cumulative rainfall (E-D) thresholds for shallow landslide occurrence, calculated thresholds for different exceedance probability levels, and assessed uncertainty using a bootstrap nonparametric technique. Their study also examined the influence of lithology and seasonal patterns on shallow landslide initiation in Sicily.

6.3.2 Physically based methods

Physically-based methods for analyzing shallow landslides often combine hydrological models with infinite slope stability analysis. These approaches typically use two modules: one to predict pore water pressure changes due to rainfall (e.g., TOPMODEL - Beven and Kirkby, 1979; TOPOG - O'Loughlin, 1986, Vertessy et al., 1994) and another to evaluate slope stability (e.g., Level I Stability Analysis LISA – Hammond et al., 1992), either coupled or uncoupled. The first simplified models combined the slope stability analysis, generally considering an infinite slope model approach, with a steady-state shallow subsurface flow model (SINMAP – Pack et al., 1998; SHALSTAB - Montgomery and Dietrich, 1994), a shallow groundwater flow model (dSLAM – Wu and Sidle, 1995), or a transient infiltration model (Transient Rainfall Infiltration and Grid-Based Regional Slope-Stability TRIGRS - Baum et al., 2002; Crosta and Frattini, 2003; HIgh REsolution Slope Stability Simulator HIRESS – Rossi et al., 2013). These last models are commonly based on the analytical solution of Richards' equation (1931), first implemented by Iverson (2000). Subsequently, models that solve the 3D Richards' equation in both saturated and unsaturated conditions, combined with the slope stability analysis (GEOtop-FS - Rigon et al., 2006; InHM - Mirus et al., 2007) were developed in order to model the transient infiltration processes catchments characterized by complex topographic conditions (e.g. Formetta et al. 2016), when stratigraphy of soils is known (e.g. Tufano et al., 2021) or/and for well-defined bedrock positions (e.g. Simoni et al. 2008; Formetta et al. 2014). Also, Capparelli and Versace (2011) introduced a physics-based approach for predicting critical rainfall by developing the Saturated Unsaturated Simulation for Hillslope Instability (SUSHI) code. Following these foundational studies, global efforts have refined physics-based rainfall thresholds at regional (Salciarini et al., 2012; Salvatici et., al 2018; Thomas et al., 2018) and basin scales (Liao et al., 2010; Wu et al., 2015; Grelle et al., 2014; Marin, 2020). Most of these applications employ the infinite slope model and the Limit Equilibrium Method (LEM) to calculate the safety factor (Montrasio and Valentino, 2008). Site-specific analyses have also provided valuable insights. For instance, De Vita et al. (2013) evaluated the influence of seasonal variations on hydrological thresholds by studying ash-fall pyroclastic deposits covering the slopes surrounding the Somma-

Vesuvius volcano. This study underscored the critical role of antecedent hydrological conditions in defining rainfall thresholds for slope instability. Additional site-specific applications, such as those by Napolitano et al. (2016) and Fusco et al. (2019), focused on areas prone to flow-like landslides in Southern Italy.

Recently, a new open-source and physics-based model for Spatial Prediction of Rainfall-Induced Shallow Landslides (SPRIn-SL; Raimondi et al., 2022) which implements the infinite slope method by incorporating the TOPOG and the Green-Ampt models to consider groundwater flow and transient rainfall infiltration, respectively, was developed and tested in a small coastal catchment of Cinque Terre (Liguria, Italy). At the slope scale, more complex physics-based models have emerged integrating vegetation dynamics into hydrological models by accounting for transpiration (e.g., Guglielmi et al., 2023; Rianna et al., 2023). These coupled hydro-thermal models have been validated using extensive geotechnical data and comprehensive on-site monitoring.

As an example of physically-based rainfall thresholds, Figure 6.3 shows the critical Intensity–Duration (I–D) curves obtained through coupled thermo-hydraulic numerical modeling of an unsaturated pyroclastic slope monitored at Mount Faito, within the Lattari Mountains, Italy (Guglielmi et al. 2023). Specifically, different threshold curves were derived as a function of the initial matric suction within the slope prior to the triggering rainfall event. Most rainfall events recorded in this geological context are located above the threshold curve corresponding to an initial suction of approximately 5 kPa, suggesting that this value may depict a representative preparatory condition for triggering. These physically-based thresholds are also compared with regional rainfall thresholds available in literature.

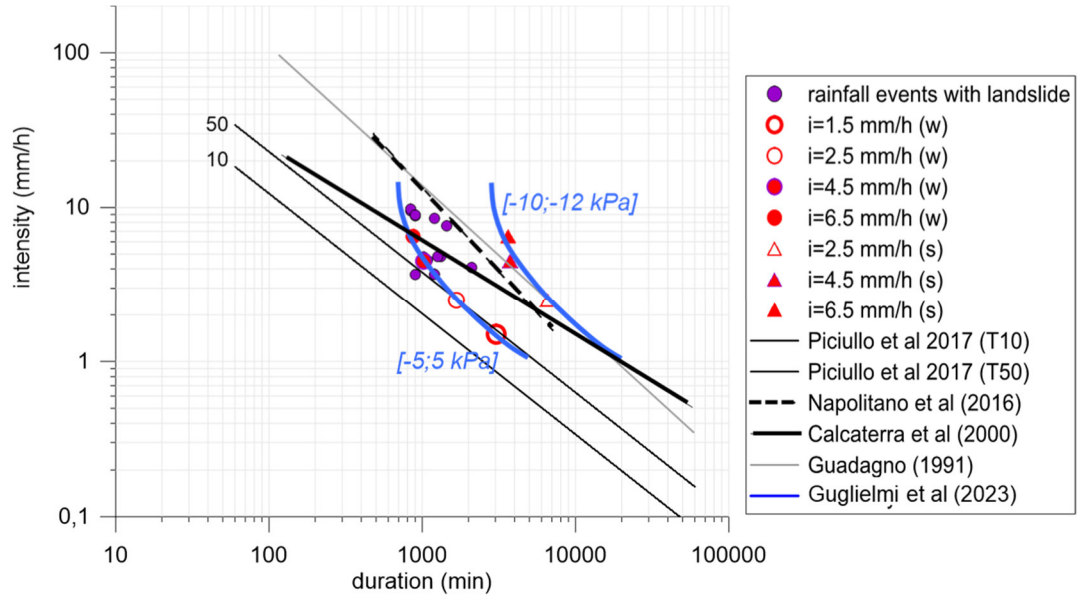

Figure 6.3: Red symbols represent points obtained from numerical analyses, where circles and triangles correspond to winter-like (w) and spring-like (s) initial hydrological conditions, respectively. Purple symbols indicate past flow-like landslide events that occurred in the Lattari Mountains. These results are compared with regional rainfall thresholds reported in the literature, developed using both empirical and physically-based approaches (Guadagno, 1991; Calcaterra et al., 2000; Napolitano et al., 2016; Piciullo et al., 2017) (Adapted from Guglielmi et al., 2023).

A recent offline early warning procedure that combines multi-factor rainfall thresholds with on-site suction monitoring before rainfall events was proposed by Pirone et al. (2025). The authors developed site-specific multi-factor rainfall thresholds, integrating mean rainfall intensity, rainfall duration, and antecedent suction. This approach employs a physics-based model calibrated with hourly on-site measurements of suction and water content, subsequently validated against historical landslide occurrences.

However, the practical application of such deterministic models, especially in terms of early-warning systems, is still limited to specific studies, due to the time effort and data demand (Boogard and Greco, 2018). In fact, the main limitations of physics-based thresholds are related to the most important disadvantages of the deterministic methods: (i) requiring a significant amount of geotechnical, mechanical, and hydrological parameters for model simulation; and (ii) reconstructing the boundary conditions which represent, in the best way, the real soil and slope behaviors (Bordoni et al., 2019).

6.4 The role of the rainfall in slow landslides: preparatory or triggering?

Slow-moving landslide movements are generally linked to intense and prolonged precipitation (Narcisi et al., 2024; Sato and Shuin, 2024; Zêzere et al., 2015). Water content is undoubtedly the most influential factor in slope movements (Leroueil and Chandler, 2001). These slow-moving failures can accelerate within days to months following the beginning of the rainfall event and decelerate during dry periods eventually halting. The imbalance between driving forces and shear strength of slope materials, caused by extreme rainfall, triggers movements. This occurs because an increase in pore water pressure leads to a reduction in effective stress and, consequently, in the soil shear strength'(Terzaghi, 1950; Glade and Crozier, 2005; Terlien, 1998). According to Berntson & Saèllfors (1984), Kenney & Lau (1984) and Vaughan (1994), seasonal fluctuations in the water table level can cause variations in pore pressure at depths ranging from 5 to 10 m. In the case of slow landslides, processes such as infiltration, deep ground-water circulation patterns, and the resulting increase in hydrostatic levels and/or pore-water pressures - accumulating over long periods before activation - must be considered (Hutchinson, 1970; Iverson and Major, 1987; Guglielmi et al., 2002; Cappa et al., 2004; de Montety et al., 2007; Matsuura et al. (2008); Ronchetti et al., 2010; Valiante et al., 2016). Failure conditions arise from a unique combination of all these factors, and the state of the slope system cannot be predicted based on rainfall alone (Berti et al., 2012). Following Guzzetti et al. (2008), Vallet et al. (2016) suggested that it is more appropriate to use "a local threshold that implicitly takes into account the landslide characteristics."

However, distinguishing between the preparatory and triggering roles of precipitation is often challenging. Typically, the minimum response time of a landslide to rainfall is proportional to the square of its depth (often approximating the saturated thickness) and inversely proportional to hydraulic diffusivity (Handwerger et al., 2013). Deeper landslides generally show more complex behavior and require more time to achieve disequilibrium conditions (Vassallo et al., 2015). Several studies have been conducted to understand this response and define the complex relationship between rainfall and landslide kinematics. Vallet et al. (2016) stated that, although the destabilization of deep-seated landslides is mainly controlled by a rainfall trigger (short-term component), site-specific time-dependent factors (long-term components), such as creep deformation or modifications in slope groundwater hydraulic connectivity, can also be significant.

Consequently, no general threshold has been proposed in the literature. Rather, three main types of studies can be recognized: the first group aims to define a local window of days or cumulative rainfall to determine a site-specific precipitation threshold, the second group focuses on understanding the

role of local groundwater recharge and the third one proposes physically-based models to investigate the hydrological impact on slope stability.

6.4.1 Cumulative rainfall threshold analysis

Van Asch et al. (1999) argued that a single day of rainfall does not significantly influence deep-seated landslides, while Bonnard and Noverraz (2001) and Trigo et al. (2005) stated that such movements are usually driven by multiple moderate-intensity storms occurring over weeks or months. Doglioni et al. (2011) analyzed precipitation trends related to the reactivation of the Maierato landslide (Calabria, Italy). By examining cumulative rainfall heights over 5, 10, 15, 20, 30, 45, and 60 days preceding the landslide, the authors identified a peculiar rainfall sequence: a prolonged period of continuous but not intense rainfall, leading to exceptionally high return periods for cumulative rainfall, with a maximum of 105 years. Martelloni et al. (2012) suggested that the hydrodynamic response of landslide aquifers is influenced more by antecedent rainfall (multiple rainfall events over a long period) than by a single rainfall event. For this reason, a single and simple rainfall trend alone does not fully explain the behavior of these phenomena (Ronchetti et al., 2010; Noverraz et al., 1998). Azañón et al. (2010) demonstrated that, for the investigated landslides (i.e. Riogordo and Diezma landslides, southeast Spain), the trigger was intense rainfall episodes that occurred after two years with annual rainfall higher than average values. However, if in the case of the Riogordo landslide the relationship between intense rainfall and slope failure is clearly established, in the case of the Diezma landslide, it occurred 20 days after an intense rainfall peak, probably as an effect of the hydrogeologic behavior of the Diezma area. Fiolleau et al. (2023) linked a landslide reactivation in the San Francisco Bay Area with an episode of heavy rainfall (about 220 mm in 30 h) following a 7-month drought through the analysis of variations in water table level, soil temperature, soil displacement, seismic wave velocity and the associated correlation coefficient measured in the autumn and in the summer seasons. Jiang et al. (2021), using displacement time-series obtained by synthetic aperture radar interferometry (InSAR) technique, observed that the Wadi Landslide (Mao Country, Sichuan Province, China) exhibited a periodic displacement with slight acceleration in 2017 and 2019, because both these years had relatively large rainfall with cumulative annual rainfall exceeding 1200 mm.

6.4.2 Groundwater recharge analysis

Fluctuations in saturation levels within landslide materials, especially loose soils and weathered geological formations, intensify the stress applied to slope materials. These processes contribute to the driving force acting on the slope to exceed the shear strength of the material and, consequently, trigger landslides (Gebremichael et al., 2024). A clear correlation between piezometric level and

acceleration and deceleration of the Papanice landslide (southern Italy) was found by Confuorto et al. (2017), which compare the piezometric level and the rainfall data with the displacement time series derived with the Coherent Pixel Technique-Temporal Sublook Coherence (CPT-TSC) algorithm in the rainy period between November 11, 2013, and December 4, 2013 (Figure 6.4).

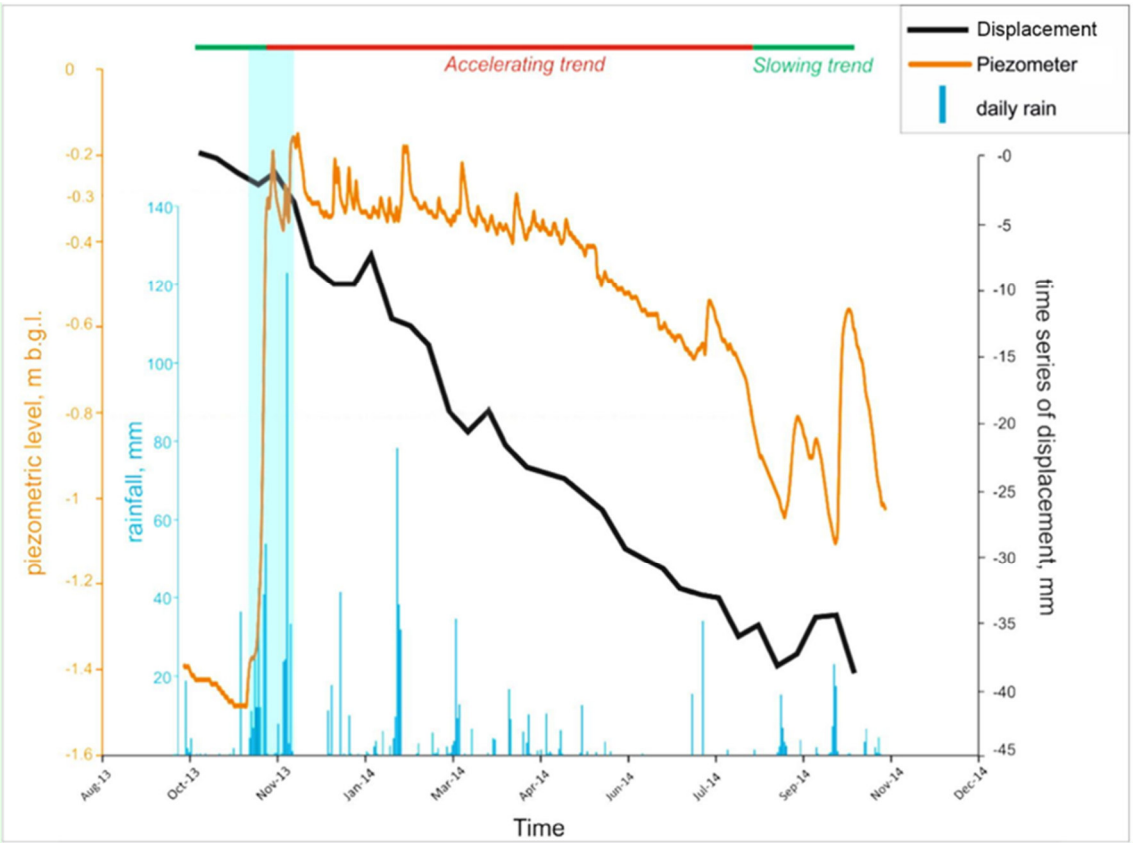

Figure 6.4: Comparison between piezometric level and rainfall data of Papanice slow landslide with time series obtained with the CPT-TSC algorithm. The blue shaded column is for the rainy period between November 11, 2013, and December 4, 2013, corresponding to a rapid rise of piezometric level (modified from Confuorto et al., 2017).

An attempt to develop a critical piezometric threshold was also carried out by Lissak et al. (2014) using long-term continuous single-point time series and shorter, but more spatially distributed, piezometric information. The Authors defined two piezometric thresholds for the landslides that occurred along the Normandy coast (France): the first one based on field surveys (short-term/high resolution) for moderate landslides at 3.50 m depth and a second threshold based on historical data (long-term/low resolution) at -10.35 m depth for the major landslides. Other Authors (i.e. Corominas et al., 2005b; Urgilez Vinueza et al., 2020; Losacco et al., 2021) also focused on the correlation

between groundwater fluctuation connected to rainfall infiltration and recurrent acceleration of landslides.

Pepe et al. (2021) analyzed the efficiency of the automatic deep-drainage system of the Mendatica landslide (Liguria, Italy) during an extreme rainfall event lasting five days, with a cumulative rainfall of 800.4 mm. The results showed that, despite the Mendatica landslide being affected by the most severe multi-day (5–6 days) rainfall event recorded in the past 75 years (Notti et al., 2021), the drainage system successfully depressed the local aquifer, preventing the landslide from reactivating. With the aim of developing a regional-scale warning system for landslides, Martelloni et al. (2012) developed a prototype algorithm based on the comparison between rainfall recordings and statistically defined thresholds, determined using a single parameter (cumulative rainfall). Based on the landslide inventory of the Emilia-Romagna region, Italy, the authors proposed a variable time-interval cumulative rainfall (up to 240 days) as a threshold for the activation of deep-seated landslides in low-permeability terrains. To identify an alert model based on cumulative rainfall for the Petacciato landslide (Molise, Italy), Doglioni et al. (2012) proposed an approach based on the evolutionary polynomial regression technique, which enabled the prediction of landslide reactivation using only cumulative rainfall. The authors obtained promising results by applying two equations: the first one considers long-term cumulative rainfall lagged up to 120 days before the reactivation event, while the second one involves cumulative rainfall up to 90 days, lagged by a maximum of 30 days before the event. Banfi and De Michele (2024) attempted to define a correlation between the spatial and temporal characteristics of precipitation clustering over the Italian territory and landslide occurrence (considering different types of phenomena) and, finally, related it to the North Atlantic Oscillation (NAO) and the Mediterranean Oscillation Index (MOI). Using specific statistical thresholds (e.g., excluding exceedances in the 90th percentile series or considering a threshold equal to the 0.7 quantile of daily precipitation, including only wet days), the authors verified the presence of temporal clustering within variable time windows of 15, 30, and 90 days preceding each landslide. They observed that, for all types of landslides except rockfalls, the majority of events were preceded by a temporal clustering of precipitation. This clustering was longer for deep-seated landslides and shorter for debris flows. For the reactivation of the Montaldo di Cosola landslide, Lollino et al. (2007) identified a time lag of approximately nine days between the occurrence of a rainfall peak (135.4 mm on November 26, 2002) and the corresponding peak in recorded movements (1.2 mm/day). This specific precipitation value and landslide activation time lag were determined by analyzing two years of precipitation data (May 2002–May 2004) and using the AIS (Automatic Inclinometric System) to quantitatively assess the local relationship between rainfall peaks and slope movement peaks. As the researchers suggested, “the time lag found has to be considered as a ‘warning time’ for this particular

landslide. It means that after a significant rainfall event, particularly in autumn, a peak in landslide movements can be expected around 8–9 days later". Lollino et al. (2023) examined the 52-hour pluviometric trend preceding the reactivation of the Montescaglioso landslide (Basilicata, Italy) and its impact on the safety factor. The authors noted that "the FS continues to decrease even after the accumulated rainfall reaches a plateau" attributing this to the rapid increase in pore water pressure following the infiltration of an exceptionally large amount of rainfall as the main factor in the reactivation. Ronchetti et al. (2010) analysed the behaviour of four large and deep mass movements involving flysch rock masses and clayey complexes: the Valoria landslide, the Lezza Nuova landslide, the Tolara landslide, and the Ca' Lita landslide, in the Emilia-Romagna region (Figure 6.5).

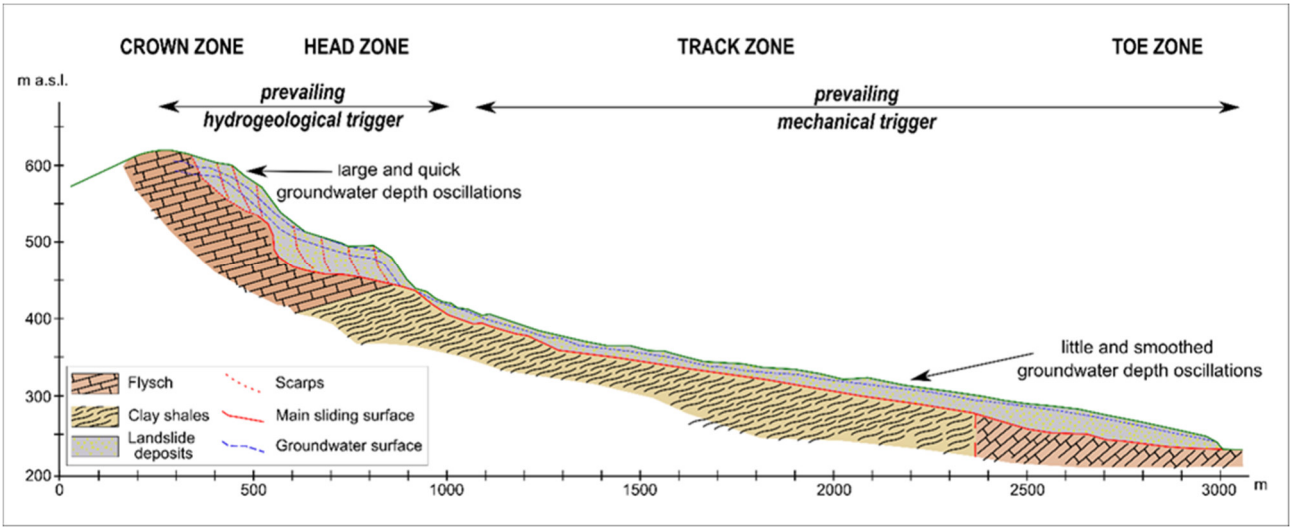

Figure 6.5: General cross section of the landslides studied by Ronchetti et al. (2010). The section highlights the hydrological features and triggering mechanisms of the different sectors of the landslides. Modified from Ronchetti et al. (2010).

This research reported Groundwater Depth (GWD) monitoring over approximately two years using piezometers equipped with electric transducers. Based on the results of this monitoring, the authors proposed a different response of landslide sectors (crown, head, track, and toe) to rainfall events. In particular, they observed a variable delay ranging from 4 to 15 days between individual rainfall events and GWD variations in the crown area, where flysch rocks remain intact and exhibit limited hydraulic conductivity (ranging from 10^{-5} to 10^{-8} m/s). In the head zone of the landslides, where hydraulic conductivity increases due to the presence of disarranged rock masses and fractures, the delay between rainfall and GWD variation is reduced to 1–8 days, with an almost instantaneous response to single rainfall events during the wet season. For the track and toe zones, which typically contain a chaotic mixture of silt, clay, and blocks, the authors observed a decrease in hydraulic conductivity

(around 10^{-8} m/s) but with a very short delay (i.e., hours) and an extremely limited GWD variation (less than 1 m). According to the obtained results, the authors proposed a different triggering mechanism for the crown/head zone, where hydrogeological factors prevail, and for the track/toe zone, where reactivation is primarily driven by mechanical causes. Vallet et al. (2016) proposed an approach for determining a statistical rainfall threshold for deep-seated landslides. In particular, the authors combined the Support Vector Machine (SVM) multidimensional rainfall threshold with a semiautomatic event detection method to define an objective and optimal threshold. Their study focused on the Séchilienne landslide (southeast of Grenoble, France), which is monitored by numerous displacement stations using a wide range of techniques, including extensometers, radar, infrared geodesy, inclinometers, and GPS. Displacement and weather data are recorded daily. For training and testing their methods, the authors analysed both low and high destabilization events, as well as rainfall trends and the recharge of the landslide's perched aquifer. Based on their results, they concluded that using recharge rather than precipitation significantly improved the delineation of a rainfall threshold distinguishing stable from unstable events.

6.4.3 Physically based models

In the realm of physics-based models, recent scientific literature emphasizes the impact of slope-vegetation-atmosphere interactions on landslide activity, with evidence suggesting these effects may extend to significant depths in natural clay slopes. The Southern Apennines (Italy), characterized by slopes composed of fissured clays, provide numerous examples of weather-induced deep landslide mechanisms. The interplay between landslide activity and hydro-mechanical processes arising from soil-vegetation-atmosphere interaction has been explored through both uncoupled and coupled two-dimensional hydro-mechanical finite element analyses (Pedone et al., 2018; Cotecchia et al., 2019; Di Lernia et al., 2022). Pedone et al. (2018) demonstrated that net rainfall accumulated over 2 and 6 months serves as effective climatic threshold variables for landslide bodies at 5 m and 20 m depths, respectively.

However, despite advances in the monitoring and analysis of active slope movements in clay, the pore pressure regime and its relationship with slope movements remain highly complex to understand due to the interaction of numerous phenomena (Pellegrino et al., 2004; Picarelli et al., 2005; Comegna et al., 2007). The effects of slope movements further complicate the reliable assessment of the pore pressure regime. Specifically, the low permeability of soil and the non-uniform state of strain and stress induced by movement often lead to the development of excess pore pressures which add to the effects induced by the infiltration of rainwater. Comegna et al. (2007), through coupled hydro-mechanical numerical analyses, demonstrated that any redistribution of internal stress associated with

the local mobilization of a mudslide body can induce excess pore pressures and subsequent deformation of the landslide. The interplay of movements and associated deformation phenomena results in a continuous alteration of soil properties, thereby affecting the hydrological and mechanical response of the slope. Comegna et al. (2020) highlighted the critical role of the shear zone in influencing the groundwater regime, based on data collected during prolonged investigations of slow-active earthflows in the Basento Valley, Southern Italy.

In some cases, even minor slope deformations can significantly alter the pore water pressure regime due to the opening of cracks, closure of fissures, or damming of permeable layers (Vieira and Fernandes, 2004). This issue is particularly relevant for stiff clays, argillaceous rocks, or clayey flysch deposits, which exhibit sharp spatial variations in hydraulic conductivity due to networks of discontinuities and changes in material properties over short distances. These characteristics make modeling the groundwater regime—and particularly the effects of rainfall—a challenging task (Picarelli et al., 2022). Technical literature has increasingly focused on this subject, emphasizing the role of fissures, cracks, and discontinuities (Cotecchia et al., 2015; Shao et al., 2015; Di Maio et al., 2021).

In light of this evidence, it is still challenging to accurately characterize the hydraulic and mechanical properties of the landslide body to understand the relationship between hydraulic regime and slope movements.

6.5 Combination of other factors with rainfall

The relationship between rainfall intensity, duration, and slope instability has been extensively studied in scientific literature since the late 20th century. However, factors influencing slope stability often evolve, moving rainfall-landslide relationships dynamic and subject to change. Such changes may result from external influences like earthquakes, fires, human activity, climatic oscillations, or even landslide activity itself.

6.5.1 Wildfire occurrence

Wildfires represent increasingly widespread phenomena that significantly alter the hydro-mechanical properties of soils, creating conditions that enhance susceptibility to natural instabilities such as shallow landslides and debris flows (Tang et al. 2019; Parsons et al. 2010; Abdollahi et al. 2024; La Porta et al. 2025). Climate change, modifications in land management and usage, and the accumulation of combustible materials contribute to the increasing frequency and severity of wildfires (Parise and Cannon, 2012). The thermal impact of fires causes chemical, physical, and biological changes in soils, with root systems among the most affected components. Vegetation,

through its root system, provides cohesion to soils, thus stabilizing slopes. However, wildfires degrade roots to varying extents, depending on factors such as the depth of heat penetration and the temperatures reached (Farid et al., 2024 and references therein). The complex interplay between wildfire-induced soil modifications and subsequent hydrological responses significantly amplifies the risk of natural instabilities, making post-fire landscapes highly susceptible to meteorological events over an extended time window (Gill and Malamud, 2014; Abdollahi et al., 2023). In this context, Vahedifard et al. (2024) report various geohazards influenced by wildfires, including rockfall, debris flows and land subsidence.

The environmental impact of fires can vary in magnitude and persist for years, depending on fire intensity, severity, and frequency (e.g., Abdollahi et al., 2023; Vahedifard et al., 2024; Farid et al., 2024). For instance, Rengers et al. (2020) indicate that complete recovery may take 3–5 years, while DeGraff (1997) reports 10 years.

Fire intensity refers to the rate of energy released during combustion, whereas fire severity describes the resultant effects on soil physical, chemical, and biological properties. Fire severity correlates with the extent of vegetation combustion and damage, which indirectly affects root degradation and the post-fire vegetation recovery process. The terms fire severity and burn severity are often used interchangeably. Fire severity is predominantly used in classifying and mapping fire events and can be assessed via remote sensing techniques, employing multispectral indices to detect spectral changes in the soil before and after fire occurrences. In situ surveys are frequently conducted for validation, assessing soil alterations such as organic matter loss and vegetation dynamics under post-fire conditions (Keeley, 2009; Parsons et al., 2010).

Following wildfires, soil and land cover are immediately impacted. However, the thermal alteration is generally confined to a very thin shallow layer of less than ten centimeters (Chicco et al., 2023). Among the effects of wildfires on slopes, notable consequences include changes in soil water repellency, reductions in hydraulic conductivity, potential formation of hydrophobic layers, degradation of soil structure, and infiltration of ash into soil pores (Vahedifard et al., 2024). These phenomena result from the interplay between soil composition, intrinsic soil properties and the thermal regime developed during combustion. DeBano (2000) reviewed experimental and field evidence regarding fire-induced water repellency, reporting negligible effects below 175°C, intense water repellency formation between 175 and 200°C, and destruction of hydrophobicity within the 280-400°C range. However, other studies have demonstrated that heating duration also influences these trends (e.g., Doerr et al., 2004). The reduction in hydraulic conductivity is attributed to void collapse following soil and vegetation combustion (Ebel & Moody, 2020). Additionally, while some studies suggest that ash layers exhibit hydrophobic behavior, others have linked them to increased

infiltration rates and water retention, delaying runoff (Ebel et al., 2012). Consequently, literature presents discrepancies regarding wildfire effects on slope stability and soil properties.

Beyond the thermo-hydraulic consequences of wildfires, soil mechanical strength may be significantly compromised. Experimental tests assessing soil-root system strength, despite variations in materials, report negligible or poor changes in friction angle but substantial reductions in cohesion (e.g. Secci et al., 2014; Peduto et al., 2022). Roots decay and tree mortality progressively reduce soil reinforcement, with effects persisting over extended periods. Lei et al. (2022) observed a time-dependent reduction in shear strength, with tests conducted on soil samples collected two months, one year and two years post-wildfire.

Rainfall exacerbates post-fire susceptibility by infiltrating fire-affected soils. The combination of reduced mechanical strength and altered hydrological behavior facilitates rapid saturation of shallow soil layers, increasing pore pressure and predisposing slopes to failure. In the initial months following a wildfire, debris flows are among the most frequent geohazards, triggered by two primary processes: erosion and material entrainment due to surface runoff, and infiltration-induced shallow landslides (Cannon & Gartner, 2005). The first process occurs immediately following significant rainfall events, whereas the second is linked to delayed root and tree mortality (Figure 6.6). Although the probability of geohazard occurrence endures for extended periods after a wildfire, it gradually reduces over time (Thomas et al., 2021).

Figure 6.6: Evolution of a slope affected first by wildfire and subsequently by rainfall, leading to instability. (a) Pre-fire condition: slope covered by soil and vegetation. (b) Wildfire event with varying burn severity, causing alterations in soil and vegetation. (c) Post-fire rainfall triggering a shallow landslide, with consequent damage to the built environment.

The assessment of rainfall-induced landslide initiation generally involves defining intensity-duration thresholds (see above). However, post-fire conditions significantly alter these thresholds, necessitating site-specific re-evaluations. Approaches for analyzing post-fire instability triggering include empirical, statistical and physically-based theoretical models. Empirical and statistical

models rely on historical data, with statistical methodologies encompassing logistic regression and machine learning techniques. However, to use such methodologies, a comprehensive inventory of post-wildfire landslides is required, which is currently lacking globally.

More recently, physically-based models have been introduced. Although these approaches are often computationally expensive and need site-specific geotechnical data, they are a valid tool to account for wildfire effects, considering the variations in root reinforcement and hydraulic conditions of the unsaturated soil covers potentially unstable (Abdollahi et al., 2023, 2024).

Observations indicate that post-fire shallow landslides evolving in floods and debris flows are predominantly triggered by short-duration and high-frequency rainfall events (Moody et al., 2013). Rainfall thresholds in burned areas are markedly lower than those in unburned areas. Despite significant advancements in wildfire and rainfall-induced geohazard research, critical knowledge gaps persist. Data on soil recovery trajectories and the evolution of post-fire geohazard susceptibility remain limited (Vahedifard et al., 2024). Given the current context of climate change and increasing wildfire frequency, advancing research to enhance understanding, prevention, and prediction of post-fire disasters is both a scientific and socio-economic priority.

6.5.2 Vegetation alteration (natural and anthropogenic)

Slope instability processes driven by rainfall can be highly influenced by the presence of vegetation cover, especially in hilly and mountainous environments susceptible to rapid and/or slow mass movements, such as soil and debris slides and flows. Vegetation can play a significant role in mitigating the impacts of mass movements occurring along natural and artificial slopes, with relevant implications in terms of risk reduction. It is widely recognized that vegetation promotes slope stability through hydro-mechanical mechanisms that concur to increase resisting forces acting along slopes (Greenway, 1987; Sidle & Ochiai, 2006; Philips et al., 2021). Among these mechanisms, root reinforcement is widely considered the most important (Figure 6.7a).

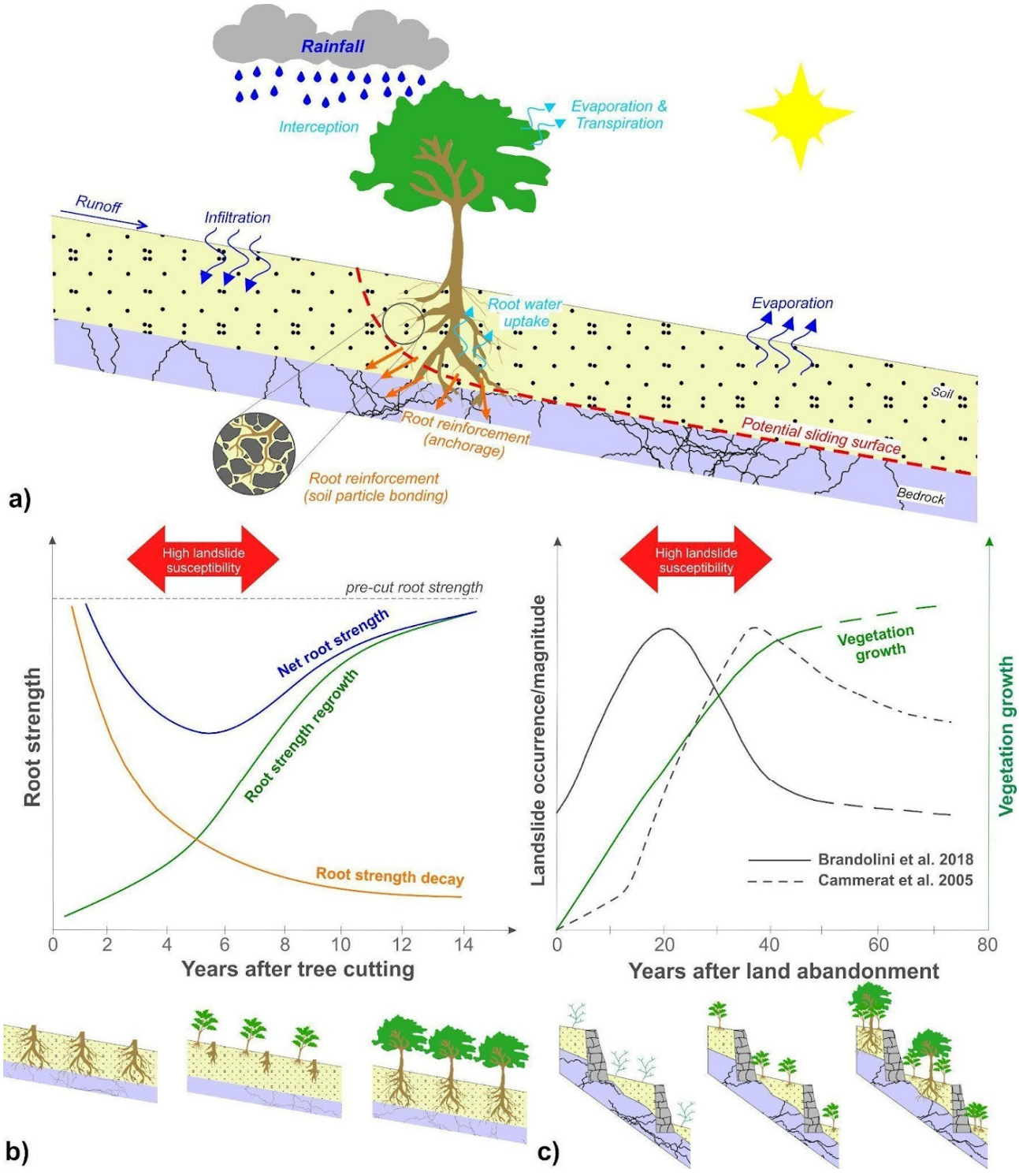

Figure 6.7: (a) Illustration of principal mechanical and hydrological mechanisms provided by vegetation on a slope. (b) Temporal variation of root strength in forested hillslopes after tree logging (redrawn and modified after Sidle & Ochiai, 2006). (c) Relationships between land abandonment, landslide occurrence/magnitude and vegetation growth in terraced slopes.

The reinforcement provided by plant roots can be twofold depending on root diameter and their spatial density (Stokes et al., 2009; Schwarz et al., 2010). On the one hand, single large (diameter >2mm)

woody roots penetrate soil covers in different directions to reach stiffer and more resistant soil horizons or the underlying bedrock, thus working as basal or lateral soil anchoring systems that exploit the root tensile strength (Figure 6.7a). On the other hand, the dense network of fine roots (diameter <2 mm) growing between granules produces more compact soil aggregates, resulting in higher overall cohesion (Figure 6.7a). Instead, the hydrological reinforcement functions of vegetation are mainly attributed to processes that concur to reduce soil moisture in the vadose zone, thus counteracting the negative role of pore water pressures (Sidle & Bogaard, 2016; Vergani et al., 2017). Namely, the action of interception operated by plant canopies, which reduces the amount of effective rainfall reaching the ground, combined with transpiration processes by roots, which enable soil desaturation and suction development (Figure 6.7a). However, the effectiveness of vegetation-related hydro-mechanical protective functions depends on several factors, such as plant species and ages, their spatial arrangements, as well as slope morphological features, climatic conditions and land management practices, making vegetation reinforcement variable both spatially and temporally (Sidle & Bogaard, 2016; Vergani et al., 2017).

The beneficial contributions of vegetation to slope stability can be altered negatively due to both natural (e.g., insect pests, diseases, wildfires) and anthropic (e.g., deforestation, timber harvesting, land use changes) causes (Conedera et al., 2003; Maringer et al., 2016; Philips et al., 2021). One of the most documented adverse effects of vegetation degradation on slope stability consists of the progressive decay of root strength following tree logging (Figure 6.7b). Although root decay is usually accompanied by the formation of soil piping (Uchida et al., 2001) that can act as preferential flow circuits for rainwater infiltrating from the ground, no straightforward evidence on their negative (i.e., increase of pore water pressure) or positive (i.e., decrease of pore water pressure) hydrological role on slope stability is still documented (Ghestem et al., 2011; Ni et al., 2019; Shao et al., 2016). Conversely, several experimental and modelling studies revealed consistent temporal patterns of root reinforcement reduction after plant removal (Ammann et al., 2009; Johnson & Wilcock, 2002; Preti, 2012; Watson et al., 1999), indicating that roots result almost totally degraded approximately 15-20 years after cutting, with the highest rates of decay recorded after 10 years (Vergani et al., 2017). Simultaneously, a significant increase in landslide magnitude and intensity (from 2 to 10 times higher) has been found until the vegetation cover is fully re-established, and a pre-logging condition is achieved (O'Loughlin & Pearce, 1976; Sidle & Wu, 1999; Dhakal & Sidle, 2003; Imaizumi & Sidle, 2012) (Figure 6.7b). Similar temporal evolutions of proneness to rain-induced mass movements were found in hilly-mountainous slopes following farmland abandonment. For example, Brandolini et al. (2018) speculated that, in terraced landscapes, the period that elapses between the cessation of farming activities and the considerable spread of natural vegetation (<25-30 years) could represent

the most hazardous scenario. Similarly, other studies in different morphological, land use and land cover (LULC) contexts indicated that the slope stabilization promoted by the progressive growth of natural vegetation can require up to 30-40 years depending on the vegetation species and the dynamics of forest regeneration as well as land management practices and policy (Cammeraat et al., 2005; Latocha, 2014; Moos et al., 2023) (Figure 6.7c). The review of literature dealing with the role of vegetation as slope stability factor clearly outlines its time dependency, thus enhancing its preparatory function on the occurrence of rainfall-induced mass-movements. As recently claimed by some authors (Vergani et al., 2017; Di Biagio et al., 2024), in order to capture reliable future landslide hazard and risk scenarios, it will be extremely important pursuing the implementation of the dynamic role of hydro-mechanical vegetation effects in slope stability modelling. This will be crucial in the light of changing climate conditions, since it can be reasonably expected that harsher weather patterns will affect both agricultural and forest ecosystems, thus also altering their protective functions (Li et al., 2023). For example, the occurrence of prolonged periods of droughts punctuated by intense or extreme rainstorms may lead to a deterioration of root mechanical reinforcement (Ma et al., 2021), which in turn can further exacerbate the severity of slope instability processes. Furthermore, new climate scenarios can also have social and economic impacts leading to climate- and economically dependent LULC change (Briner et al., 2013) that can modify over time the response of slopes prone to landslides driven by rainfall.

6.5.3 Earthquakes and rainfall

The simultaneous occurrence of seismic ground motion and other destabilizing factors, such as soil saturation from rainfall (Figure 6.8), plays a crucial role in assessing landslide hazards and the associated risks to settlements and infrastructure (Bird and Bommer, 2004; Li et al., 2012; Ruggeri et al., 2020, Kumar et al., 2021; Khadka et al., 2025;). Martino et al. (2022) conducted a comprehensive quantitative analysis to evaluate changes in landslide activity at the basin scale following a 5.1 Mw earthquake in Central Italy's Molise region in August 2018.

The study combined direct field observations with Differential SAR Interferometry (DInSAR) analysis over a three-year period, spanning two years before and one year after the earthquake. This approach identified both first-time and reactivated landslides within a region of high landslide susceptibility, characterized by lithologies such as marly clays and flysch.

Findings revealed that seasonal rainfall interacting with slopes destabilized by the earthquake triggered a significantly higher number of landslides compared to previous years under similar rainfall conditions. Notably, the number of reactivation events increased by approximately 118%, during one year after the low-magnitude earthquake. This increase in activity was observed in both first-time and

reactivated landslides, marked by shorter periods of inactivity and prolonged periods of sustained activity.

Martino et al. (2020) investigated the 2016-2017 earthquake-induced landslide scenarios for seismic microzonation in the Accumoli area (central Italy). Since the seismic sequence exacerbated the region's vulnerability to landslides, this study focused on the triggering of slow landslides, such as earthflows and planar or rotational slides, in this highly susceptible area following a low-magnitude (5.1 Mw) earthquake. Through field surveys conducted immediately after the event, the authors documented the distribution of seismically induced effects, particularly landslides in cohesive soils and structural collapses. They analyzed how the spatial distribution of these phenomena correlated with seismic and rainfall intensities. The intense rainfall, delivering approximately 120 mm over three days before and during the earthquake, significantly worsened slope stability: the soil saturation during seismic shaking played a critical role, influencing both the extent of induced effects and their spatial concentration relative to epicentral distance and earthquake magnitude. This led to a more severe landslide scenario than would typically be expected for an earthquake of such low magnitude. Specifically, the affected area extended far beyond the traditional Keefer radius (Keefer, 1984) of approximately 2 km, reaching distances up to 20 km, indicating that saturated soil conditions dramatically amplify the impact of seismic activity on slope stability. This phenomenon does not extend to disrupted or rapid landslides, such as collapses or fast flows (Rodriguez et al., 1999).

Beyond the Italian case studies, the scientific literature offers a range of approaches to study multi-hazard landslide scenarios. Sassa et al. (2007) emphasized that the combined effect of earthquakes and rainfall can trigger landslides even under conditions that would not be critical if considered separately. Faris & Wang (2014) used stochastic analysis to evaluate the impact of rainfall on earthquake-induced landslides in Indonesia, showing that variability in the hydraulic response of slopes significantly modifies risk scenarios. More recently, Nguyen & Kim (2020) applied Monte Carlo simulations to predict rainfall–earthquake-induced landslides in Seoul, South Korea, demonstrating the effectiveness of probabilistic approaches.

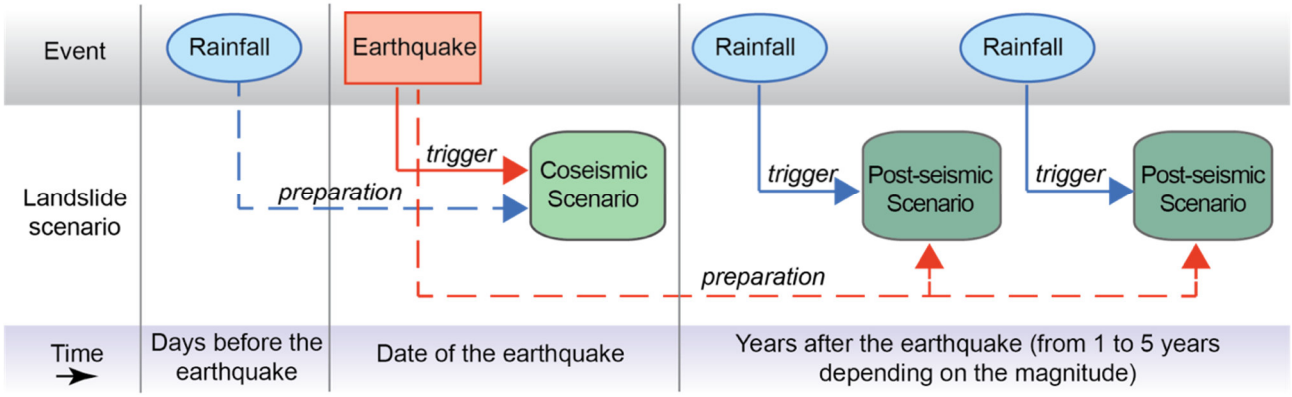

Figure 6.8: Role of antecedent rainfall in the earthquake-triggered shallow landslides involving unsaturated slope covers.

7. Ground instability scenarios of effects under a changing climate

7.1 Toolchains for modelling the role of rainfall in landslide preparation and triggering

Operational toolchains are defined as sequences of computational and analytical tools designed to produce scenarios of ground instability effects linked to specific types of preparation processes and triggering actions, characterized by a given intensity.

Based on the principle of leveraging existing knowledge, the VS2 spoke first focused on the identification and rationalization of computational tools useful for constructing these logical-operational analysis flows, characterizing each operational tool according to various criteria and initially designing their interconnection.

The resulting toolchains (Figure 7.1) specifically address rainfall-induced shallow landslides commonly observed in mountainous and hilly environments (Table 5.1). They are designed to model and simulate the role of rainfall in both the preparation (time-dependent processes) and triggering (transient processes) of slope failures. Accordingly, tools dedicated to susceptibility or predisposing factor analysis (e.g., SZplugin, Titti et al., 2022, 2025) and those developed for run-out modelling (e.g., QPROTO, Castelli et al., 2021; STONE, Guzzetti et al., 2002; RASH3D, Pirulli et al., 2007) are not included in the present framework. The compiled toolchains (Figure 11) can thus address, with varying levels of detail, the following types of shallow landslides commonly observed in Italian mountainous and hilly environments:

- Rapid-kinematics phenomena: rockfalls/topples and debris/mud flows.
- Slow-kinematics phenomena: shallow planar slides and roto-translational landslides.

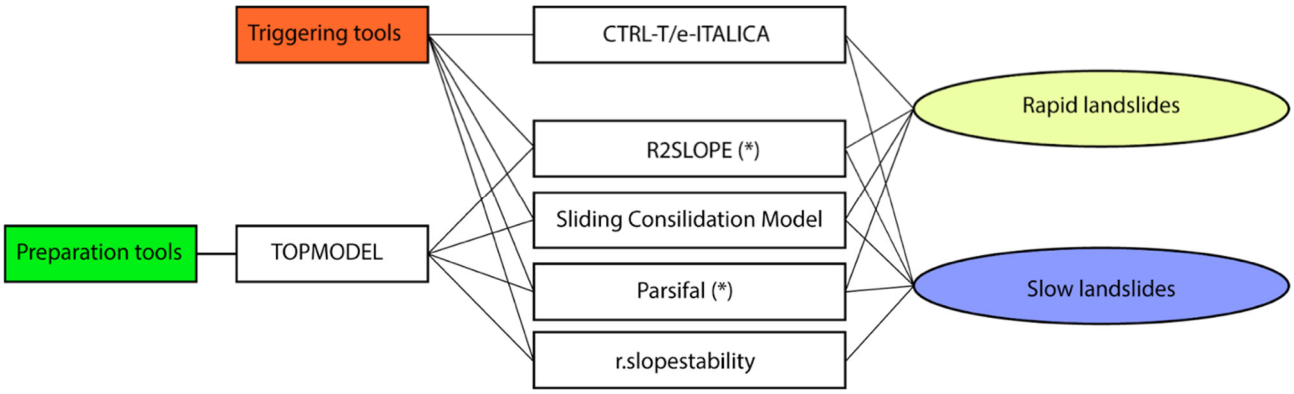

Figure 7.1: Inventory of tools compiled for modeling rainfall-induced preparation and triggering of ground instabilities. (*) These tools also support seismic forcing, potentially enabling multi-hazard scenario assessment.

7.1.1 Tools for the Evaluation of Preparatory Conditions

- **TOPMODEL**

TOPMODEL (TOPography-based hydrological MODEL) is derived from the seminal work of Beven et al. (1995) and critically reviewed in Beven (1997). Its core concept is the topographic index, defined as the ratio of upslope contributing area to the local slope angle. This index provides a measure of hydrological similarity, under the assumption that locations with equal values respond in comparable ways to rainfall and groundwater dynamics. Areas with higher index values are expected to saturate first and thus contribute more readily to surface and subsurface runoff.

To capture the complexity of catchment hydrology in a simplified manner, TOPMODEL assumes that subsurface runoff is generated uniformly within zones sharing the same index, that the hydraulic gradient of the water table parallels the land surface slope, and that soil transmissivity declines exponentially with depth. These simplifying assumptions allow the model to be implemented effectively with digital terrain data and GIS.

By simulating water table fluctuations in shallow soil deposits following rainfall events, provided the relevant hydro-mechanical parameters are available, TOPMODEL outputs can be used for two key purposes:

i) to assess how rainfall intensifies pre-existing slope instability conditions, and

ii) to generate input data for quantitative slope stability analyses in soil-mantled terrains, particularly with respect to shallow translational and, to a lesser degree, rotational–translational failure mechanisms.

7.1.2 Tools for the Evaluation of Triggering Effects

- **e-ITALICA-CTRL-T**

The empirical rainfall threshold approach emerges as the key methodological tool for assessing rainfall-triggered slope instabilities, as it provides a unified framework applicable to different landslide kinematics. In particular, e-ITALICA (enhanced ITAlian rainfall-induced LandslIdes CAtalogue; Brunetti et al., 2025) is a comprehensive Italian landslide catalogue that documents 6,312 rainfall-induced landslides recorded between 1996 and 2021. These events, originally listed in the ITALICA catalogue (Peruccacci et al., 2023), are now enriched with detailed information on their rainfall triggering conditions, expressed in terms of rainfall duration D (hours) and cumulative event rainfall E (mm). The triggering conditions were derived from hourly rainfall measurements collected

at 4,033 gauges and processed using a rigorous and reproducible methodology. In addition to rainfall information, the catalogue also includes topographic and land cover attributes, making it a valuable dataset for analyzing rainfall conditions capable of triggering landslides, calibrating and validating physically based prediction models, and defining empirical rainfall thresholds from local to national scales, thereby contributing to landslide risk reduction in Italy. To process these data, the CTRL-T tool (Calculation of Thresholds for Rainfall-induced Landslides–Tool; Melillo et al., 2018) was applied. Developed in R, CTRL-T automatically reconstructs rainfall events from standard rainfall series and landslide records, identifies multiple rainfall conditions responsible for slope failures, and defines frequentist rainfall thresholds for different non-exceedance probabilities. The tool further incorporates machine learning algorithms to refine empirical rainfall thresholds by correlating the spatial and temporal occurrence of landslides with their triggering rainfall. When historical rainfall series are available, these thresholds can also be characterized in terms of hazard.

Although e-ITALICA produces binary forecasts (landslide/no landslide) without pinpointing exact locations, these can be linked to inventoried landslides (reactivations) or to highly susceptible areas (potential first-time activations). The catalogue supports analysis of rainfall conditions that trigger landslides, calibration and validation of physically-based prediction models, and the definition of empirical rainfall thresholds across Italy, contributing to landslide risk reduction. It is applicable to all types of landslides, from rapid to slow-moving.

- **R2SLOPE**

The R2SLOPE tool (Rollo & Rampello, 2023) is a GIS-based probabilistic model designed for the regional assessment of slope stability under both rainfall and seismic forcing. For rainfall-induced shallow landslides in soil, it couples a hydrological framework (TOPMODEL), with the infinite slope stability equation to simulate how infiltration raises pore-water pressures and lowers the factor of safety, allowing different rainfall scenarios to be translated into probabilities of failure. For earthquake-induced instability, it uses semi-empirical relationships to estimate expected co-seismic displacements for both rock sliding, including planar and wedge mechanisms, and shallow soil landslides. These displacements are computed from peak ground acceleration and peak ground velocity values in combination with the yield coefficient Ky. By linking distributed hydrological response to slope failure thresholds and integrating seismic predictive relationships, R2SLOPE can be applied to both rapid and slow landslides, offering a versatile framework for assessing multi-hazard scenarios.

- **Sliding-Consolidation Model**

The Sliding-Consolidation Model (Rollo & Buscarnera, 2023) is a hydro-mechanical framework developed to estimate deformations in slopes caused by changes in pore water pressure, particularly those induced by rainfall. It is designed to capture the complex interplay between infiltration-driven pore pressure build-up, consolidation processes, and shear deformation within the basal shear zone, thereby providing a mechanistic understanding of how hydrologic forcing translates into deformation velocity and the potential evolution of shallow failures into either rapid or slow-moving landslides. By linking hydrological inputs from models such as TOPMODEL, the Sliding-Consolidation Model can account for the preparatory effects of rainfall, including spatially variable infiltration and soil saturation, allowing for a more realistic representation of rainfall-triggered instability.

The model is applicable to a wide range of landslide types, from slow, creeping slopes to fast, catastrophic failures, making it a versatile tool for both research and practical hazard assessment. Its strength lies in its ability to connect pore water pressure dynamics with slope mechanical behavior over both short- and long-time scales, offering insight into long-term slope dynamics, deformation velocities, and the conditions under which shallow landslides may accelerate. However, the model is limited in its scope as it does not include the effects of seismic triggers or other rapid-loading mechanisms, which constrains its applicability in multi-hazard scenarios where rainfall and earthquakes might act in combination. Despite this limitation, the Sliding-Consolidation Model remains a powerful framework for understanding rainfall-driven landslide processes and for predicting the potential timing, magnitude, and evolution of slope failures under varying hydrological conditions.

- **PARSIFAL**

The PARSIFAL (Probabilistic Approach to pRovide Scenarios of earthquake-Induced slope FAiLures) framework was developed as an integrated computational tool for the prediction of slope-failure scenarios induced by seismic loading, under predefined hydraulic conditions of the slopes, and with reference to failure mechanisms related to rock-block instabilities (planar, wedge, and toppling failures) and shallow translational soil slides (Esposito et al., 2016; Martino et al., 2020; Giannini et al., 2022). The analysis follows a stepwise procedure that, with specific reference to first-time failures, can be summarized as follows:

i) assessment of static stability conditions for different hydraulic states (expressed in terms of joint saturation percentage for rock masses, and pore pressure ratio – Ru – for shallow soil slides);

ii) definition of the critical acceleration coefficient (Ky) and pseudo-static stability analysis for given PGA values and hydraulic conditions;

iii) estimation of coseismic displacement approach and related exceedance probability of a given critical displacement threshold using a pseudo-dynamic method.

The implemented analytical solutions are based on the global limit equilibrium approach (static and pseudo-static stability analysis) and the Newmark rigid-block method (pseudo-dynamic analysis).

Originally conceived as a modular collection of computational tools, the PARSIFAL framework has been specifically updated and integrated to meet the requirements of the project's Proof of Concept (PoC). In particular, to enhance its performance, two distinct processing chains were developed: one dedicated to rock-mass instabilities (PARSIFAL-R) and the other to shallow soil instabilities (PARSIFAL-T), depending also on the nature of the required input data. Both PARSIFAL-R and PARSIFAL-T include a final module that allows for the estimation of coseismic displacement as a function of Ky based on a semi-empirical relation (Rollo and Rampello, 2021), without requiring the use of spectrum-compatible accelerograms needed for the Newmark analysis.

Furthermore, regarding hydraulic conditions – crucial for assessing the effects of meteorological and climatic forcings independently from multi-hazard interactions – while no computational tool is currently available for rock masses to transform rainfall input into hydraulic head along the joint network, for soil translational slides the TOPMODEL hydrological model (Beven et al., 1995) has been integrated by means of a dedicated script providing an estimation of the water table depth - and, thus, the Ru factor – following a given rainfall. Although simplified, this model enables the evaluation of the preparatory and/or triggering effects of rainfall events.

- **r.slopestability**

r.slopestability is a spatially distributed, physically based model for landslide susceptibility analysis. It is open-source and was developed by Mergili et al. (2014) as a C- and Python-based raster module of the GRASS GIS software package. Its application ranges from shallow soil slips to deep-seated mass movements in geologically complex areas, being suitable for large areas, including tens to hundreds of square kilometres or more appropriately accounting for the natural variability of the governing parameters.

It offers five modes of physically based slope stability simulations. Four are based on randomly located and sized ellipsoidal slip surfaces, and one employs the infinite slope stability model. The ellipsoidal approaches allow the user to consider either only the ellipsoid bottom or also the bottoms

of soil layers intersecting the ellipsoid. In addition, the tool can be run with a single ellipsoid of fixed parameters for targeted analysis. The model requires as inputs a digital elevation model (DEM), the saturated water content (via TOPMODEL), ranges of geotechnical parameter values derived from laboratory tests, and estimates of soil depth obtained in the field. Each soil class or layer must be associated with geometric and geotechnical properties such as thickness, cohesion, friction angle, and bulk density.

The model calculates the factor of safety (FoS) and the probability of slope failure (Pf) for each surface. Probability density functions are exploited to assign Pf to each ellipsoid. The minimum value of FoS and the maximum value of Pf recorded for each pixel are then taken as indicators of slope instability. The final output consists of raster maps of FoS and Pf, providing spatially distributed estimates of slope stability conditions and allowing identification of areas with higher landslide susceptibility.

7.2 Scenario simulations - the demonstrator case of Calabria coastal railway

In order to validate the above-described toolchains, the VS2 spoke identified a set of demonstrator cases, among which a sector of the Tyrrhenian Calabria region, where a coastal railway is repeatedly threatened by rapid landslides.

Once the toolchains have been validated in the demonstrator cases (see VS2 Deliverable 2.5.3), we have run the same toolchains (with the same input parameters except rainfall) to provide scenarios of effects under variable climate, using rainfall data from climatic models provided by the DS spoke.

7.2.1 Precipitation modelling

Among the most recent advances in climate modelling, Struglia et al. (2025) performed a downscaling of the CMIP6 global climate projections to local scales for the Mediterranean and Italian regions, aiming to produce high-resolution climate information for the assessment of climate change signals, with a focus on precipitation extreme events. The Authors performed hindcast (i.e., ERA5-driven) and historical simulations (driven by the MPI-ESM1-2-HR model) to simulate the present (1980–2014) and future (2015–2100) climate under three different emission scenarios (SSP1-2.6, SSP2-4.5, SSP5-8.5). For each experiment, they adopted a double-nesting approach to dynamically downscale global data to the regional domain of interest, firstly over the Europe (EURO) COordinated Regional climate Downscaling Experiment (CORDEX) domain, at a spatial resolution of 15 km, and then

further refined (second nesting) over Italy and the northwestern Mediterranean at a resolution of 5 km, i.e., in the so-called gray zone (5–10 km), close to the convection-permitting (CP) limit.
This study exploits 1-hour precipitation extremes with a 50-year return period, calculated by applying a Gumbel distribution to a 30-year reference dataset, both for the present time and for the 2071-2100 projections, under the worst emission scenario (SSP5-8.5).

7.2.2 Landslide scenarios

Figures 7.2 and 7.3 show the results of the computational run performed with the VS2 toolchain in the Calabria demonstrator case. The results obtained for the two different climatic scenarios do not shows significant increment of landslide areas in the worst future scenario. Such preliminary results encourage to increase the simulations with different duration/return period under different emission , also taking into account the landslide preparatory condition variables.

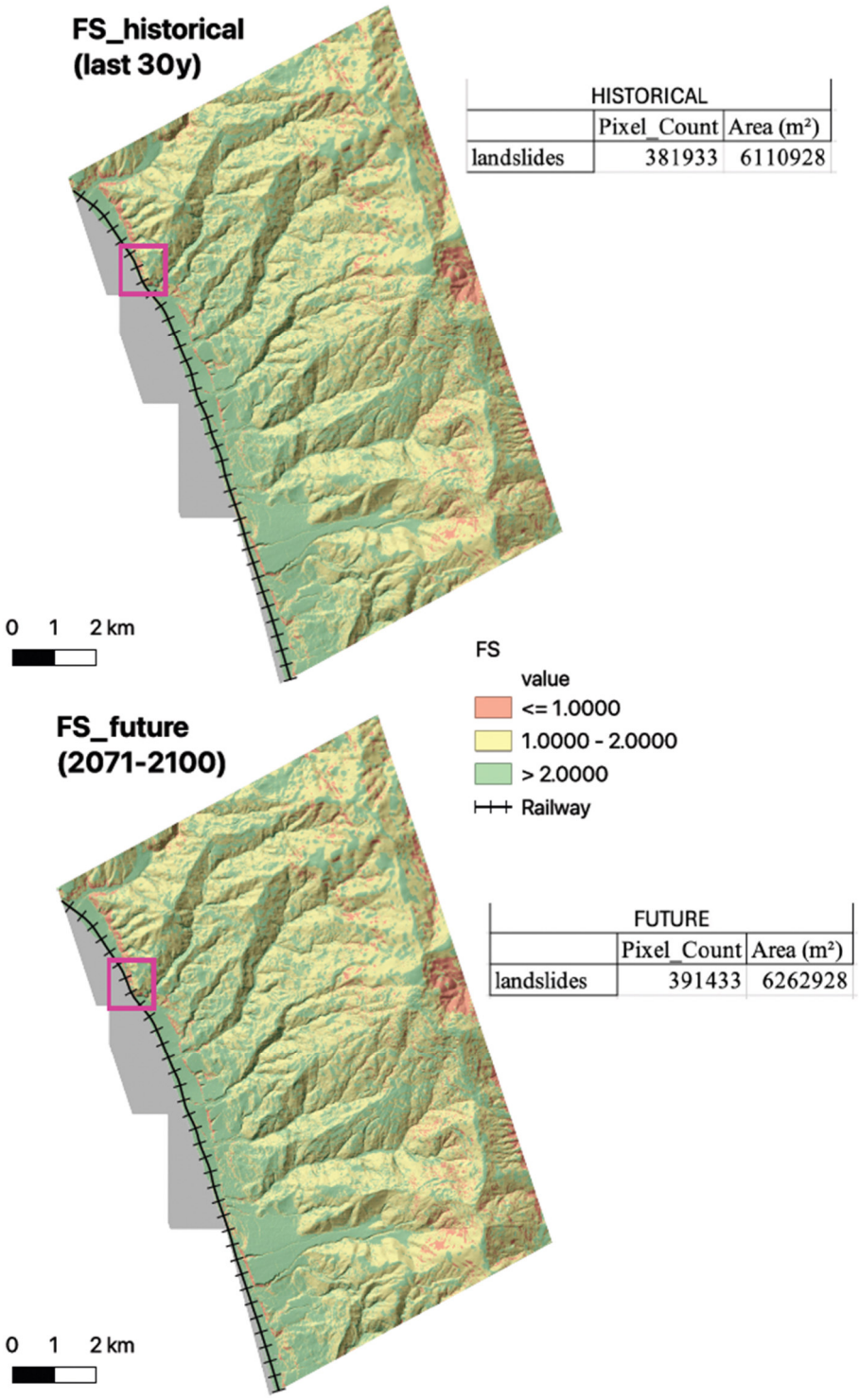

Figure 7.2: Landslide scenarios (Safety Factor FS <= 1) computed by running the VS2 toolchains with 1-hour precipitation extremes with a 50-year return period for both historical conditions and end-century climate projections, under the worst emission scenario (SSP5-8.5). The tables indicate the total extent of landslide areas in the two scenarios. The magenta box is the frame zoomed in Figure 7.3.

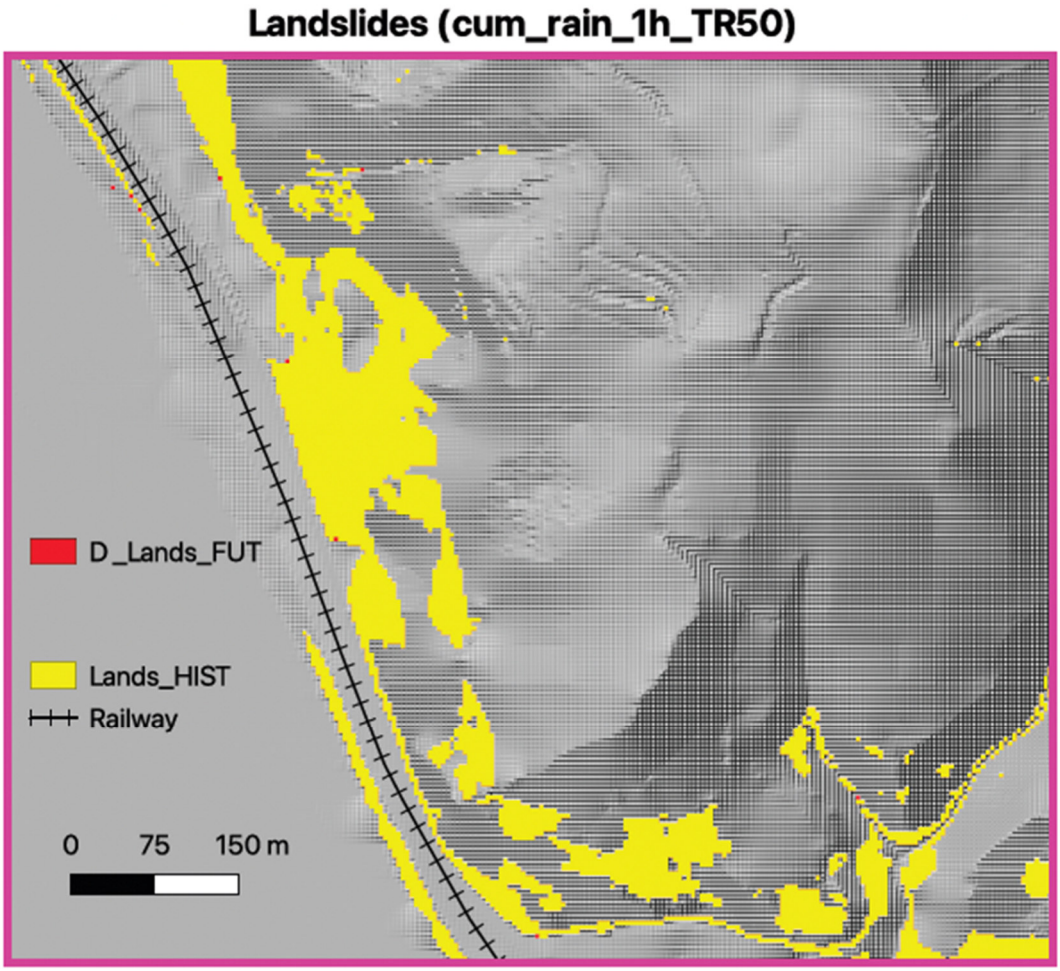

Delta_Pixel_Count	Delta_Area (m²)
9500	152000

Figure 7.3: Landslide areas for the historical (yellow) and future scenarios (red, incremental areas). The table shows the very low amount if incremental landslide area for the whole study case.

7.3 Scenario simulations - the RETURNLAND Virtual Test Bed

The RETURNLAND virtual environment (VTB) provides an integrated analytical framework for simulating the multi-hazard and multi-risk scenarios under changing climate, deriving from the interactions of all the RETURN Project spokes. Some toolchains of the VS2 spoke have been selected to contribute to build such scenarios in the RETURNLAND VTB. Two virtual environments ("Inland" and "Coastal") have been identified, where virtual cities (RETURNVILLE) are expected to be damaged by concatenated hazardous processes.

We simulated both landslide scenarios under changing rainfall regimes (both in the Inland and Coastal environments) and sinkhole scenarios in the Coastal environment) under changing sea-level.

7.3.1 Precipitation modelling

This study exploits 1-hour precipitation extremes with a 100-year return period (same rainfall data as those used for river flood scenarios) for both historical conditions and end-century climate projections. The analysis integrates kilometre-scale convection-permitting climate models (CPMs) with the SMEV (Simplified Metastatistical Extreme Value) framework. CPMs, which explicitly resolve deep convection, provide physically realistic simulations of intense short-duration rainfall compared to traditional regional climate models. Here we rely on the high-resolution simulations developed by Dallan et al. (2024a), which deliver suitable temporal detail for extreme-value applications. To obtain stable and unbiased quantile estimates, rainfall time series were analysed using SMEV, building on metastatistical extreme value theory introduced by Marani and collaborators and further advanced for practical hydrometeorological use by Marra et al. (2019, 2020). SMEV models the distribution of all ordinary rainfall events rather than relying exclusively on annual maxima or threshold exceedances, making it well suited to relatively short yet information-dense CPM outputs. Using this methodology, we estimated historical and future 100-year quantiles and produced spatial maps describing their geographic variability. These products support the evaluation of how hourly extremes may intensify under climate change and form a robust basis for shallow landslide hazard assessment for climate-adaptation planning. Foundational research that informs this workflow includes Ban et al. (2014), Prein et al. (2015), Fosser et al. (2024), for CPMs, alongside Marani & Ignaccolo (2015), Marra et al (2019, 2020), Dallan et al., 2024a, 2024b), Correa Sánchez et al. (2025), and Lompi et al. (2025) for SMEV and the integration of CPM and SMEV.

7.3.2 Landslide scenarios

Figures 7.4 and 7.5 show the results of the computational run performed with the VS2 toolchain in the RETURN-Land Inland environment.

The results obtained for the two different climatic scenarios do not shows significant increment of landslide areas in the worst future scenario. In this case, however, the use of 1-hour precipitation extremes with a 100-year return period (to fine-tune the chain effects related to landslide and river flood scenarios) provided quite severe landslide scenarios also for historical conditions, again suggesting to increase the simulations with different duration/return period under different emission scenarios, also taking into account the landslide preparatory condition variables. Similar results have been obtained for the RETURN-Land Coastal environment (Figures 7.6 and 7.7)

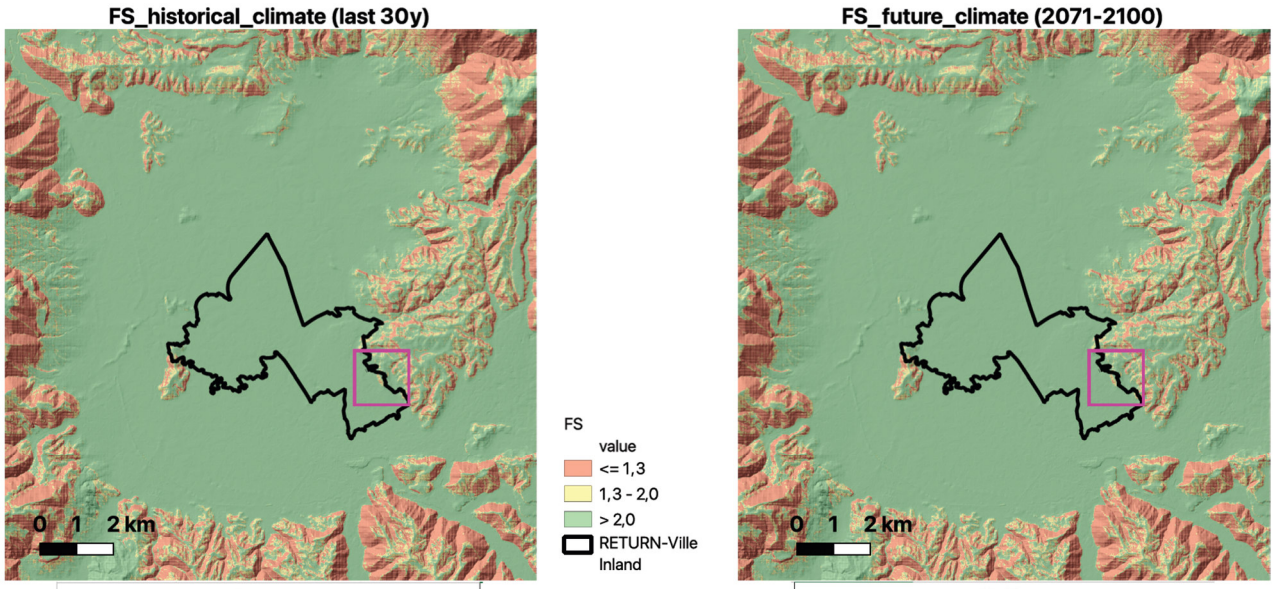

HISTORICAL		
	Pixel_Count	Area (m²)
landslides	388394	38839400

FUTURE		
	Pixel_Count	Area (m²)
landslides	394158	39415800

Figure 7.4: Landslide scenarios (Safety Factor FS <= 1,3) for the Inland environment of RETURNLAND, computed by running the VS2 toolchains with 1-hour precipitation extremes with a 100-year return period for both historical conditions and end-century climate projections, under the worst emission scenario (SSP5-8.5). The tables indicate the total extent of landslide areas in the two scenarios. The magenta box is the frame zoomed in Figure 7.5.

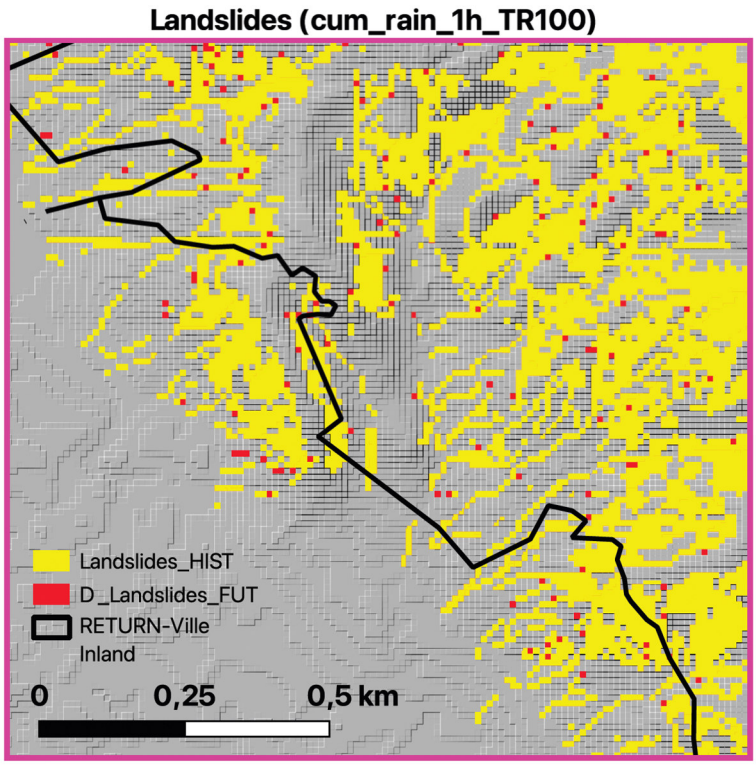

Delta_Pixel_Count	Delta_Area (m²)
5764	576400

Figure 7.5: Landslide scenarios (Safety Factor FS <= 1) or the Inland environment of RETURNLAND, computed by running the VS2 toolchains with 1-hour precipitation extremes with a 50-year return period for both historical conditions and end-century climate projections, under the worst emission scenario (SSP5-8.5). The tables indicate the total extent of landslide areas in the two scenarios.

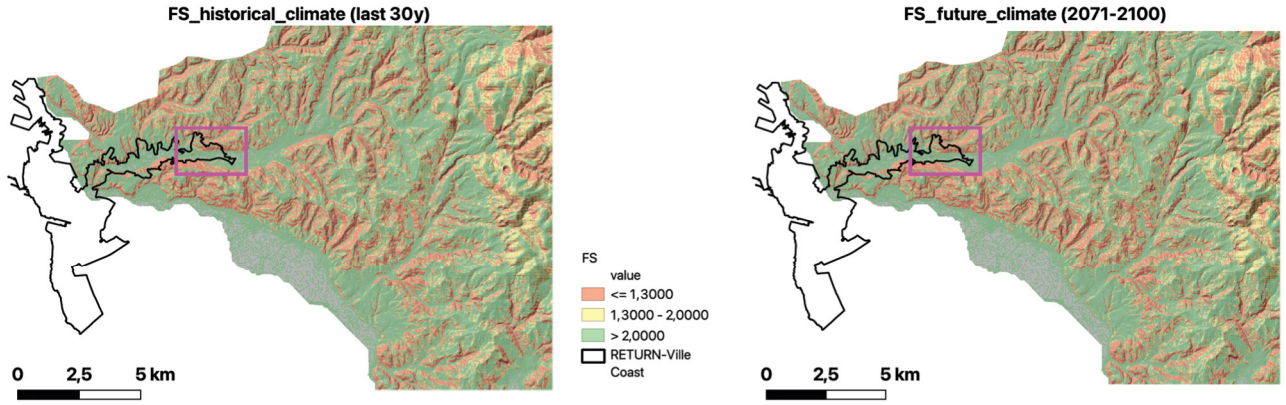

HISTORICAL		
	Pixel_Count	Area (m²)
landslides	528766	52876600

FUTURE		
	Pixel_Count	Area (m²)
landslides	533285	53328500

Figure 7.6: Landslide scenarios (Safety Factor FS <= 1,3) for the Coastal environment of RETURNLAND, computed by running the VS2 toolchains with 1-hour precipitation extremes with a 100-year return period for both historical conditions and end-century climate projections, under the worst emission scenario (SSP5-8.5). The tables indicate the total extent of landslide areas in the two scenarios. The magenta box is the frame zoomed in Figure 7.7.

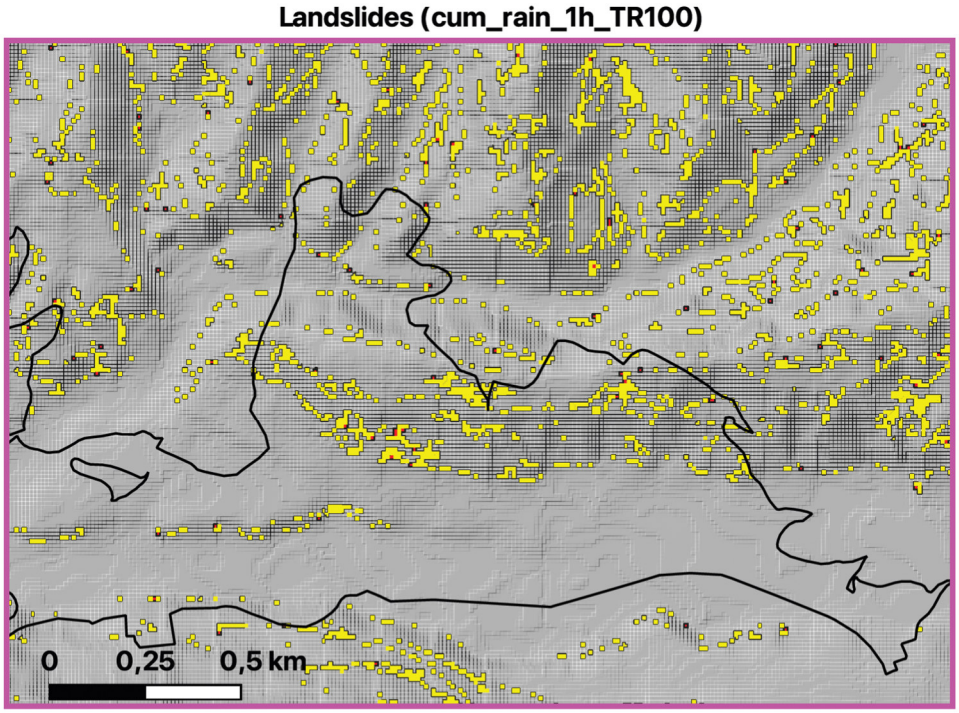

Delta_Pixel_Count	Delta_Area (m²)
4519	451900

Figure 7.7: Landslide scenarios (Safety Factor FS <= 1) for the Coastal environment of RETURNLAND, computed by running the VS2 toolchains with 1-hour precipitation extremes with a 50-year return period for both historical conditions and end-century climate projections, under the worst emission scenario (SSP5-8.5). The tables indicate the total extent of landslide areas in the two scenarios.

7.3.3 Sinkhole scenarios

By combining geological, geomorphological, hydrogeological, and remotely sensed data, both the long-term shoreline shifts and climate-driven impacts on geohazards have been assessed. Two modelling components were developed: (i) a reconstruction of past shoreline positions to quantify retreat and progradation rates, and (ii) forward-looking simulations (up to 2175) of shoreline migration and coastal flooding. Complementary machine learning analyses were implemented to evaluate the influence of coastal processes on sinkhole formation and to produce predictive susceptibility scenarios under rising sea-level conditions.

The first modelling phase (Figure 7.8) focused on Marine Isotope Stage 5 (MIS 5; 125–80 ka), a period characterized by rapid sea-level oscillations. Five shoreline positions were reconstructed, corresponding to three transgressive and two regressive phases, with the MIS 5.5 highstand representing the only peak exceeding the present-day sea level. Corrected for vertical tectonic

displacement, these paleo-shorelines delineate a coastal migration belt approximately 42 km-wide across the RETURNLAND region.

Sea-level projections were obtained from the Coupled Model Intercomparison Project Phase 6 (CMIP6), integrating contributions from:

- atmosphere–ocean general circulation models (AOGCMs);
- surface mass balance and dynamic ice-sheet contributions from Greenland and Antarctica;
- glacier and land water storage contributions;
- glacial isostatic adjustment;
- inverse barometer effect.

To assess coastal flooding, two scenarios were considered: SSP1–2.6 and SSP5–8.5, corresponding to, respectively, low and high greenhouse gas concentration pathways, therefore representative of best- and worst-case projections (Palma et al., 2020; Sannino et al., 2022).

Future shoreline evolution was evaluated using a bathtub model that combines CMIP6 sea-level rise (SLR) projections with Vertical Land Motion (VLM) derived from InSAR and GNSS data (2014–2021). VLM-corrected DEMs and SLR projections were applied across multiple time horizons (2050–2175). Under the high-end SSP5–8.5 scenario, inundation is projected to increase progressively, reaching 152.3 km² by 2175, with low-lying coastal areas undergoing permanent submergence and significant land loss.

Sinkhole susceptibility was analyzed using an ensemble machine-learning framework combining Random Forest, Gradient Boosting Machines, and MaxEnt. Models were trained on MIS 5 shoreline reconstructions and applied to future conditions (Figure 7.9) under SSP5–8.5 (2050–2175). Predisposing factors included:

- overburden thickness;
- lithology, slope;
- Relative Slope Position;
- Topographic Wetness Index;
- coastline density.

Training and validation relied on two independent sinkhole inventories. Model performance was evaluated using ROC/AUC metrics, yielding excellent accuracy for the training phase (AUC = 0.978) and very good performance for the 2175 projections (AUC = 0.865). Variable-importance analyses highlighted coastline density, lithology, and slope as the dominant controlling factors. Response

curves indicated increased susceptibility in areas with higher coastline density, carbonate lithologies, and low-gradient topography. Ensemble projections produced spatially explicit sinkhole susceptibility scenarios aligned with trends of future shoreline migration and flooding.

Overall, the combined modelling approaches enable a robust assessment of climate-driven coastal instability and provide suitable insights aimed at long-term sinkhole/coastal flooding susceptibility within RETURNLAND.

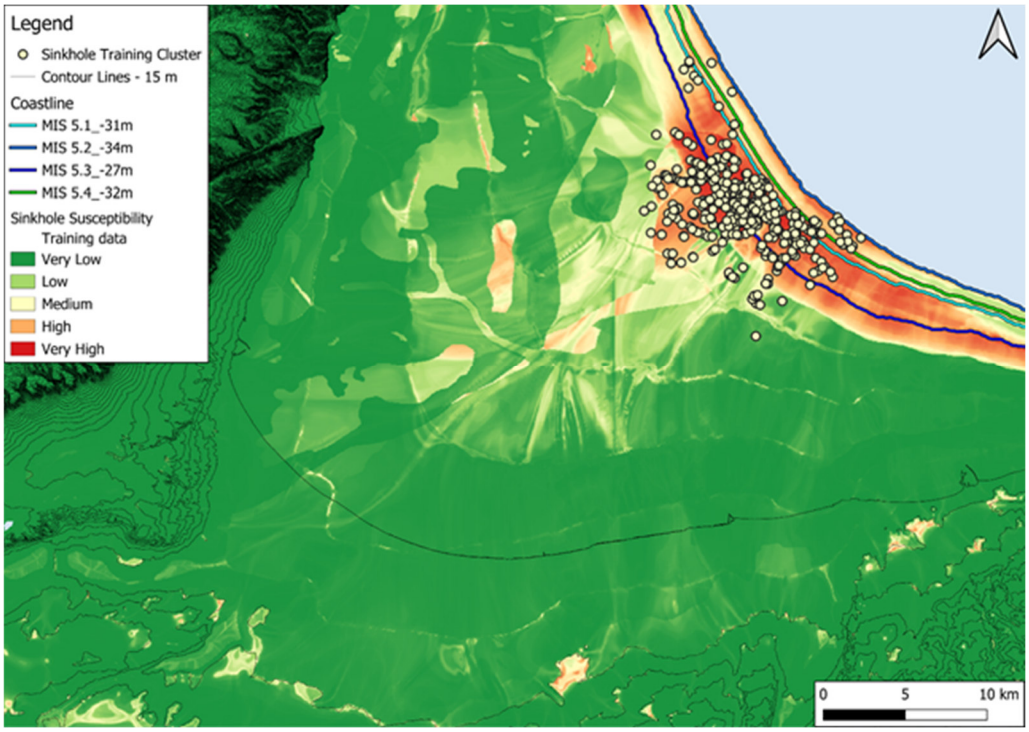

Figure 7.8: Ensemble sinkhole susceptibility map during MIS 5, referring to the training dataset.

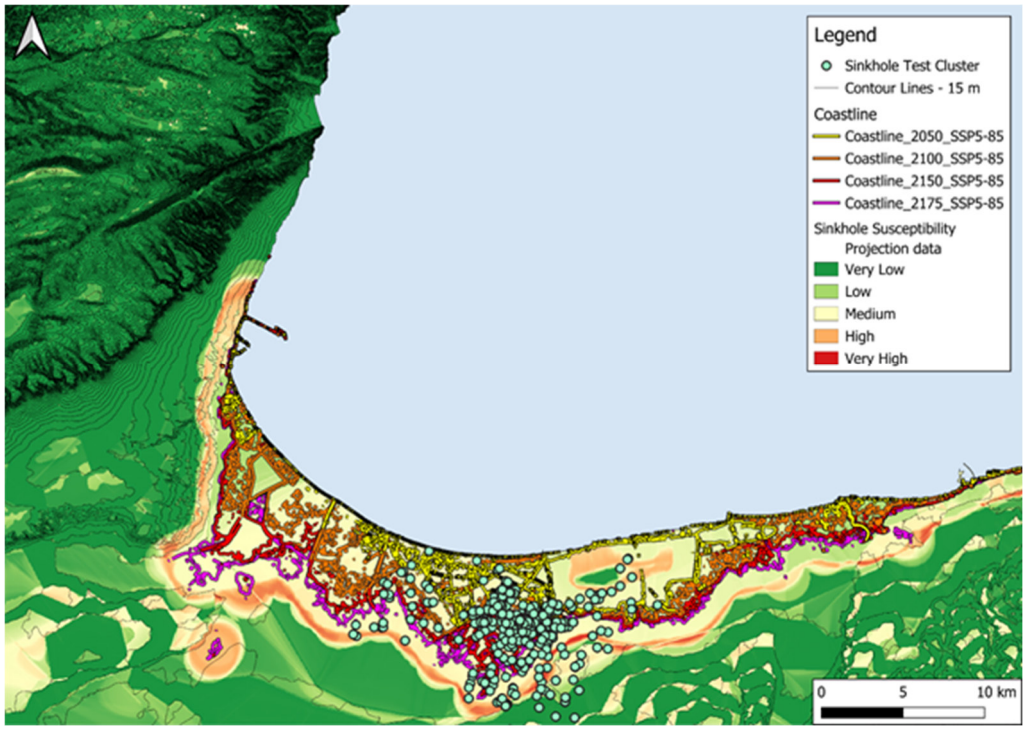

Figure 7.9: Ensemble sinkhole susceptibility map for 2050, 2100, 2150 and 2175, referring to the projected dataset.

7.4 Further scenario simulations

The above preliminary results outlined the need of further simulation, in order to better define ground instability scenarios of effects under a changing climate. In particular, 1h rainfall duration events with shorter return periods have been taken into account for both the demonstrator case of Calabria coastal railway (5-year return period) and the RETURNLAND Virtual Test Bed (2-year return period), in order to test the sensitivity of the VS2 toolchain to changing climate scenarios.

7.4.1 Further landslide scenario simulation in the demonstrator case of Calabria coastal railway

Further investigations on the sensitivity to the triggering role of rainfall under climate change have been performed, since using 1h rainfall duration events with 50-year return period led almost unchanging scenarios of effects related to historical and end-century projected rainfalls. By referring also to the e-ITALICA rainfall thresholds (Brunetti et al., 2025), a different rainfall duration/return period combination (1h/5-years return period) has been tested. In fact, the preliminary analysis of rainfall threshold data for landslide initiation in the Calabria area, according to the e-ITALICA database, outlined that these threshold values are considerably lower than the duration/intensity curves obtained by applying the Gumbel distribution for precipitation extremes with a 10-years return

period (Fig. 7.10), both for the present time and for the 2071-2100 projections, under the worst emission scenario (SSP5-8.5).

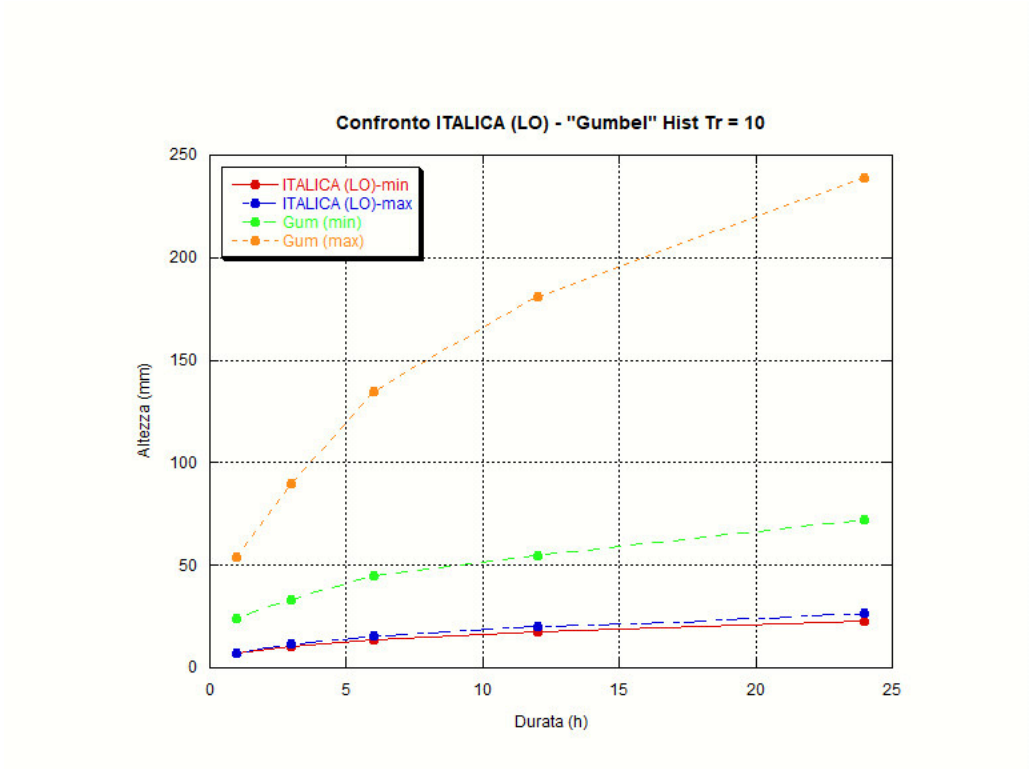

Figure 7.10: Comparison between e-ITALICA rainfall thresholds for landslide initiation and duration/intensity precipitation extremes with a 10-year return period, calculated by applying a Gumbel distribution to a 30-year reference dataset, both for the present time and for the 2071-2100 projections, under the worst emission scenario (SSP5-8.5).

Figure 7.11 show the results of the computational run performed with the VS2 toolchain in the Calabria demonstrator exploiting 1-hour precipitation extremes with a 5-year return period, calculated by applying a Gumbel distribution to a 30-year reference dataset, both for the historical computation (last 30 years; average intensity: 28 mm/h) and for the 2071-2100 projections under the worst emission scenario (SSP5-8.5; average intensity: 32 mm/h).

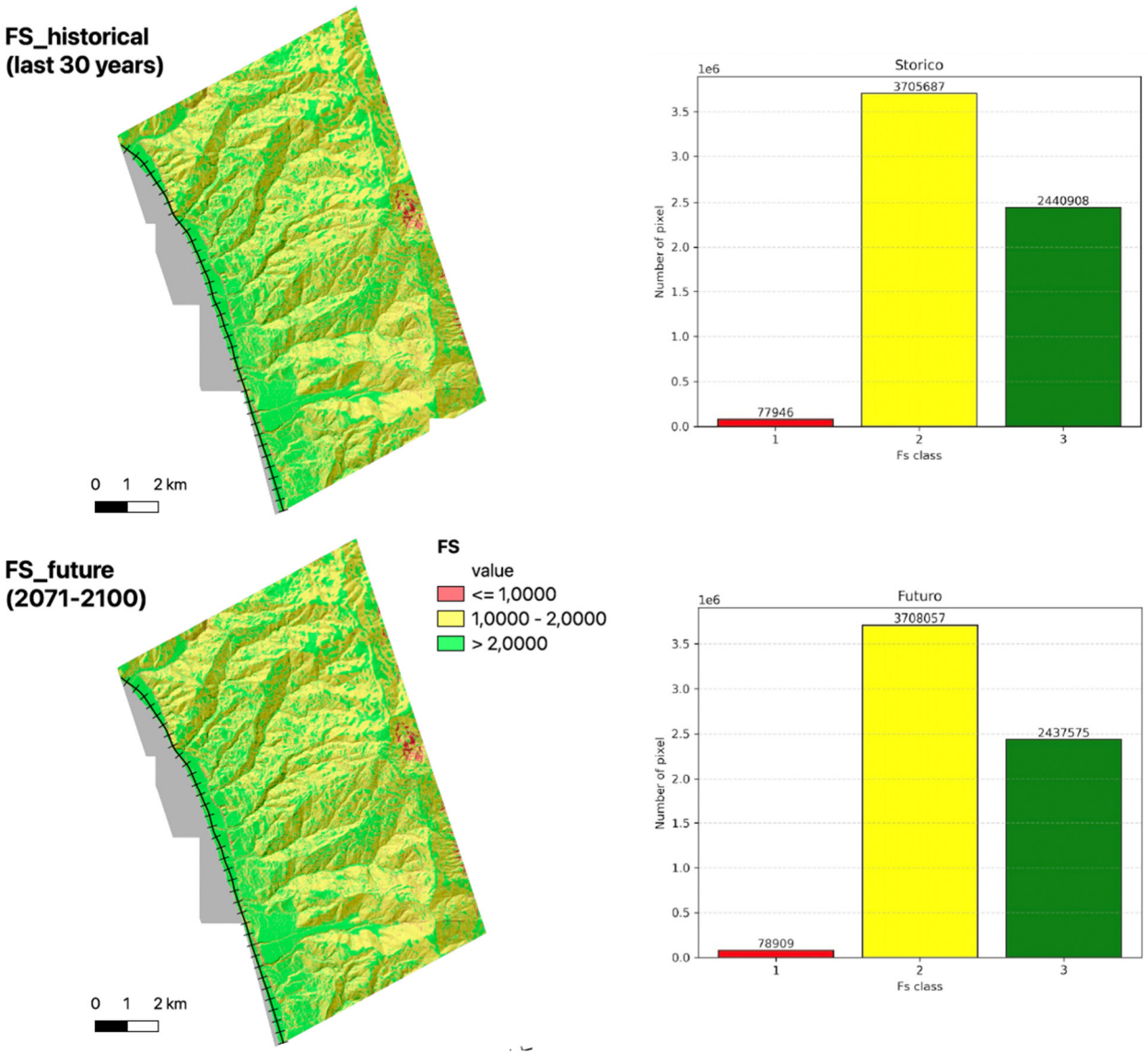

Figure 7.11: Landslide scenarios for the demonstrator case of Calabria coastal railway (Safety Factor FS <= 1) computed by running the VS2 toolchains with 1-hour precipitation extremes with a 5-year return period for both historical conditions and end-century climate projections, under the worst emission scenario (SSP5-8.5). Plots indicate the frequency distribution of FS values for both the historical and future landslide scenarios.

The results obtained for the two different climatic scenarios again do not shows significant increment of landslide areas in the worst future scenario. Such an unexpected result could be biased by the different space and time resolution and uncertainty of rainfall and other input parameters data related mainly to soil properties.

Therefore, the outcomes suggest the need of deeper sensitivity analyses on the toolchain with respect to the input parameters. Furthermore, deepening the analysis of the preparatory role of rainfall, by analysing soil moisture data derived by climate models (both historical and end-century projection),

despite the uncertainty linked to these estimates, would be very useful to have impact scenarios that also account for soil moisture (and, more importantly, for its changes between historical and future conditions, rather than for absolute values). This will allow to refine the parameter configuration for the proper functioning of the toolchains.

7.4.2 Further landslide scenario simulation in the RETURNLAND Virtual Test Bed

In light of the preliminary analyses outlined above, a new run of the toolchains has been carried out for the VTB Inland area, using historical (last 30 years; average intensity: 24 mm/h for the Inland area and 21 mm/h for the Coastal area) and projected data (2071-2100; average intensity: 27 mm/h for the Inland area and 25 mm/h for the Coastal area), as provided by the University of Padua, with 1h duration and 2-years return periods. This has allowed simulations that are decoupled from the cascading effects associated with river flooding phenomena, which had originally required the adoption of a return period of 100 years.

Figures 7.12 and 7.13 show the results of the computational run performed with the VS2 toolchain in both the VTB Inland and Coastal areas, exploiting 1-hour precipitation extremes with a 2-years return period, calculated both for the present time and for the 2071-2100 projections, under the worst emission scenario (SSP5-8.5).

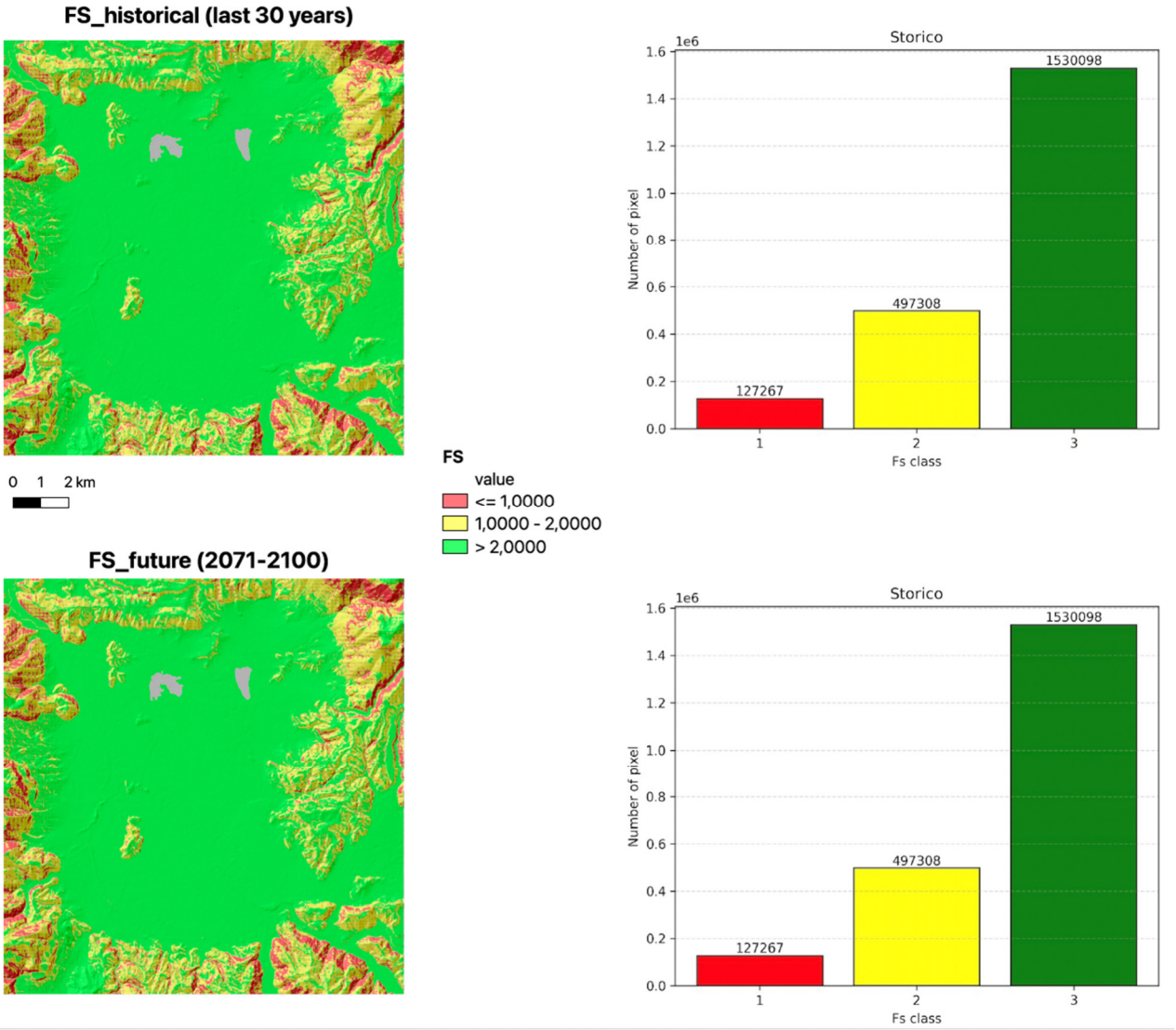

Figure 7.12: Landslide scenarios for the RETURNLAND Virtual Test Bed Inland area (Safety Factor FS <= 1) computed by running the VS2 toolchains with 1-hour precipitation extremes with a 5-year return periods for both historical conditions and end-century climate projections, under the worst emission scenario (SSP5-8.5). Plots indicate the frequency distribution of FS values for both the historical and future landslide scenarios.

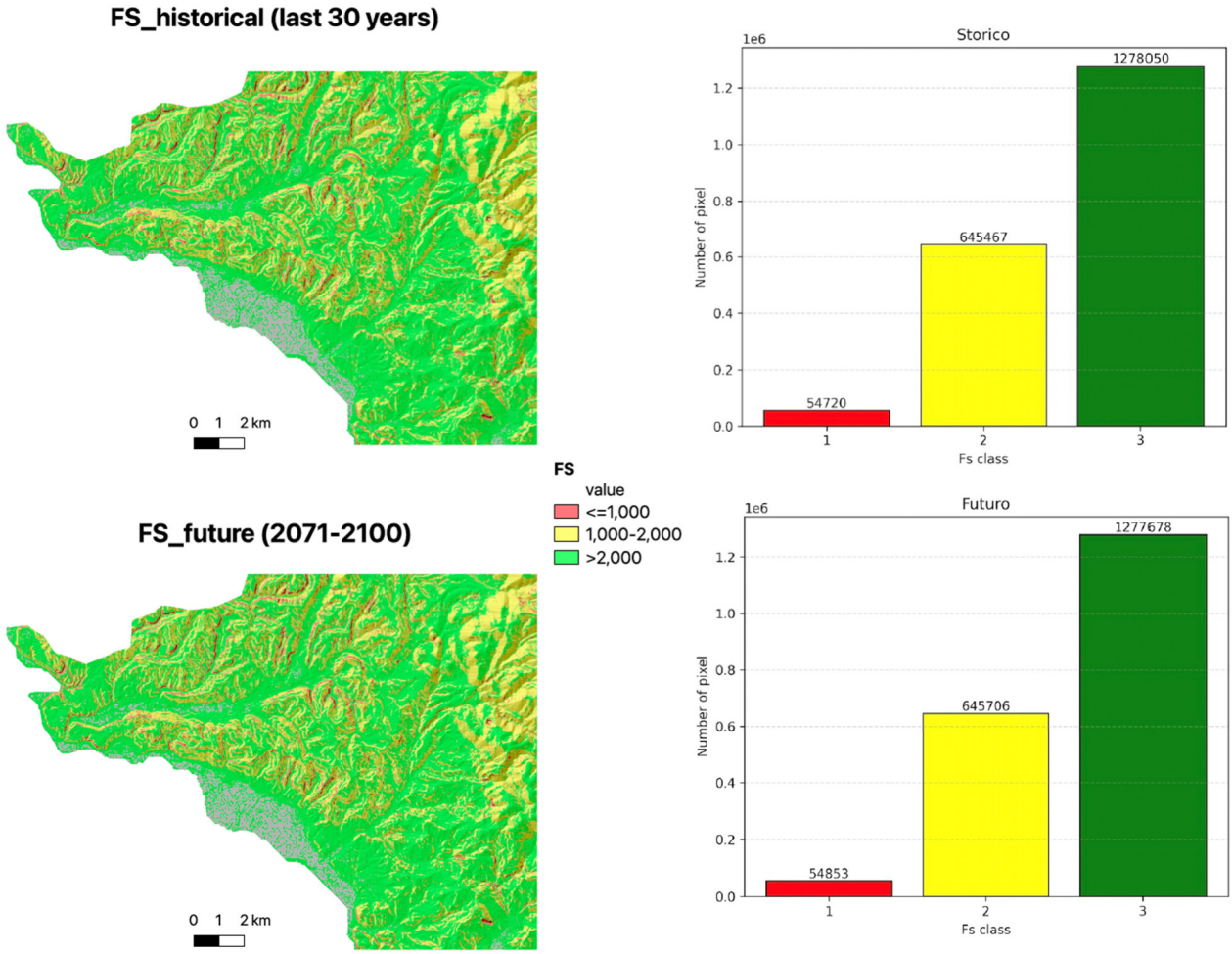

Figure 7.13: Landslide scenarios for the RETURNLAND Virtual Test Bed Coastal area (Safety Factor FS <= 1) computed by running the VS2 toolchains with 1-hour precipitation extremes with a 5-year return periods for both historical conditions and end-century climate projections, under the worst emission scenario (SSP5-8.5). Plots indicate the frequency distribution of FS values for both the historical and future landslide scenarios.

The results obtained in the two different climatic scenarios again do not shows significant increment of landslide areas in the worst future scenario. Such an unexpected result could be biased by the different space and time resolution and uncertainty of rainfall and other input parameters data related mainly to soil properties.

Therefore, the outcomes suggest the need of deeper sensitivity analyses on the toolchain with respect to the input parameters. Furthermore, deepening the analysis of the preparatory role of rainfall, by analysing soil moisture data derived by climate models (both historical and end-century projection), despite the uncertainty linked to these estimates, would be very useful to have impact scenarios that also account for soil moisture (and, more importantly, for its changes between historical and future conditions, rather than for absolute values). This will allow to refine the parameter configuration for the proper functioning of the toolchains.

8. Conclusions

The results of the VS2-DS interactions highlight several key findings and recommendations on climate-driven ground instabilities in Italy.

Landslides, influenced by the interplay of static and dynamic factors, are particularly susceptible to changing rainfall regimes and extreme events, that show a trend toward increased spatial and temporal variability, especially for sub-hourly and hourly precipitation extremes in northern and mountainous regions. Despite these trends, impacts remain locally variable and require duration-specific, regionally resolved analyses for reliable forecasting.

Sinkhole susceptibility is amplified by rising sea levels and coastal migration, with ensemble machine learning models providing robust spatial predictions. The dominant factors controlling sinkhole risk include coastline density, carbonate lithologies, and low-gradient topography, with future coastal flooding significantly exacerbating instability risks.

There is no shared or standardized national framework yet to systematically assess the climate influence on ground instabilities, though the RETURN project sets important groundwork through high-resolution climate downscaling and procedural toolchains. Validation of climate and hazard models remains a priority to support operational and adaptation practices.

9. References

Abdollahi, M., Vahedifard, F. and Tracy, F.T., 2023. Post-wildfire stability of unsaturated hillslopes against rainfall-triggered landslides. Earth's Future, 11(3). https://doi.org/10.1029/2022EF003213

Abdollahi, M., Vahedifard, F., and Leshchinsky, B. A., 2024. Hydromechanical modeling of evolving post-wildfire regional-scale landslide susceptibility. Engineering Geology, 335, 107538. https://doi.org/10.1016/j.enggeo.2024.107538

Abraham, M. T., Satyam, N., Kushal, S., Rosi, A., Pradhan, B., & Segoni, S. (2020). Rainfall threshold estimation and landslide forecasting for Kalimpong, India using SIGMA model. Water, 12(4), 1195. https://doi.org/10.3390/w12041195

Agenzia Regionale Prevenzione Ambiente Energia Emilia-Romagna (ARPAE) - https://www.arpae.it/it/notizie/alluvione-19-20-ottobre-un-analisi-preliminare (Accessed 15/07/2025)

Agenzia Regionale per la Protezione dell'Ambiente del Friuli Venezia Giulia (ARPA-FVG) - https://www.meteo.fvg.it/clima/clima_fvg/03_cambiamenti_climatici/07_GRUPPO_DI_LAVORO_CLIMA_FVG_e_Segnali_dal_Clima/SegnaliDalClimaFVG2024.pdf (accessed 15/07/2025)

Agenzia regionale per la protezione dell'ambiente ligure (ARPAL) - https://www.arpal.liguria.it/home-page/notizie-tematiche/item/ciaran-e-vaia-nel-video-le-mareggiate-a-confronto.html (accessed 15/07/2025)

Ahmad, R. (2003). Developing early warning systems in Jamaica: rainfall thresholds for hydrogeological hazards. In National Disaster Management Conference. Ocho Rios: UDS, 2003.

Aleotti, P. (2004). A warning system for rainfall-induced shallow failures. Engineering geology, 73(3-4), 247-265. https://doi.org/10.1016/j.enggeo.2004.01.007

Ammann, M., Böll, A., Rickli, C., Speck, T., & Holdenrieder, O. (2009). Significance of tree root decomposition for shallow landslides. For Snow Landsc Res, 82(79-94), 79.

Arboleda, R. A., & Martinez, M. (1996). 1992 lahars in the Pasig-Potrero River system. In Fire and mud: eruptions and lahars of Mount Pinatubo (p. 1126). Seattle: Quezon City and University of Washington Press.

Arnone, E., Pumo, D., Viola, F., Noto, L. V., & La Loggia, G. (2013). Rainfall statistics changes in Sicily. Hydrology and Earth System Sciences, 17(7), 2449-2458. https://doi.org/10.5194/hess-17-2449-2013

Avanzi, F., De Michele, C., Gabriele, S., Ghezzi, A., & Rosso, R. (2015). Orographic signature on extreme precipitation of short durations. Journal of Hydrometeorology, 16(1), 278–294. https://doi.org/10.1175/JHM-D-14-0063.1.

Avino, A., Cimorelli, L., Furcolo, P., Noto, L. V., Pelosi, A., Pianese, D., ... & Manfreda, S. (2024). Are rainfall extremes increasing in southern Italy?. Journal of Hydrology, 631, 130684. https://doi.org/10.1016/j.jhydrol.2024.130684

Ayat, H., Evans, J. P., Sherwood, S. C., & Soderholm, J. (2022). Intensification of subhourly heavy rainfall. Science, 378(6620), 655–659. https://doi.org/10.1126/science.abn8657

Azañón, J. M., Azor, A., Yesares, J., Tsige, M., Mateos, R. M., Nieto, F., Delgado, J., Lòpez-Chicano, M., Martìn, W., & Rodríguez-Fernández, J. (2010). Regional-scale high-plasticity clay-bearing

formation as controlling factor on landslides in Southeast Spain. Geomorphology, 120(1-2), 26-37. http://dx.doi.org/10.1016/j.geomorph.2009.09.012

Ban, N., Schmidli, J., & Schär, C. (2014). Evaluation of the new convective-resolving regional climate modeling approach in decade-long simulations. Journal of Geophysical Research, 119, 7889–7907. https://doi.org/10.1002/2014JD021478

Ban, N., Caillaud, C., Coppola, E., Pichelli, E., Sobolowski, S., Adinolfi, M., Ahrens, B., Alias, A., Anders, I., Bastin, S., Belušić, D., Berthou, S., Brisson, E., Cardoso, R.M., Chan, S.C., Christensen, O.B., Fernández, J., Fita, L., Frisius, T., Gašparac, G., Giorgi, F., Goergen, K., Haugen, J. E., Hodnebrog, Ø., Kartsios, S., Katragkou, E., Kendon, E.J., Keuler, K., Lavin-Gullon, A., Lenderink, G., Leutwyler, D., Lorenz, T., Maraun, D., Mercogliano, P., Milovac, J., Panitz, H.-J., Raffa, M., Reca Remedio, A., Schär, C., Soares, P. M. M., Srnec, L., Steensen, B. M., Stocchi, P., Tolle, M.H., Truhetz, H., Vergara- Temprado, J., de Vries, M.H., Warrach-Sagi, K., Wulfmeyer, V. and Zander, M.J. (2021). The first multi-model ensemble of regional climate simulations at kilometer-scale resolution, part I: evaluation of precipitation. Climate Dynamics, 57(1), 275-302. https://doi.org/10.1007/s00382-021-05708-w

Ban, N., Rajczak, J., Schmidli, J., & Schär, C. (2020). Analysis of Alpine precipitation extremes using generalized extreme value theory in convection-resolving climate simulations. Climate Dynamics, 55(1–2), 61–75. https://doi.org/10.1007/s00382-018-4339-4

Banfi, F., & De Michele, C. (2024). Temporal clustering of precipitation driving landslides over the Italian territory. Earth's Future, 12(5). https://doi.org/10.1029/2023EF003885

Baum, R. L., Savage, W. Z., & Godt, J. W. (2002). TRIGRS—A FORTRAN program for transient rainfall infiltration and grid-based regional slope-stability analysis (U.S. Geological Survey Open-File Report 02-0424). U.S. Geological Survey.

Baum, R. L., Godt, J. W., Harp, E. L., McKenna, J. P., & McMullen, S. R. (2005). Early warning of landslides for rail traffic between Seattle and Everett, Washington, USA. In Landslide risk management (pp. 741-750). CRC Press.

Benz, S. A., & Blum, P. (2019). Global detection of rainfall-triggered landslide clusters. Natural Hazards and Earth System Sciences, 19(7), 1433-1444. https://doi.org/10.5194/nhess-19-1433-2019

Berntson, J. A. & Saèllfors, G. B. (1984). Pore pressure variations in marine clay deposits. Proc. 4th Int. Symp. Landslides, Toronto 1, 363-366.

Berti, M., Martina, M. L. V., Franceschini, S., Pignone, S., Simoni, A., & Pizziolo, M. (2012). Probabilistic rainfall thresholds for landslide occurrence using a Bayesian approach. Journal of Geophysical Research: Earth Surface, 117(4). https://doi.org/10.1029/2012JF002367

Berti, M., Pizziolo, M., Scaroni, M., Generali, M., Critelli, V., Mulas, M., ... & Corsini, A. (2025). RER2023: the landslide inventory dataset of the May 2023 Emilia-Romagna meteorological event. Earth System Science Data, 17(3), 1055-1074. https://doi.org/10.5194/essd-17-1055-2025

Beven, K. J., & Kirkby, M. J. (1979). A physically based, variable contributing area model of basin hydrology. Hydrological Sciences Journal, 24(1), 43–69. https://doi.org/10.1080/02626667909491834

Beven, K. J., Lamb, R., Quinn, P., Romanowicz, R., and Freer, J. (1995). TOPMODEL. in V. P. Singh (Ed.), Computer Models of Watershed Hydrology. Water Resource Publications, Colorado, pp. 627–668.

Beven, K. (1997). TOPMODEL: a critique. Hydrological processes, 11(9), 1069-1085. https://doi.org/10.1002/(SICI)1099-1085(199707)11:9%3C1069::AID-HYP545%3E3.0.CO;2-O

Biondi, A., Facheris, L., Argenti, F., & Cuccoli, F. (2024). Comparison of Different Quantitative Precipitation Estimation Methods Based on a Severe Rainfall Event in Tuscany, Italy, November 2023. Remote Sensing, 16(21), 3985. https://doi.org/10.3390/rs16213985

Bird, J. F., & Bommer, J. J. (2004). Earthquake losses due to ground failure. Engineering geology, 75(2), 147-179.https://doi.org/10.1016/j.enggeo.2004.05.006

Bittelli, M., Valentino, R., Salvatorelli, F., & Pisa, P. R. (2012). Monitoring soil-water and displacement conditions leading to landslide occurrence in partially saturated clays. Geomorphology, 173, 161-173. https://doi.org/10.1016/j.geomorph.2012.06.006

Bloomfield, H. C., Hillier, J., Griffin, A., Kay, A. L., Shaffrey, L. C., Pianosi, F., ... & Bates, P. D. (2023). Co-occurring wintertime flooding and extreme wind over Europe, from daily to seasonal timescales. Weather and Climate Extremes, 39, 100550. https://doi.org/10.1016/j.wace.2023.100550

Bogaard, T. A., & Greco, R. (2016). Landslide hydrology: from hydrology to pore pressure. Wiley Interdisciplinary Reviews: Water, 3(3), 439-459. https://doi.org/10.1002/wat2.1126

Bonaccorso, B., Cancelliere, A., & Rossi, G. (2005). Detecting trends of extreme rainfall series in Sicily. Advances in Geosciences, 2, 7-11. https://doi.org/10.5194/adgeo-2-7-2005

Bonanno, R., Lacavalla, M., & Sperati, S. (2019). A new high-resolution meteorological reanalysis Italian dataset: MERIDA. Quarterly Journal of the Royal Meteorological Society, 145(721), 1756-1779. https://doi.org/10.1002/qj.3530

Bonnard, C. H., & Noverraz, F. (2001). Influence of climate change on large landslides: Assessment of long-term movements and trends. In: Proceedings of the International Conference on Landslides Causes, Impact and Countermeasures (pp.121-138).

Bordoni, M., Corradini, B., Lucchelli, L., Valentino, R., Bittelli, M., Vivaldi, V., & Meisina, C. (2019). Empirical and physically based thresholds for the occurrence of shallow landslides in a prone area of northern Italian Apennines. Water, 11(12), 2653. https://doi.org/10.3390/w11122653

Brandolini, P., Cevasco, A., Capolongo, D., Pepe, G., Lovergine, F., & Del Monte, M. (2018). Response of terraced slopes to a very intense rainfall event and relationships with land abandonment: A case study from Cinque Terre (Italy). Land Degradation & Development, 29(3), 630-642. https://doi.org/10.1002/ldr.2672

Briner, S., Elkin, C., and Huber, R. 2013. Evaluating the relative impact of climate and economic changes on forest and agricultural ecosystem services in mountain regions. J. of Environ. Man. 129: 414-422. https://doi.org/10.1016/j.jenvman.2013.07.018

Brunetti, M. T., Gariano, S. L., Melillo, M., Rossi, M., & Peruccacci, S. (2025). An enhanced rainfall-induced landslide catalogue in Italy. Scientific Data, 12(1), 216. https://doi.org/10.1038/s41597-025-04551-6

Brunetti, M., Lentini, G., Maugeri, M., Nanni, T., Auer, I., Böhm, R., & Schöner, W. (2009). Climate variability and change in the Greater Alpine Region over the last two centuries based on multi-variable analysis. International Journal of Climatology, 29(15), 2197–2225. https://doi.org/10.1002/joc.1857.

Brunetti, M. T., Peruccacci, S., Rossi, M., Luciani, S., Valigi, D., & Guzzetti, F. (2010). Rainfall thresholds for the possible occurrence of landslides in Italy. Natural Hazards and Earth System Sciences, 10(3), 447–458. https://doi.org/10.5194/nhess-10-447-2010

Buzzi, A., N. Tartaglione, and P. Malguzzi, 1998. Numerical simulations of the 1994 Piedmont flood: Role of orography and moist processes. Mon. Wea. Rev., 126, 2369–2383, https://doi.org/10.1175/1520-0493(1998)126,2369:NSOTPF.2.0.CO;2 .

Caine, N. (1980). The rainfall intensity-duration control of shallow landslides and debris flows. Geografiska annaler: series A, physical geography, 62(1-2), 23-27.

Calcaterra, D., Parise, M., Palma, B., & Pelella, L. (2000). The influence of meteoric events in triggering shallow landslides in pyroclastic deposits of Campania, Italy. In E. Bromhead, N. Dixon, & M. L. Ibsen (Eds.), Landslides in research, theory and practice: Proceedings of the 8th International Symposium on Landslides (pp. 209–214). A. A. Balkema.

Caleca, F., Confuorto, P., Raspini, F., Segoni, S., Tofani, V., Casagli, N., & Moretti, S. (2024). Shifting from traditional landslide occurrence modeling to scenario estimation with a "glass-box" machine learning. Science of the total environment, 950, 175277. https://doi.org/10.1016/j.scitotenv.2024.175277

Cammeraat E, van Beek R, Kooijman A. 2005. Vegetation succession and its consequences for slope stability in SE Spain. Plant and Soil 278:135–147. https://doi.org/10.1007/s11104-005-5893-1

Cancelli A, Nova R (1985) Landslides in soil debris cover triggered by rainstorms in Valtellina (central Alps – Italy). In Proc. IV international conference and field workshop on landslides, Tokyo, August 1985 (pp. 267-272).

Cannarozzo, M., L. Noto, F. Viola, 2006. Spatial distribution of rainfall trends in Sicily (1921–2000). Phys. Chem. Earth, 31, 1201–1211, doi:10.1016/j.pce.2006.03.022.

Cannon, S. H. (1985). Rainfall conditions for abundant debris avalanches, San Francisco Bay region, California. Geology, 38, 267-272.

Cannon, S.H. and Gartner, J.E. (2005). Wildfire-related debris flow from a hazards perspective. In: Debris-flow hazards and related phenomena. Jakub, M., Hungr, O. (Eds.), pp.363-385.

Cantonati, F., Lissari, G., Vagnon, F., et al. (2025). From Alpine Catchment Classification to Debris Flow Monitoring. GeoHazards 6, 15. https://doi.org/10.3390/geohazards6010015

Caporali, E., Lompi, M., Pacetti, T., Chiarello, V., Fatichi, S., 2021. A review of studies on observed precipitation trends in Italy. Int J. Clim. 41 (. 1), E1–E25. https://doi.org/10.1002/joc.6741.

Cappa, F., Guglielmi, Y., Soukatchoff, V. M., et al. (2004). Hydromechanical modeling of a large moving rock slope inferred from slope levelling coupled to spring long-term hydrochemical monitoring: Example of the La Clapière landslide (Southern Alps, France). Journal of Hydrology, 291, 67–90. https://doi.org/10.1016/j.jhydrol.2003.12.013

Capparelli, G., & Versace, P. (2011). FLaIR and SUSHI: Two mathematical models for early warning of landslides induced by rainfall. Landslides, 8(1), 67–79. https://doi.org/10.1007/s10346-010-0228-6

Castelli, M., Torsello, G., & Vallero, G. (2021). Preliminary modeling of rockfall runout: Definition of the input parameters for the QGIS plugin QPROTO. Geosciences, 11(2), 88. https://doi.org/10.3390/geosciences11020088

Catani, F., Lagomarsino, D., Segoni, S., & Tofani, V. (2013). Landslide susceptibility estimation by random forests technique: sensitivity and scaling issues. Natural Hazards and Earth System Sciences, 13(11), 2815-2831. https://doi.org/10.5194/nhess-13-2815-2013

Ceriani, M. (1992). Rainfall and landslides in the Alpine area of Lombardia Region, central Alps, Italy. In Proceedings, Interpraevent Int. Symp, Bern (Vol. 2, pp. 9-20).

Chelli S, Wellstein C, Campetella G, Canullo R, Tonin R, Zerbe S, Gerdol R (2017) Climate change response of vegetation across climatic zones in Italy. Climate Research, 71:249-262 https://doi.org/10.3354/cr01443

Chicco, J.M., Mandrone, G. and Vacha, D., 2023. Effects of wildfire on soils: field studies and modelling on induced underground temperature variations. Frontiers in Earth Science, 11. https://doi.org/10.3389/feart.2023.1307569

Chien-Yuan, C., Tien-Chien, C., Fan-Chieh, Y., Wen-Hui, Y., & Chun-Chieh, T. (2005). Rainfall duration and debris-flow initiated studies for real-time monitoring. Environmental Geology, 47(5), 715-724. https://doi.org/10.1007/s00254-004-1203-0

Clarizia, M., Gullà, G., & Sorbino, G. (1996). Sui meccanismi di innesco dei soil slip. In International conference Prevention of hydrogeological hazards: the role of scientific research (Vol. 1, pp. 585-597).

Collison, A., Wade, S., Griffiths, J., & Dehn, M. (2000). Modelling the impact of predicted climate change on landslide frequency and magnitude in SE England. Engineering Geology, 55(3), 205–218. https://doi.org/10.1016/S0013-7952(99)00121-0

Comegna, L., Picarelli, L., & Urciuoli, G. (2007). The mechanics of mudslides as a cyclic undrained–drained process. Landslides, 4(3), 217-232. https://doi.org/10.1007/s10346-007-0083-2

Comegna, L., Picarelli, L., & Urciuoli, G. (2020). Effects of slope movements on soil structure and hydrological response. Geotechnical and Geological Engineering, 38(5), 5633-5647. https://doi.org/10.1007/s10706-020-01341-2

Confuorto, P., Di Martire, D., Centolanza, G., Iglesias, R., Mallorqui, J. J., Novellino, A., Plank, S., Ramondini, M., Thuro, K., & Calcaterra, D. (2017). Post-failure evolution analysis of a rainfall-triggered landslide by multi-temporal interferometry SAR approaches integrated with geotechnical analysis. Remote sensing of environment, 188, 51-72. http://dx.doi.org/10.1016/j.rse.2016.11.002

Conedera, M., Larissa, P.,Marxer, P., Forster, F., Rickenmann, D., Re, L. 2003. Consequences of forest fires on the hydrogeological response of mountain catchments: a case study of the Riale Buffaga, Ticino, Switzerland. Earth Surf. Process. Landf. 28, 117–129. https://doi.org/10.1002/esp.425

Conrad, J. L., Morphew, M. D., Baum, R. L., & Mirus, B. B. (2021). HydroMet: a new code for automated objective optimization of hydrometeorological thresholds for landslide initiation. Water, 13(13), 1752. https://doi.org/10.3390/w13131752

Conte, E., Pugliese, L., & Troncone, A. (2022). A simple method for predicting rainfall-induced shallow landslides. Journal of Geotechnical and Geoenvironmental Engineering, 148(10), 04022079. https://doi.org/10.1061/(ASCE)GT.1943-5606.0002877

Coppola, E., Sobolowski, S., Pichelli, E., Raffaele, F., Ahrens, B., Anders, I., Ban, N., Bastin, S., Belda, M., Belusic, D., Caldas-Alvarez, A., Cardoso, R. M. , Davolio, S. , Dobler, A. , Fernandez, J. , Fita, L. , Fumiere, Q. , Giorgi, F. , Goergen, K., Güttler, I. , Halenka, T. , Heinzeller, D. , Hodnebrog, Ø. , Jacob, D. , Kartsios, S. , Katragkou, E. , Cornes, R. C., Van Der Schrier, G., Van Den Besselaar, E. J., & Jones, P. D. (2018). An ensemble version of the E-OBS temperature and precipitation data sets. Journal of Geophysical Research: Atmospheres, 123(17), 9391-9409. https://doi.org/10.1029/2017JD028200

Cornes, R., van der Schrier, G., van den Besselaar, E.J.M., Jones, P., (2018): An Ensemble Version of the E-OBS Temperature and Precipitation Datasets, J. Geophys. Res. Atmos., 123.

Corominas, J., Ayala, F. J., Cendrero, A., Chacón, J., Díaz de Terán, J. R., Gonzáles, A., Moja, J., Vilaplana, J. M. (2005a). Impacts on natural hazard of climatic origin. ECCE final report: a preliminary assessment of the impacts in Spain due to the effects of climate change. Ministerio de Medio Ambiente.

Corominas, J., Moya, J., Ledesma, A., Lloret, A., & Gili, J. A. (2005b). Prediction of ground displacements and velocities from groundwater level changes at the Vallcebre landslide (Eastern Pyrenees, Spain). Landslides, 2(2), 83-96. https://doi.org/10.1007/s10346-005-0049-1

Correa-Sánchez, E. Dallan, F. Marra, G. Fosser, M. Borga (2025). Orographic control on bias and uncertainty in extreme sub-daily precipitation simulations from a convection-permitting ensemble. J. Hydrol., 659 (2025), Article 133324, https://doi.org/10.1016/j.jhydrol.2025.133324

Cotecchia, F., Vitone, C., Santaloia, F., Pedone, G., & Bottiglieri, O. (2015). Slope instability processes in intensely fissured clays: case histories in the Southern Apennines. Landslides, 12(5), 877-893. https://doi.org/10.1007/s10346-014-0516-7

Cotecchia, F., Tagarelli, V., Pedone, G., Ruggieri, G., Guglielmi, S., & Santaloia, F. (2019). Analysis of climate-driven processes in clayey slopes for early warning system design. Proceedings of the Institution of Civil Engineers-Geotechnical Engineering, 172(6), 465-480. https://doi.org/10.1680/jgeen.18.00217

Crespi, A., Brunetti, M., Lentini, G., and Maugeri, M.: 1961–1990 high-resolution monthly precipitation climatologies for Italy (2018), Int. J. Climatol., 3, 878–895, https://doi.org/10.1002/joc.5217, 2018.

Crisci, A., Gozzini, B., Meneguzzo, F., Pagliara, S., & Maracchi, G. (2002). Extreme rainfall in a changing climate: regional analysis and hydrological implications in Tuscany. Hydrological Processes, 16(6), 1261-1274. https://doi.org/10.1002/hyp.1061

Crosta, G. B., & Frattini, P. (2001, October). Rainfall thresholds for triggering soil slips and debris flow. In Proc. of the 2nd EGS Plinius Conference on Mediterranean Storms: Publication CNR GNDCI (Vol. 2547, pp. 463-487).

Crosta, G. B., & Frattini, P. J. N. H. (2003). Distributed modelling of shallow landslides triggered by intense rainfall. Natural Hazards and Earth System Sciences, 3(1/2), 81-93. https://doi.org/10.5194/nhess-3-81-2003

Crozier, M. J. (2010). Deciphering the effect of climate change on landslide activity: A review. Geomorphology, 124(3-4), 260-267. https://doi.org/10.1016/j.geomorph.2010.04.009

Dahal, R. K., & Hasegawa, S. (2008). Representative rainfall thresholds for landslides in the Nepal Himalaya. Geomorphology, 100(3-4), 429-443. https://doi.org/10.1016/j.geomorph.2008.01.014

Dai, J.-Y., & Cheng, S.-T. (2022). Modeling shallow soil moisture dynamics in mountainous landslide active regions. Frontiers in Environmental Science, 10, 913059. https://doi.org/10.3389/fenvs.2022.913059

Dallan, E., Borga, M., Zaramella, M., & Marra, F. (2022). Enhanced summer convection explains observed trends in extreme subdaily precip-itation in the Eastern Italian Alps. Geophysical Research Letters, 49(5), e2021GL096727. https://doi.org/10.1029/2021GL096727.

Dallan, E., Borga, M., Fosser, G., Canale, A., Roghani, B., Marani, M., & Marra, F. (2024a). A method to assess and explain changes in sub-daily precipitation return levels from convection-permitting simulations. Water Resources Research, 60(5), e2023WR035969. https://doi.org/10.1029/2023WR035969

Dallan, E., Marra, F., Fosser, G., Marani, M., & Borga, M. (2024b). Dynamical factors heavily modulate the future increase of sub-daily extreme precipitation in the alpine-mediterranean region. Earth's Future, 12, e2024EF005185. https://doi. org/10.1029/2024EF005185 .

Dallan, E., Marra, F., Fosser, G., Marani, M., Formetta, G., Schär, C., & Borga, M. (2023). How well does a convection-permitting regional climate model represent the reverse orographic effect of extreme hourly precipitation? Hydrology and Earth System Sciences, 27(5), 1133– 1149. https://doi.org/10.5194/hess-27-1133-2023

de Montety, V., Marc, V., Emblanch, C., Malet, J. P., Bertrand, C., Maquaire, O., & Bogaard, T. A. (2007). Identifying the origin of groundwater and flow processes in complex landslides affecting black marls: Insights from a hydrochemical survey. Earth Surface Processes and Landforms, 32, 32–48. https://doi.org/10.1002/esp.1370

De Vita, P., Napolitano, E., Godt, J. W., Baum, R. L., & Allocca, V. (2013). Deterministic estimation of hydrological thresholds for shallow landslide initiation and slope stability models: Case study from the Somma-Vesuvius area of southern Italy. Landslides, 10(6), 713–728. https://doi.org/10.1007/s10346-012-0348-2

DeBano, L.F., 2000. The role of fire and soil heating on water repellency in wildland environments: a review. Journal of hydrology, 231, pp.195-206. https://doi.org/10.1016/S0022-1694(00)00194-3

DeGraff, J., 1997. Geologic investigation of the pilot ridge debris flow, Groveland Ranger District, Stanislaus National Forest. United States Department of Agriculture Forest Service FS-6200-7 (10/73)

Delchiaro, M., Della Seta, M., Martino, S., Moumeni, M., Nozaem, R., Marmoni, G. M., & Esposito, C. (2024a). The role of long-term preparatory factors in mass rock creep deforming slopes: insights from the Zagros Mts. belt (Iran). Landslides, 1-21. https://doi.org/10.1007/s10346-024-02252-6

Delchiaro, M., Iacobucci, G., Della Seta, M., Gribenski, N., Piacentini, D., Ruscitto, V., ... & Troiani, F. (2024b). A fluvial record of late Quaternary climate changes and tectonic uplift along the Marche Piedmont Zone of the Apennines: New insights from the Tesino River (Italy). Geomorphology, 445, 108971. https://doi.org/10.1016/j.geomorph.2023.108971

Delchiaro, M., Ruscitto, V., Schwanghart, W., Brignone, E., Piacentini, D., & Troiani, F. (2025). BankfullMapper: a semi-automated MATLAB tool on high-resolution Digital Terrain Models for spatio-temporal monitoring of bankfull geometry and discharge. Computers & Geosciences, 106001. https://doi.org/10.1016/j.cageo.2025.106001

Dehn, M., Bürger, G., Buma, J., & Gasparetto, P. (2000). Impact of climate change on slope stability using expanded downscaling. Engineering Geology, 55(3), 193–204. https://doi.org/10.1016/S0013-7952(99)00123-4

Desiato, F., Fioravanti, G., Fraschetti, P., Perconti, W., & Toreti, A. (2011). Climate indicators for Italy: calculation and dissemination. Advances in Science and Research, 6(1), 147-150. https://doi.org/10.5194/asr-6-147-2011

Devò, P., Caruso, M. F., Borga, M., & Marani, M. (2025). Estimates of rare rainfall extremes in ungauged areas. Geophysical Research Letters, 52, e2024GL113576. https://doi.org/10.1029/2024GL113576

Dhakal, A.S., Sidle, R.C. 2003. Long-term modeling of landslides for different forest management practices. Earth Surf. Process. Landf. 28, 853–868. https://doi.org/10.1002/esp.499

di Lernia, A., Cotecchia, F., Elia, G., Tagarelli, V., Santaloia, F., & Palladino, G. (2022). Assessing the influence of the hydraulic boundary conditions on clay slope stability: The Fontana Monte case study. Engineering Geology, 297, 106509. https://doi.org/10.1016/j.enggeo.2021.106509

Di Maio, C., De Rosa, J., & Vassallo, R. (2021). Pore water pressures and hydraulic conductivity in the slip zone of a clayey earthflow: Experimentation and modelling. Engineering Geology, 292, 106263. https://doi.org/10.1016/j.enggeo.2021.106263

Di Biagio, A., Capobianco, V., Oen, A., & Tallaksen, L. M. 2024. State-of-the-art: parametrization of hydrological and mechanical reinforcement effects of vegetation in slope stability models for shallow landslides. Landslides, 21(10), 2417-2446. https://doi.org/10. 1007/s10346- 024- 02300-1

Dixon, N., & Brook, E. (2007). Impact of predicted climate change on landslide reactivation: Case study of Mam Tor, UK. Landslides, 4(2), 137–147. https://doi.org/10.1007/s10346-006-0071-y

Distefano, P., Peres D.J., Scandura, P., Cancelliere, A. (2022) Brief communication: introducing rainfall thresholds for landslide triggering based on artificial neural networks. Nat Hazard 22:1151–1157. https://doi.org/10.5194/nhess-22-1151-2022

Doerr, S.H., Blake, W.H., Shakesby, R.A., Stagnitti, F., Vuurens, S.H., Humphreys, G.S. and Wallbrink, P., 2004. Heating effects on water repellency in Australian eucalypt forest soils and their value in estimating wildfire soil temperatures. International Journal of Wildland Fire, 13(2), pp.157-163. https://doi.org/10.1071/WF03051

Doglioni, A., Di Bari, P., Ponte, M., & Simeone, V. (2011). Analysis of the rainfall preceding the activation of the large Maierato landslide in 2010. In: Margottini, C., Canuti, P., & Sassa, K. (Eds.), Landslide Science and Practice: Volume 4 – Global Environmental Change (pp. 107–114). Springer, Berlin, Heidelberg. https://doi.org/10.1007/978-3-642-31337-0_14

Doglioni, A., Fiorillo, F., Guadagno, F. M., & Simeone, V. (2012). Evolutionary polynomial regression to alert rainfall-triggered landslide reactivation. Landslides, 9(1), 53–62. https://doi.org/10.1007/s10346-011-0274-8

Ducrocq, V., Braud, I., Davolio, S., Ferretti, R., Flamant, C., Jansa, A., ... & Tamayo, J. (2014). HyMeX-SOP1: The field campaign dedicated to heavy precipitation and flash flooding in the northwestern Mediterranean. Bulletin of the American Meteorological Society, 95(7), 1083-1100. https://doi.org/10.1175/BAMS-D-12-00244.1

Ebel, B.A., Moody, J.A. and Martin, D.A., 2012. Hydrologic conditions controlling runoff generation immediately after wildfire. Water Resources Research, 48(3). https://doi.org/10.1029/2011WR011470

Ebel, B.A. and Moody, J.A., 2020. Parameter estimation for multiple post-wildfire hydrologic models. Hydrological Processes, 34(21), pp.4049-4066. https://doi.org/10.1002/hyp.13865

Emberson, R., Kirschbaum, D., & Stanley, T. (2021). Global connections between El Nino and landslide impacts. Nature communications, 12(1), 2262. https://doi.org/10.1038/s41467-021-22398-4

EM-DAT, CRED / UCLouvain, Brussels, Belgium - www.emdat.be

Esposito, C., Martino, S., Pallone, F., Martini, G., & Romeo, R. (2016). A methodology for a comprehensive assessment of earthquake-induced landslide hazard, with an application to pilot sites in Central Italy. In Landslides and engineered slopes: Experience, theory and practice (Vol. 2, pp. 869–877). Taylor & Francis.

European Space Agency (ESA) - https://www.esa.int/ESA_Multimedia/Images/2024/10/Valencia_flood_disaster (Accessed 15/07/2025)

Fantini A (2019) Ph. D. Thesis: climate change impact on flood hazard over Italy. http://hdl.handle.net/11368/2940009

Fares, A., Temimi, M., Morgan, K., & Kelleners, T. J. (2013). In-Situ and Remote Soil Moisture Sensing Technologies for Vadose Zone Hydrology. Vadose Zone Journal, 12(2), 1–3. https://doi.org/10.2136/vzj2013.03.0058

Farid, A., Alam, M. K., Goli, V. S. N. S., Akin, I. D., Akinleye, T., Chen, X., Cheng, Q., Cleall, P., Cuomo, S., Foresta, V., Ge, S., Iervolino, L., Iradukunda, P., Luce, C. H., Koda, E., Mickovski, S. B., O'Kelly, B. C., Paleologos, E. K., Peduto, D., … Winkler, J., 2024. A Review of the Occurrence and Causes for Wildfires and Their Impacts on the Geoenvironment. Fire, 7(8), 295. https://doi.org/10.3390/fire7080295

Faris, F., & Wang, F. (2014). Stochastic analysis of rainfall effect on earthquake induced shallow landslide of Tandikat, West Sumatra, Indonesia. Geoenvironmental Disasters, 1(1), 12. https://doi.org/10.1186/s40677-014-0012-3

Fiolleau, S., Uhlemann, S., Wielandt, S., & Dafflon, B. (2023). Understanding slow-moving landslide triggering processes using low-cost passive seismic and inclinometer monitoring. Journal of Applied Geophysics, 215, 105090. https://doi.org/10.1016/j.jappgeo.2023.105090

Flaounas, E., Davolio, S., Raveh-Rubin, S., Pantillon, F., Miglietta, M. M., Gaertner, M. A., ... & Ricard, D. (2022). Mediterranean cyclones: Current knowledge and open questions on dynamics, prediction, climatology and impacts. Weather and Climate Dynamics, 3(1), 173-208. https://doi.org/10.5194/wcd-3-173-2022

Floris, M., Mari, M., Romeo, R. W., & Gori, U. (2004). Modelling of landslide-triggering factors-A case study in the northern Apennines, Italy. In Engineering Geology for Infrastructure Planning in Europe: A European Perspective (pp. 745-753). Berlin, Heidelberg: Springer Berlin Heidelberg.

Formetta, G., Bancheri, M., David, O., & Rigon, R. (2016). Performance of site-specific parameterizations of longwave radiation. Hydrology and Earth System Sciences, 20(11), 4641–4654. https://doi.org/10.5194/hess-20-4641-2016

Formetta, G., Rago, V., Capparelli, G., Rigon, R., Muto, F., & Versace, P. (2014). Integrated physically based system for modeling landslide susceptibility. Procedia Earth and Planetary Science, 9, 74–82. https://doi.org/10.1016/j.proeps.2014.06.016

Fosser, G., Tölle, M., Kendon, E. J., Adinolfi, M., Ban, N., Belušić, D., et al. (2024). Convection-permitting climate models offer more certain extreme rainfall projections. NPJ Climate and atmospheric science. https://doi.org/10.1038/s41612-024-00600-w

Frei, C., and C. Schär, 1998. A precipitation climatology of the Alps from high-resolution rain-gauge observations. Int. J. Climatol., 18, 873–900 https://doi.org/10.1002/(SICI)1097-0088(19980630)18:8%3C873::AID-JOC255%3E3.0.CO;2-9

Fusco, F., De Vita, P., Mirus, B. B., Baum, R. L., Allocca, V., Tufano, R., Di Clemente, E., & Calcaterra, D. (2019). Physically based estimation of rainfall thresholds triggering shallow landslides in volcanic slopes of southern Italy. Water, 11(9), 1915. https://doi.org/10.3390/w11091915

Galvincio, J. D., De Queiroga Miranda, R., & Da Luz, G. G. (2024). Use of Soil Moisture as an Indicator of Climate Change in the SUPer System. Hydrology, 11(5), 65. https://doi.org/10.3390/hydrology1105006

Gariano, S. L., Brunetti, M. T., Iovine, G., Melillo, M., Peruccacci, S., Terranova, O., Vennari, C., & Guzzetti, F. (2015). Calibration and validation of rainfall thresholds for shallow landslide forecasting in Sicily, southern Italy. Geomorphology, 228, 653–665. https://doi.org/10.1016/j.geomorph.2014.10.019

Gariano, S. L., & Guzzetti, F. (2016). Landslides in a changing climate. Earth-science reviews, 162, 227-252. https://doi.org/10.1016/j.earscirev.2016.08.011

Gariano, S. L., & Rianna, G. (2025). How will the projected climate change influence rainfall-induced landslides in Europe? A review of modelling approaches. Landslides 22, 3011–3027 (2025). https://doi.org/10.1007/s10346-025-02550-7

Gebremichael, E., Hernandez, R., Alsleben, H., Ahmed, M., Denne, R., & Harvey, O. (2024). Kinematics and Controlling Factors of Slow-Moving Landslides in Central Texas: A Multisource Data Fusion Approach. Geosciences, 14(5), 133. https://doi.org/10.3390/geosciences14050133

Gelaro, R., McCarty, W., Suárez, M. J., Todling, R., Molod, A., Takacs, L., ... & Zhao, B. (2017). The modern-era retrospective analysis for research and applications, version 2 (MERRA-2). Journal of climate, 30(14), 5419-5454. https://doi.org/10.1175/JCLI-D-16-0758.1

Gemitzi, A., Kofidou, M., Falalakis, G., Fang, B., & Lakshmi, V. (2024). Estimating high-resolution soil moisture by combining data from a sparse network of soil moisture sensors and remotely sensed MODIS LST information. Hydrology Research, 55(9), 905–920. https://doi.org/10.2166/nh.2024.043

Ghestem, M., Sidle, R. C., & Stokes, A. 2011. The influence of plant root systems on subsurface flow: Implications for slope stability. Bioscience, 61, 869–879. https://doi.org/10.1525/bio.2011.61.11.6

Giannini, L. M., Varone, C., Esposito, C., Marmoni, G. M., Scarascia Mugnozza, G., & Schilirò, L. (2022). Earthquake-induced reactivation of landslides under variable hydrostatic conditions: evaluation at regional scale and implications for risk assessment. Landslides, 19(8), 2005-2019. https://doi.org/10.1007/s10346-022-01882-y

Gill, J. C., and Malamud, B. D., 2014. Reviewing and visualizing the interactions of natural hazards. Reviews of Geophysics, 52(4), 680–722. https://doi.org/10.1002/2013RG000445

Giordani, A., Cerenzia, I. M. L., Paccagnella, T., & Di Sabatino, S. (2023). SPHERA, a new convection-permitting regional reanalysis over Italy: Improving the description of heavy rainfall. Quarterly Journal of the Royal Meteorological Society, 149(752), 781-808. https://doi.org/10.1002/qj.4428

Giorgi, F. (2006). Climate change hot-spots. Geophysical research letters, 33(8). https://doi.org/10.1029/2006GL025734

Giorgi F, Jones C, Asrar G (2009) Addressing climate information needs at the regional level: the CORDEX framework. WMO Bull 58(3):175–183

Glade, T., & Crozier, M. J. (2005). The nature of landslide hazard and impact. In: Glade, T., Anderson, M. G., & Crozier, M. J. (Eds.), Landslide Hazard and Risk (pp. 43–74). Wiley, Chichester.

Gleckler, P. J., K. E. Taylor, and C. Doutriaux (2008), Performance metrics for climate models, J. Geophys. Res., 113, D06104,https://doi.org/10.1029/2007JD008972

Greco R, Giorgio M, Capparelli G, Versace P (2013) Early warning of rainfall-induced landslides based on empirical mobility function predictor. Eng Geol 153:68–79. https://doi.org/10.1016/j.enggeo.2012.11.009

Greenway, D.R. 1987. Vegetation and slope stability. In: Anderson, M.G., Richards, K.S. (Eds.), Slope Stability, Geotechnical Engineering and Geomorphology. John Wiley & Sons, Chichester, UK, pp. 187–230.

Grelle, G., Soriano, M., Revellino, P., Guerriero, L., & Guadagno, F. M. (2014). Space–time prediction of rainfall-induced shallow landslides through a combined probabilistic/deterministic approach, optimized for initial water table conditions. Bulletin of Engineering Geology and the Environment, 73, 877–890. https://doi.org/10.1007/s10064-013-0546-8

Guadagno, F. M. (1991). Debris flows in the Campanian volcaniclastic soils. Slope Stability Engineering: Developments and Applications, 125.

Guglielmi, Y., Vengeon, J. M., Bertrand, C., et al. (2002). Hydrogeochemistry: An investigation tool to evaluate infiltration into large moving rock masses (case studies of La Clapière and Séchilienne alpine landslides). Bulletin of Engineering Geology and the Environment, 61, 311–324. https://doi.org/10.1007/s10064-002-0163-4

Guglielmi, S., Pirone, M., Dias, A. S., Cotecchia, F., & Urciuoli, G. (2023). Thermohydraulic numerical modeling of slope–vegetation–atmosphere interaction: Case study of the pyroclastic slope cover at Monte Faito, Italy. Journal of Geotechnical and Geoenvironmental Engineering, 149(11), 05023005. https://doi.org/10.1061/(ASCE)GT.1943-5606.0002960

Guzzetti, F., Crosta, G., Detti, R., & Agliardi, F. (2002). STONE: a computer program for the three-dimensional simulation of rock-falls. Computers & Geosciences, 28(9), 1079-1093. https://doi.org/10.1016/S0098-3004(02)00025-0

Guzzetti, F., Peruccacci, S., Rossi, M., & Stark, C. P. (2007). Rainfall thresholds for the initiation of landslides in central and southern Europe. Meteorology and atmospheric physics, 98(3), 239-267. https://doi.org/10.1007/s00703-007-0262-7

Guzzetti, F., Peruccacci, S., Rossi, M., & Stark, C. P. (2008). The rainfall intensity-duration control of shallow landslides and debris flows: An update. Landslides, 5(1), 3–17. https://doi.org/10.1007/s10346-007-0112-1

Guzzetti, F., Melillo, M., & Mondini, A. C. (2025). Landslide predictions through combined rainfall threshold models. Landslides, 22(1), 137-147. https://doi.org/10.1007/s10346-024-02340-7

Halter, T., Lehmann, P., Wicki, A., Aaron, J., & Stähli, M. (2024). Optimising landslide initiation modelling with high-resolution saturation prediction based on soil moisture monitoring data. Landslides, 1-18. https://doi.org/10.1007/s10346-024-02304-x

Hammond, C., Hall, D., Miller, S., & Swetik, P. (1992). Level I stability analysis (LISA) documentation for version 2.0 (General Technical Report INT-285). U.S. Department of Agriculture, Forest Service.

Handwerger, A. L., Roering, J. J., & Schmidt, D. A. (2013). Controls on the seasonal deformation of slow-moving landslides. Earth and Planetary Science Letters, 377, 239-247. https://doi.org/10.1016/j.epsl.2013.06.047

Harris, I., Osborn, T. J., Jones, P., & Lister, D. (2020). Version 4 of the CRU TS monthly high-resolution gridded multivariate climate dataset. Scientific data, 7(1), 109. https://doi.org/10.1038/s41597-020-0453-3

Hays, J. D., Imbrie, J., & Shackleton, N. J. (1976). Variations in the Earth's Orbit: Pacemaker of the Ice Ages: For 500,000 years, major climatic changes have followed variations in obliquity and precession. science, 194(4270), 1121-1132. https://doi.org/10.1126/science.194.4270.1121

Held, I. M., & Soden, B. J. (2006). Robust responses of the hydrological cycle to global warming. Journal of climate, 19(21), 5686-5699. https://doi.org/10.1175/JCLI3990.1

Hong, Y., Hiura, H., Shino, K., Sassa, K., Suemine, A., Fukuoka, H., & Wang, G. (2005). The influence of intense rainfall on the activity of large-scale crystalline schist landslides in Shikoku Island, Japan. Landslides, 2(2), 97-105. https://doi.org/10.1007/s10346-004-0043-z

Hong, M., Kim, J., & Jeong, S. (2018). Rainfall intensity–duration thresholds for landslide prediction in South Korea by considering the effects of antecedent rainfall. Landslides, 15, 523–534. https://doi.org/10.1007/s10346-017-0892-x

Hutchinson, J. N. (1970). A coastal mudflow on the London Clay cliffs at Beltinge, North Kent. Géotechnique, 20(4), 412–438. https://doi.org/10.1680/geot.1970.20.4.412

Iacobucci, G., Ruscitto, V., Delchiaro, M., Troiani, F., Della Seta, M., & Piacentini, D. (2025). The contribution of Geomorphology on climate services: recent developments on the assessment of climate-impact indicators in the frame of the PNRR RETURN project. Geografia Fisica e Dinamica Quaternaria, 48(1-2), 59-71. https://doi.org/10.4454/fgrt74jk

Imaizumi, F., Sidle, R.C. 2012. Effect of forest harvesting on hydrogeomorphic processes in steep terrain of central Japan. Geomorphology 169-170, 109–122. https://doi.org/10.1016/j.geomorph.2012.04.017

IPCC, 2023: Summary for Policymakers. In: Climate Change 2023: Synthesis Report. Contribution of Working Groups I, II and III to the Sixth Assessment Report of the Intergovernmental Panel on Climate Change [Core Writing Team, H. Lee and J. Romero (eds.)]. IPCC, Geneva, Switzerland, pp. 1-34, https://doi.org/10.59327/IPCC/AR6-9789291691647.001

Isotta, F. A., Frei, C., Weilguni, V., Perčec Tadić, M., Lassegues, P., Rudolf, B., ... & Vertačnik, G. (2014). The climate of daily precipitation in the Alps: development and analysis of a high-resolution grid dataset from pan-Alpine rain-gauge data. International Journal of Climatology, 34(5), 1657-1675. https://doi.org/10.1002/joc.3794

Iverson, R. M., Major, J.J. (1987). Rainfall, groundwater flow, and seasonal motion at Minor Creek landslide, northwestern California: Physical interpretation of empirical relations. Geological Society of America Bulletin, 99, 579–594. https://doi.org/10.1130/0016-7606(1987)99<0579:RGFASM>2.0.CO;2

Iverson, R. M. (2000). Landslide triggering by rain infiltration. Water Resources Research, 36(7), 1897–1910. https://doi.org/10.1029/2000WR900090

Jacob, D., Teichmann, C., Sobolowski, S. et al. (2020) Regional climate downscaling over Europe: perspectives from the EURO-CORDEX community. Reg Environ Change 20, 51. https://doi.org/10.1007/s10113-020-01606-9

Jaiswal, P., van Westen, C. J. (2009). Estimating temporal probability for landslide initiation along transportation routes based on rainfall thresholds. Geomorphology 112:96–105. https://doi.org/10.1016/j.geomorph.2009.05.008

Jakob, M., & Weatherly, H. (2003). A hydroclimatic threshold for landslide initiation on the North Shore Mountains of Vancouver, British Columbia. Geomorphology, 54(3-4), 137-156. https://doi.org/10.1016/S0169-555X(02)00339-2

Jakob, M., & Lambert, S. (2009). Climate change effects on landslides along the southwest coast of British Columbia. Geomorphology, 107(3–4), 275–284. https://doi.org/10.1016/j.geomorph.2008.12.009

Jakob, M., & Owen, T. (2021). Projected effects of climate change on shallow landslides, North Shore Mountains, Vancouver, Canada. Geomorphology, 393, 107921. https://doi.org/10.1016/j.geomorph.2021.107921

Jiang, M., Zhao, X., & Shi, X. (2021). Kinematic behavior analysis of the wadi landslide from time-series sentinel-1 data. IEEE Journal of Selected Topics in Applied Earth Observations and Remote Sensing, 15, 127-135. https://doi.org/10.1109/JSTARS.2021.3134177

Jibson, R. W. (1989). Debris flows in southern Puerto Rico. Geological Society of America, special paper 236, pp 29–55. https://doi.org/10.1130/SPE236-p29

Jin, B., Liu, S., Zeng, T., Li, Y., Wang, T., Gui, L., ... & Yin, K. (2024). Spatio-temporal forecasting of landslide hazard in Chongqing National Transmission Protection Regions, China. International Journal of Digital Earth, 17(1), 2392843. https://doi.org/10.1080/17538947.2024.2392843

Jomelli, V., Brunstein, D., Déqué, M., Vrac, M., & Grancher, D. (2009). Impacts of future climatic change (2070–2099) on the potential occurrence of debris flows: A case study in the Massif des Ecrins (French Alps). Climatic Change, 97(1–2), 171–191. https://doi.org/10.1007/s10584-009-9616-0

Johnson, A.C., Wilcock, P. 2002. Association between cedar decline and hillslope stability in mountainous regions of southeast Alaska. Geomorphology 46, 129–142. https://doi.org/10.1016/S0169-555X(02)00059-4

Kanjanakul, C., Chub-Uppakarn, T., & Chalermyanont, T. (2016). Rainfall thresholds for landslide early warning system in Nakhon Si Thammarat. Arab J Geosci 9:584. https://doi.org/10.1007/s12517-016-2614-4

Kanungo, D. P., & Sharma, S. (2014). Rainfall thresholds for prediction of shallow landslides around Chamoli-Joshimath region, Garhwal Himalayas, India. Landslides, 11(4), 629-638. https://doi.org/10.1007/s10346-013-0438-9

Keefer, D. K. (1984). Landslides caused by earthquakes. Geological Society of America Bulletin, 95(4), 406-421. https://doi.org/10.1130/0016-7606(1984)95<406:LCBE>2.0.CO;2

Keeley, J. E., 2009. Fire intensity, fire severity and burn severity: A brief review and suggested usage. International Journal of Wildland Fire, 18(1), 116–126. https://doi.org/10.1071/WF07049

Kendon M, McCarthy M, Jevrejeva S, Matthews A, Legg T. State of the UK climate (2018). Int J Climatol. 2019; 39 (Suppl. 1): 1–55. https://doi.org/10.1002/joc.6213

Kenney, T. C., & Lau, K. C. (1984). Temporal changes of groundwater pressure in a natural slope of nonfissured clay. Canadian Geotechnical Journal, 21(1), 138-146. https://doi.org/10.1139/t84-011

Khadka, P., Kolawole, O., Amenuvor, A. C., & Ankah, M. L. (2025). Coupled effects of earthquake and rainfall on landslide susceptibility in non-tropical coastal areas: assessing governing mechanisms and innovative slope protection strategy. Discover Civil Engineering, 2(1), 69. https://doi.org/10.1007/s44290-025-00227-7

Kim, S. W., Chun, K. W., Kim, M., Catani, F., Choi, B., & Seo, J. I. (2021). Effect of antecedent rainfall conditions and their variations on shallow landslide-triggering rainfall thresholds in South Korea. Landslides, 18(2), 569-582. https://doi.org/10.1007/s10346-020-01505-4

Kirschbaum, D. B., Adler, R., Hong, Y., Lerner-Lam, A. (2009). Evaluation of a preliminary satellite-based landslide hazard algorithm using global landslide inventories. Nat Hazards Earth Syst Sci 9:673–686. https://doi.org/10.5194/nhess-9-673-2009

Kirschbaum, D. B., Adler, R., Hong, Y., et al. (2012). Advances in landslide nowcasting: evaluation of a global and regional modeling approach. Environ Earth Sci 66:1683–1696. https://doi.org/10.1007/s12665-011-0990-3

Kumar, V., Cauchie, L., Mreyen, A. S., Micu, M., & Havenith, H. B. (2021). Evaluating landslide response in a seismic and rainfall regime: a case study from the SE Carpathians, Romania. Natural Hazards and Earth System Sciences, 21(12), 3767-3788. https://doi.org/10.5194/nhess-21-3767-2021

La Porta, G., Leonardi, A., La Ferlita, S., Pirulli, M. (2025).. Post-wildfire debris flow in the Northwestern Italian Alps: description and numerical analysis of the June 2018 Bussoleno event. Landslides 22, 3625–3640 (2025). https://doi.org/10.1007/s10346-025-02605-9

Larsen, M. C., & Simon, A. (1993). A rainfall intensity-duration threshold for landslides in a humid-tropical environment, Puerto Rico. Geografiska Annaler: Series A, Physical Geography, 75(1-2), 13-23. https://doi.org/10.1080/04353676.1993.11880379

Lee, M. L., Ng, K. Y., Huang, Y. F., & Li, W. C. (2014). Rainfall-induced landslides in Hulu Kelang area, Malaysia. Nat Hazards 70:353–375. https://doi.org/10.1007/s11069-013-0814-8

Lee, S., Won, J. S., Jeon, S. W., Park, I., & Lee, M. J. (2015). Spatial landslide hazard prediction using rainfall probability and a logistic regression model. Math Geosci 47(5):565–589. https://doi.org/10.1007/s11004-014-9560-z

Leroueil, S., & Chandler, R. J. (2001). Natural slopes and cuts: movement and failure mechanisms. Géotechnique, 51(3), 197-243. https://doi.org/10.1680/geot.2001.51.3.197

Li, Y., Chen, G., Tang, C., Zhou, G., & Zheng, L. (2012). Rainfall and earthquake-induced landslide susceptibility assessment using GIS and Artificial Neural Network. Natural Hazards and Earth System Sciences, 12(8), 2719-2729. https://doi.org/10.5194/nhess-12-2719-2012

Li S, Wang Z, Stutz HH 2023. State-of-the-art review on plant-based solutions for soil improvement. Biogeotechnics. https://doi.org/10. 1016/j. bgtech. 2023. 100035

Liang, X., Segoni, S., Fan, W., Yin, K., Deng, L., Xiao, T., ... & Casagli, N. (2025). Integration of effective antecedent rainfall to improve the performance of rainfall thresholds for landslide early warning in Wanzhou District, China. International Journal of Disaster Risk Reduction, 119, 105317. https://doi.org/10.1016/j.ijdrr.2025.105317

Liao, Z., Hong, Y., Wang, J., Fukuoka, H., Sassa, K., Karnawati, D., & Fathani, T. F. (2010). Prototyping an experimental early warning system for rainfall-induced landslides in Indonesia using satellite remote sensing and geospatial datasets. Landslides, 7(3), 317–324. https://doi.org/10.1007/s10346-010-0219-7

Libertino, A., Ganora, D., & Claps, P. (2019). Evidence for increasing rainfall extremes remains elusive at large spatial scales: The case of Italy. Geophysical Research Letters, 46(13), 7437–7446. https://doi.org/10.1029/2019GL083371

Lissak, C., Maquaire, O., Davidson, R., & Malet, J. P. (2014). Piezometric thresholds for triggering landslides along the Normandy coast, France. Géomorphologie: relief, processus, environnement, 20(2), 145-158. https://doi.org/10.4000/geomorphologie.10607

Liu, S., Du, J., Yin, K., Zhou, C., Huang, C., Jiang, J., & Yu, J. (2024). Regional early warning model for rainfall induced landslide based on slope unit in Chongqing, China. Engineering Geology, 333, 107464. https://doi.org/10.1016/j.enggeo.2024.107464

Liu, Y., Deng, Z., & Wang, X. (2021). The effects of rainfall, soil type and slope on the processes and mechanisms of rainfall-induced shallow landslides. Applied Sciences, 11(24), 11652. https://doi.org/10.3390/app112411652

Liu, Z., Gilbert, G., Cepeda, J. M., Lysdahl, A. O. K., Piciullo, L., Hefre, H., Lacasse, S. (2021). Modelling of shallow landslides with machine learning algorithms. Geosci Front 12:385–393. https://doi.org/10.1016/j.gsf.2020.04.014

Löbmann, M. T., Geitner, C., Wellstein, C., & Zerbe, S. (2020). The influence of herbaceous vegetation on slope stability–a review. Earth-Science Reviews, 209, 103328. https://doi.org/10.1016/j.earscirev.2020.103328

Lollino, G., Arattano, M., Allasia, P., & Giordan, D. (2007). Time response of a landslide to meteorological events. Natural Hazards and Earth System Sciences, 6, 179–184. https://doi.org/10.5194/nhess-6-179-2006

Lollino, P., Ugenti, A., de Lucia, D., Parise, M., Vennari, C., Allasia, P., & Fazio, N. L. (2023). Failure mechanism of a rainfall-triggered landslide in clay slopes. Geosciences, 13(4). https://doi.org/10.3390/geosciences13040125

Lompi M., F Marra, R Deidda, E Caporali, M Borga, E Dallan (2025). Non-stationary frequency analysis of long-term Convection Permitting simulations reveals sub-daily extreme precipitation changes in central-southern Europe. Advances in Water Resources, 105071. https://doi.org/10.1016/j.advwatres.2025.105071

Losacco, N., Bottiglieri, O., Santaloia, F., Vitone, C., & Cotecchia, F. (2021). The Geo-Hydro-Mechanical Properties of a Turbiditic Formation as Internal Factors of Slope Failure Processes. Geosciences, 11(10), 429. https://doi.org/10.3390/geosciences11100429

Lucas-Picher, P., Argüeso, D., Brisson, E., Tramblay, Y., Berg, P., Lemonsu, A., Kotlarski, S., & Caillaud, C. (2021). Convection-permitting modeling with regional climate models: Latest developments and next steps. Wiley Interdisciplinary Reviews: Climate Change, 12(6), e731. https://doi.org/10.1002/wcc.731

Lynas, M., Houlton, B. Z., & Perry, S. (2021). Greater than 99% consensus on human caused climate change in the peer-reviewed scientific literature. Environmental Research Letters, 16(11), 114005. https://doi.org/10.1088/1748-9326/ac2966

Ma, T., Li, C., Lu, Z., & Wang, B. (2014). An effective antecedent precipitation model derived from the power-law relationship between landslide occurrence and rainfall level. Geomorphology 216:187–192. https://doi.org/10.1016/j.geomorph.2014.03.033

Makris, C. V., Tolika, K., Baltikas, V. N., Velikou, K., & Krestenitis, Y. N. (2023). The impact of climate change on the storm surges of the Mediterranean Sea: Coastal sea level responses to deep depression atmospheric systems. Ocean Modelling, 181, 102149. https://doi.org/10.1016/j.ocemod.2022.102149

Marani, M, Ignaccolo, M. (2015). A metastatistical approach to rainfall extremes. Advances in Water Resources 79 (2015) 121–126.

Maraun, D. and Widmann, M. (2018). Statistical Downscaling and Bias Correction for Climate Research,Cambridge University Press, Cambridge

Marchi, L., Arattano, M., & Deganutti, A. M. (2002). Ten years of debris-flow monitoring in the Moscardo Torrent (Italian Alps). Geomorphology, 46(1-2), 1-17. https://doi.org/10.1016/S0169-555X(01)00162-3

Marin, R. J. (2020). Physically based and distributed rainfall intensity and duration thresholds for shallow landslides. Landslides, 17, 2907–2917. https://doi.org/10.1007/s10346-020-01481-9

Maringer, J., Ascoli, D., Dorren, L., Bebi, P., & Conedera, M. (2016). Temporal trends in the protective capacity of burnt beech forests (Fagus sylvatica L.) against rockfall. European Journal of Forest Research, 135(4), 657-673. https://doi.org/10.1007/s10342-016-0962-y

Marino, P., Peres, D. J., Cancelliere, A., Greco, R., & Bogaard, T. A. (2020). Soil moisture information can improve shallow landslide forecasting using the hydrometeorological threshold approach. Landslides, 17(9), 2041-2054. https://doi.org/10.1007/s10346-020-01420-8

Marra, F., Zoccatelli ,D., Armon M., Morin E., (2019). A simplified MEV formulation to model extremes emerging from multiple nonstationary underlying processes. Advances in Water Resources 127 (2019) 280–290. https://doi.org/10.1016/j.advwatres.2019.04.002.

Marra, F., Borga, M., & Morin, E. (2020). A unified framework for extreme subdaily precipitation frequency analyses based on ordinary events. Geophysical Research Letters, 47, e2020GL090209. https://doi.org/10.1029/2020GL090209

Marra, F., Dallan, E., Borga, M., Greco, R., and Bogaard, T. (2025). Brief communication: Threshold not probability. The conceptual difference between ID thresholds for landslide initiation and IDF curves, EGUsphere [preprint], https://doi.org/10.5194/egusphere-2025-3378

Martelloni, G., Segoni, S., Fanti, R., & Catani, F. (2012). Rainfall thresholds for the forecasting of landslide occurrence at regional scale. Landslides, 9(4), 485-495. https://doi.org/10.1007/s10346-011-0308-2

Martino, S., Battaglia, S., D'alessandro, F., Della Seta, M., Esposito, C., Martini, G., ... & Troiani, F. (2020). Earthquake-induced landslide scenarios for seismic microzonation: Application to the Accumoli area (Rieti, Italy). Bulletin of Earthquake Engineering, 18(12), 5655-5673. https://doi.org/10.1007/s10518-019-00589-1

Martino, S., Marmoni, G. M., Fiorucci, M., Ceci, A. F., Discenza, M. E., Rouhi, J., & Tedoradze, D. (2022). Role of antecedent rainfall in the earthquake-triggered shallow landslides involving unsaturated slope covers. Applied Sciences, 12(6), 2917. https://doi.org/10.3390/app12062917

Mathew, J., Babu, D. G., Kundu, S., Pant, C. C., & Kumar, K. V. (2014). Integrating intensity–duration-based rainfall threshold and antecedent rainfall-based probability estimate towards generating early warning for rainfall-induced landslides in parts of the Garhwal Himalaya, India. Landslides, 11, 575–588. https://doi.org/10.1007/s10346-013-0408-2

Matsuura S, Asano S, Okamoto T (2008) Relationship between rain and/or meltwater, pore-water pressure and displacement of a reactivated landslide. Engineering Geology, 101(1–2), 49–59. https://doi.org/10.1016/j.enggeo.2008.03.007

Mazzoglio P., Butera I., Alvioli M., Claps P. (2022). The role of morphology in the spatial distribution of short-duration rainfall extremes in Italy. Hydrology and Earth System Sciences, 26, 1659–1672, https://doi.org/10.5194/hess-26-1659-2022.

Mazzoglio P., Butera I., Claps P. (2023). A local regression approach to analyze the orographic effect on the spatial variability of sub-daily rainfall annual maxima. Geomatics, Natural Hazards and Risk, 14(1), 2205000, https://doi.org/10.1080/19475705.2023.2205000.

Mazzoglio P., Lompi M., Marra F., Dallan E., Deidda R., Claps P., Manfreda S., Noto L.V., Viglione A., Raffa M., Mercogliano P., Marani M., Caporali E., Borga M. (2025a). Orographic and land-sea contrast effects in convection-permitting simulations of extreme sub-daily precipitation. Weather and Climate Extremes, 100798. https://doi.org/10.1016/j.wace.2025.100798.

Mazzoglio, P., Viglione, A., Ganora, D., Claps, P. (2025b). Mapping the uneven temporal changes in ordinary and extraordinary rainfall extremes in Italy. Journal of Hydrology: Regional Studies 58 (2025) 102287. https://doi.org/10.1016/j.ejrh.2025.102287.

Melillo, M., Brunetti, M. T., Peruccacci, S., Gariano, S. L., Roccati, A., & Guzzetti, F. (2018). A tool for the automatic calculation of rainfall thresholds for landslide occurrence. Environmental Modelling & Software, 105, 230-243. https://doi.org/10.1016/j.envsoft.2018.03.024

Mergili, M., Marchesini, I., Rossi, M., Guzzetti, F., Fellin, W. (2014): Spatially distributed three-dimensional slope stability modelling in a raster GIS. Geomorphology 206: 178-195. https://doi.org/10.1016/j.geomorph.2013.10.008

Mirus, B. B., Ebel, B. A., Loague, K., & Wemple, B. C. (2007). Simulated effect of a forest road on near-surface hydrologic response. Earth Surface Processes and Landforms, 32(1), 126–142. https://doi.org/10.1002/esp.1387

Mirus, B. B., Morphew, M. D., & Smith, J. B. (2018). Developing hydro-meteorological thresholds for shallow landslide initiation and early warning. Water, 10(9), 1274. https://doi.org/10.3390/w10091274

Mondini, A. C., Guzzetti, F., & Melillo, M. (2023). Deep learning forecast of rainfall-induced shallow landslides. Nature communications, 14(1), 2466. https://doi.org/10.1038/s41467-023-38135-y

Muñoz-Sabater, J., Dutra, E., Agustí-Panareda, A., Albergel, C., Arduini, G., Balsamo, G., ... & Thépaut, J. N. (2021). ERA5-Land: A state-of-the-art global reanalysis dataset for land applications. Earth system science data, 13(9), 4349-4383. https://doi.org/10.5194/essd-13-4349-2021

Montrasio, L., & Valentino, R. (2008). A model for triggering mechanisms of shallow landslides. Natural Hazards and Earth System Sciences, 8(5), 1149–1159. https://doi.org/10.5194/nhess-8-1149-2008

Montgomery, D. R., & Dietrich, W. E. (1994). A physically based model for the topographic control on shallow landsliding. Water Resources Research, 30(4), 1153–1171. https://doi.org/10.1029/93WR02979

Montgomery, D. R., Schmidt, K. M., Greenberg, H. M., & Dietrich, W. E. (2000). Forest clearing and regional landsliding. Geology, 28(4), 311-314. https://doi.org/10.1130/0091-7613(2000)28%3C311:FCARL%3E2.0.CO;2

Moody, J.A., Shakesby, R.A., Robichaud, P.R., Cannon, S.H. and Martin, D.A., 2013. Current research issues related to post-wildfire runoff and erosion processes. Earth-science reviews, 122, pp.10-37. https://doi.org/10.1016/j.earscirev.2013.03.004

Moos C, Stritih A, Teich M, Alessandra B 2023. Mountain protective forests under threat? An in-depth review of global change impacts on their protective effect against natural hazards. Front For Glob Change 6:1223934. https://doi.org/10.3389/ffgc.2023.1223934

Moser, M., & Hohensinn, F. (1983). Geotechnical aspects of soil slips in Alpine regions. Engineering Geology, 19(3), 185-211. https://doi.org/10.1016/0013-7952(83)90003-0

Napolitano, E., Fusco, F., Baum, R. L., Godt, J. W., & De Vita, P. (2016). Effect of antecedent-hydrological conditions on rainfall triggering of debris flows in ash-fall pyroclastic mantled slopes of Campania (southern Italy). Landslides, 13, 967–983. https://doi.org/10.1007/s10346-015-0647-5

Narcisi, R., Pappalardo. S.E., Taddia, G., De Marchi, M. (2024). Assessing climate impacts on slow-moving landslides in the western Alps of Piemonte: integration of monitoring techniques for detecting displacements. Frontiers in Earth Science, 12: 1365469. https://doi.org/10.3389/feart.2024.1365469

Ng, C. W. W., Yang, B., Liu, Z. Q., Kwan, J. S. H., & Chen, L. (2021). Spatiotemporal modelling of rainfall-induced landslides using machine learning. Landslides 18:2499–2514. https://doi.org/10.1007/s10346-021-01662-0

Nguyen, V. B. Q., & Kim, Y. T. (2020). Rainfall-earthquake-induced landslide hazard prediction by Monte Carlo simulation: A case study of MT. Umyeon in Korea. KSCE Journal of Civil Engineering, 24(1), 73-86. https://doi.org/10.1007/s12205-020-0963-8

Ni, J.J., Leung, A.K., Ng, C.W.W. (2019). Modelling effects of root growth and decay on soil water retention and permeability. Can Geotech J 56(7):1049–1055. https://doi.org/10.1139/cgj-2018-0402

Nocentini, N., Rosi, A., Segoni, S., & Fanti, R. (2023). Towards landslide space-time forecasting through machine learning: the influence of rainfall parameters and model setting. Frontiers in Earth Science, 11, 1152130. https://doi.org/10.3389/feart.2023.1152130

Nocentini, N., Medici, C., Barbadori, F., Gatto, A., Franceschini, R., del Soldato, M., ... & Segoni, S. (2024a). Optimization of rainfall thresholds for landslide early warning through false alarm reduction and a multi-source validation. Landslides, 21(3), 557-571. https://doi.org/10.1007/s10346-023-02176-7

Nocentini, N., Rosi, A., Piciullo, L., Liu, Z., Segoni, S., & Fanti, R. (2024b). Regional-scale spatiotemporal landslide probability assessment through machine learning and potential applications for operational warning systems: a case study in Kvam (Norway). Landslides, 21(10), 2369-2387. https://doi.org/10.1007/s10346-024-02287-9

Notti, D., Wrzesniak, A., Dematteis, N., Lollino, P., Fazio, N. L., Zucca, F., & Giordan, D. (2021). A multidisciplinary investigation of deep-seated landslide reactivation triggered by an extreme rainfall event: The Monesi di Mendatica landslide, Ligurian Alps. Landslides, 18(7), 2341–2365. https://doi.org/10.1007/s10346-021-01651-3

Noverraz, F., Bonnard, C., Dupraz, H., & Huguenin, L. (1998). Grands glissements de versants et climat – VERSINCLIM: Comportement passé, présent et futur des grands versants instables subactifs en fonction de l'évolution climatique, et évolution en continu des mouvements en profondeur. In: Rapport final PNR 31 (p. 314). Hochschulverlag AG an der ETH Zurich.

O'Loughlin, E. M. (1986). Prediction of surface saturation zones in natural catchments by topographic analysis. Water Resources Research, 22(5), 794–804. https://doi.org/10.1029/WR022i005p00794

O'Loughlin, C. L., & Pearce, A. J. (1976). Influence of Cenozoic geology on mass movement and sediment yield response to forest removal, North Westland, New Zealand. Bulletin of the International Association of Engineering Geology-Bulletin de l'Association Internationale de Géologie de l'Ingénieur, 13(1), 41-46.

Pack, R. T., Tarboton, D. G., & Goodwin, C. N. (1998). The SINMAP approach to terrain stability mapping. In Proceedings of the 8th International Congress of the International Association of Engineering Geology and the Environment (Vol. 2, pp. 1157–1165). A. A. Balkema.

Palau, R. M., Berenguer, M., Hürlimann, M., & Sempere-Torres, D. (2023). Implementation of hydrometeorological thresholds for regional landslide warning in Catalonia (NE Spain). Landslides, 20(10), 2039-2054. https://doi.org/10.1007/s10346-023-02094-8

Palma, M., Iacono, R., Sannino, G. et al. Short-term, linear, and non-linear local effects of the tides on the surface dynamics in a new, high-resolution model of the Mediterranean Sea circulation. Ocean Dynamics 70, 935–963 (2020). https://doi.org/10.1007/s10236-020-01364-6

Parise, M. and Cannon, S.H., (2012). Wildfire impacts on the processes that generate debris flows in burned watersheds. Natural Hazards, 61, pp.217-227. https://doi.org/10.1007/s11069-011-9769-9

Paronuzzi, P., Coccolo, A., Garlatti, G. (1998). Eventi meteorici critici e debris flows nei bacini montani del Friuli. L'Acqua, Sezione I/Memorie, 6, 39-50.

Parsons, A., Robichaud, P. R., Lewis, S. A., Napper, C., and Clark, J. T., (2010). Field guide for mapping post-fire soil burn severity (No. RMRS-GTR-243; p. RMRS-GTR-243). U.S. Department of Agriculture, Forest Service, Rocky Mountain Research Station. https://doi.org/10.2737/RMRS-GTR-243

Pavan, V., Antolini, G., Barbiero, R., Berni, N., Brunier, F., Cacciamani, C., ... & Torrigiani Malaspina, T. (2019). High resolution climate precipitation analysis for north-central Italy, 1961–2015. Climate Dynamics, 52(5), 3435-3453. https://doi.org/10.1007/s00382-018-4337-6

Pedone, G., Ruggieri, G., & Trizzino, R. (2018). Characterisation of climatic variables used to identify instability thresholds in clay slopes. Géotechnique Letters, 8(3), 231-239. https://doi.org/10.1680/jgele.18.00020

Peduto, D., Iervolino, L. and Foresta, V., 2022. Experimental analysis of the fire-induced effects on the physical, mechanical, and hydraulic properties of sloping pyroclastic soils. Geosciences, 12(5), p.198. https://doi.org/10.3390/geosciences12050198

Pellegrino, A., Picarelli, L., & Urciuoli, G. (2004). Experiences of mudslides in Italy (general report). In Occurrence and mechanisms of flow-like landslides in natural slopes and earthfills (Vol. 1, pp. 191-206).

Peng, J., & Loew, A. (2017). Recent Advances in Soil Moisture Estimation from Remote Sensing. Water, 9(7), 530. https://doi.org/10.3390/w9070530

Pepe, G., Cevasco, A., Piazza, M., Macciò, R., Arrighetti, F., & Casagli, N. (2021). On the efficiency and effectiveness of automatic deep drainage systems during an extreme rainfall event: The Mendatica landslide case study (western Liguria, Italy). Landslides, 18(12), 3799–3820. https://doi.org/10.1007/s10346-021-01740-3

Persiano, S., Ferri, E., Antolini, G., Domeneghetti, A., Pavan, V., & Castellarin, A. (2020). Changes in seasonality and magnitude of sub-daily rainfall extremes in Emilia-Romagna (Italy) and potential influence on regional rainfall frequency estimation. Journal of Hydrology: Regional Studies, 32, 100751. https://doi.org/10.1016/j.ejrh.2020.100751

Peruccacci, S., Gariano, S. L., Melillo, M., Solimano, M., Guzzetti, F., & Brunetti, M. T. (2023). The ITAlian rainfall-induced LandslIdes CAtalogue, an extensive and accurate spatio-temporal catalogue of rainfall-induced landslides in Italy. Earth System Science Data, 15(7), 2863-2877. https://doi.org/10.5194/essd-15-2863-2023

Petropoulos, G. P., Ireland, G., & Barrett, B. (2015). Surface soil moisture retrievals from remote sensing: Current status, products & future trends. Physics and Chemistry of the Earth, Parts A/B/C, 83–84, 36–56. https://doi.org/10.1016/j.pce.2015.02.009

Picarelli, L., Urciuoli, G., Ramondini, M., & Comegna, L. (2005). Main features of mudslides in tectonised highly fissured clay shales. Landslides, 2(1), 15-30. https://doi.org/10.1007/s10346-004-0040-2

Picarelli, L., Di Maio, C., Tommasi, P., Urciuoli, G., & Comegna, L. (2022). Pore water pressure measuring and modeling in stiff clays and clayey flysch deposits: A challenging problem. Engineering Geology, 296, 106442. https://doi.org/10.1016/j.enggeo.2021.106442

Pichelli, E., Coppola, E., Sobolowski, S., Ban, N., Giorgi, F., Stocchi, P., ... & Vergara-Temprado, J. (2021). The first multi-model ensemble of regional climate simulations at kilometer-scale resolution part 2: historical and future simulations of precipitation. Climate Dynamics, 56(11), 3581-3602. https://doi.org/10.1007/s00382-021-05657-4

Piciullo, L., Gariano, S. L., Melillo, M., Brunetti, M. T., Peruccacci, S., Guzzetti, F., & Calvello, M. (2017). Definition and performance of a threshold-based regional early warning model for rainfall-induced landslides. Landslides, 14(3), 995–1008. https://doi.org/10.1007/s10346-016-0750-2

Pirone, M., Forte, G., Santo, A., & Urciuoli, G. (2025). Novel rainfall thresholds for shallow slip prediction based on field monitoring: Case study of the Lattari Mountains, Italy. Journal of Geotechnical and Geoenvironmental Engineering, 151(3), 04025016. https://doi.org/10.1061/JGGEFK.GTENG-12797

Ponziani, F., Pandolfo, C., Stelluti, M., et al. (2012). Assessment of rainfall thresholds and soil moisture modeling for operational hydrogeological risk prevention in the Umbria region (central Italy). Landslides, 9, 229–237. https://doi.org/10.1007/s10346-011-0287-3

Pourghasemi, H. R., Teimoori Yansari, Z., Panagos, P., & Pradhan, B. (2018). Analysis and evaluation of landslide susceptibility: a review on articles published during 2005–2016 (periods of 2005–2012 and 2013–2016). Arabian Journal of Geosciences, 11(9), 193. https://doi.org/10.1007/s12517-018-3531-5

Prein, A. F., Langhans, W., Fosser, G., Ferrone, A., Ban, N., Goergen, K., et al. (2015). A review on regional convection-permitting climate modeling: Demonstrations, prospects, and challenges. Reviews of Geophysics, 53(2), 323–361. https://doi.org/10.1002/2014RG000475.

Preti, F. 2012. Forest protection and protection forest: tree root degra- dation over hydrological shallow landslides triggering. Ecol. Eng. http://dx.doi.org/10.1016/j.ecoleng.2012.11.009

Raffa, M., Reder, A., Marras, G. F., Mancini, M., Scipione, G., Santini, M., & Mercogliano, P. (2021). VHR-REA_IT dataset: very high resolution dynamical downscaling of ERA5 reanalysis over Italy by COSMO-CLM. Data, 6(8), 88. https://doi.org/10.3390/data6080088

Raffa, M., Adinolfi, M., Reder, A., Marras, G. F., Mancini, M., Scipione, G., ... & Mercogliano, P. (2023). Very high resolution projections over Italy under different CMIP5 IPCC scenarios. Scientific Data, 10(1), 238. https://doi.org/10.1038/s41597-023-02144-9

Raimondi, L., Pepe, G., Firpo, M., Calcaterra, D., & Cevasco, A. (2023). An open-source and QGIS-integrated physically based model for spatial prediction of rainfall-induced shallow landslides (SPRIn-SL). Environmental Modelling & Software, 160, 105587. https://doi.org/10.1016/j.envsoft.2023.105587

Ran, Q., Hong, Y., Li, W., & Gao, J. (2018). A modelling study of rainfall-induced shallow landslide mechanisms under different rainfall characteristics. Journal of Hydrology, 563, 790-791. https://doi.org/10.1016/j.jhydrol.2018.06.040

Reichenbach, P., Rossi, M., Malamud, B. D., Mihir, M., & Guzzetti, F. (2018). A review of statistically-based landslide susceptibility models. Earth-science reviews, 180, 60-91. https://doi.org/10.1016/j.earscirev.2018.03.001

Rengers, F. K., McGuire, L. A., Oakley, N. S., Kean, J. W., Staley, D. M., and Tang, H., 2020. Landslides after wildfire: Initiation, magnitude, and mobility. Landslides, 17(11), 2631–2641. https://doi.org/10.1007/s10346-020-01506-3

Richards, L. A. (1931). Capillary conduction of liquids through porous mediums. Physics, 1(5), 318–333. https://doi.org/10.1063/1.1745010

Rianna, G., Reder, A., & Pagano, L. (2023). From empirically to physically based early warning predictions of rainfall induced landslides in silty volcanic soils: The Lattari Mountains case study. Bulletin of Engineering Geology and the Environment, 82, 223. https://doi.org/10.1007/s10064-023-03228-x

Ridal, M., Bazile, E., Le Moigne, P., Randriamampianina, R., Schimanke, S., Andrae, U., ... & Wang, Z. Q. (2024). Cerra, the copernicus european regional reanalysis system. Quarterly Journal of the Royal Meteorological Society, 150(763), 3385-3411. https://doi.org/10.1002/qj.4764

Rigon, R., Bertoldi, G., & Over, T. M. (2006). GEOtop: A distributed hydrological model with coupled water and energy budgets. Journal of Hydrometeorology, 7(3), 371–388. https://doi.org/10.1175/JHM497.1

Rodolfo, K. S., & Arguden, A. T. (1991). Rain-lahar generation and sediment-delivery systems at Mayon Volcano, Philippines. In: Sedimentation in volcanic settings (Fisher RV, Smith GA, eds), vol. 45. Society of Economic Paleontologists and Mineralogists, special publication, pp 71–88

Rodrıguez, C. E., Bommer, J. J., & Chandler, R. J. (1999). Earthquake-induced landslides: 1980–1997. Soil Dynamics and Earthquake Engineering, 18(5), 325-346. https://doi.org/10.1016/S0267-7261(99)00012-3

Rollo F., & Buscarnera, G. (2023). Modelling seasonal landslide motion: Does it only depend on fluctuations in normal effective stress? Int J Numer Anal Methods Geomech., 1-20. https://doi.org/10.1002/nag.3625.

Rollo, F., Rampello, S., (2021). Probabilistic assessment of seismic-induced slope displacements: an application in Italy. Bull Earthquake Eng 19, 4261–4288. https://doi.org/10.1007/s10518-021-01138-5

Rollo, F., & Rampello, S. (2023). Influence of the Displacement Predictive Relationships on the Probabilistic Seismic Analysis of Slopes. Journal of Geotechnical and Geoenvironmental Engineering, 149(6), 04023033. https://doi.org/10.1061/JGGEFK.GTENG-11162

Ronchetti, F., Borgatti, L., Cervi, F., & Corsini, A. (2010). Hydro-mechanical features of landslide reactivation in weak clayey rock masses. Bulletin of Engineering Geology and the Environment, 69(2), 267–274. https://doi.org/10.1007/s10064-009-0249-3

Roseto, R., Dellino, P., & Capolongo, D. (2024). Spatial distribution and trend analysis of extreme rainfall time series in Apulia region (Italy). Phys. Geogr. Quat. Dyn, 46, 163-177. https://doi.org/10.4454/jt76er4b

Rosi, A., Segoni, S., Catani, F., & Casagli, N. (2012). Statistical and environmental analyses for the definition of a regional rainfall threshold system for landslide triggering in Tuscany (Italy). Journal of Geographical Sciences, 22(4), 617–629. https://doi.org/10.1007/s11442-012-0951-0

Rossi, G., Catani, F., Leoni, L., Segoni, S., & Tofani, V. (2013). HIRESSS: A physically based slope stability simulator for HPC applications. Natural Hazards and Earth System Sciences, 13(1), 151–166. https://doi.org/10.5194/nhess-13-151-2013

Rudari, R., D. Entekhabi, and G. Roth, 2005. Large-scale atmospheric patterns associated with mesoscale features leading to extreme precipitation events in northwestern Italy. Adv. Wa-ter Resour., 28, 601–614, https://doi.org/10.1016/j.advwatres.2004.10.017.

Ruggeri, P., Fruzzetti, V. M., Ferretti, A., & Scarpelli, G. (2020). Seismic and rainfall induced displacements of an existing landslide: Findings from the continuous monitoring. Geosciences, 10(3), 90. https://doi.org/10.3390/geosciences10030090

Ruti, P. M., Somot, S., Giorgi, F., Dubois, C., Flaounas, E., Obermann, A., ... & Vervatis, V. (2016). MED-CORDEX initiative for Mediterranean climate studies. Bulletin of the American Meteorological Society, 97(7), 1187-1208. https://doi.org/10.1175/BAMS-D-14-00176.1

Rutllant, J. A., Matus, F., Rudloff, V., & Rondanelli, R. (2023). The role of atmospheric rivers in rainfall-induced landslides: A study from the Elqui valley. Journal of Arid Environments, 216, 105016. https://doi.org/10.1016/j.jaridenv.2023.105016

Salvatici, T., Tofani, V., Rossi, G., D'Ambrosio, M., Tacconi Stefanelli, C., Masi, E. B., Rosi, A., Pazzi, V., Vannocci, P., Petrolo, M., Catani, F., Ratto, S., Stevenin, H., & Casagli, N. (2018). Application of a physically based model to forecast shallow landslides at a regional scale. Natural Hazards and Earth System Sciences, 18(7), 1919–1935. https://doi.org/10.5194/nhess-18-1919-2018

Salciarini, D., Tamagnini, C., Conversini, P., & Rapinesi, S. (2012). Spatially distributed rainfall thresholds for the initiation of shallow landslides. Natural Hazards, 61(1), 229–245. https://doi.org/10.1007/s11069-011-9739-2

Sannino, G., Carillo, A., Iacono, R. et al. (2022) Modelling present and future climate in the Mediterranean Sea: a focus on sea-level change. Clim Dyn 59, 357–391 (2022). https://doi.org/10.1007/s00382-021-06132-w

Sassa, K., Fukuoka, H., Wang, F., Wang, G. (2007). Landslides Induced by a Combined Effect of Earthquake and Rainfall. In: Sassa, K., Fukuoka, H., Wang, F., Wang, G. (eds) Progress in Landslide Science. Springer, Berlin, Heidelberg. https://doi.org/10.1007/978-3-540-70965-7_14

Sato, T., & Shuin, Y. (2024). Rainfall characteristics and magnitude control the volume of shallow and deep-seated landslides: Inferences from analyses using a simple runoff model. Geomorphology, 466, 109453. https://doi.org/10.1016/j.geomorph.2024.109453

Pirulli M, Bristeau M-O, Mangeney A, Scavia C (2007) The effect of the earth pressure coefficients on the runout of granular material. Environ Model Softw 22(10):1437–1454

Schilirò, L., Bosman, A., Caielli, G. M., Corazza, A., Crema, S., Di Salvo, C., ... & Tommasi, P. (2025). The May 2023 Rainstorm-Induced Landslides in the Emilia-Romagna Region (Northern Italy): Considerations from UAV Investigations Under Emergency Conditions. Geosciences, 15(3), 101. https://doi.org/10.3390/geosciences15030101

Schmidt, M., & Glade, T. (2003). Linking global circulation model outputs to regional geomorphic models: A case study of landslide activity in New Zealand. Climate Research, 25, 135–152. https://doi.org/10.3354/cr025135

Schwarz, M., Cohen, D., & Or, D. 2010. Root-soil mechanical interactions during pullout and failure of root bundles. Journal of Geophysical Research, 115, F04035. https://doi.org/10.1029/2009JF001603

Secci, R., Calcina, S.V., Ranieri, G. and Uras, G., 2014. Analysis of the stability variation of a slope crossed by forest fire. International Journal of Civil Engineering, 3(1), pp.41-50.

Segoni, S., Ajin, R. S., Nocentini, N., & Fanti, R. (2024). Insights gained from the review of landslide susceptibility assessment studies in Italy. Remote Sensing, 16, 1-31. https://doi.org/10.3390/rs16234491

Segoni, S., Piciullo, L., & Gariano, S. L. (2018). A review of the recent literature on rainfall thresholds for landslide occurrence. Landslides, 15(8), 1483-1501. https://doi.org/10.1007/s10346-018-0966-4

Shao,W., Bogaard, T.A., Bakker,M., Greco, R. 2015. Quantification of the influence of preferential flow on slope stability using a numerical modelling approach. Hydrol. Earth Syst. Sci. 19, 2197–2212. http://dx.doi.org/10.5194/hess-19-2197-2015

Shao, W., Bogaard, T., Bakker, M., & Berti, M. (2016). The influence of preferential flow on pressure propagation and landslide triggering of the Rocca Pitigliana landslide. Journal of Hydrology, 543, 360-372. https://doi.org/10.1016/j.jhydrol.2016.10.015

Sharma, A., Sajjad, H., Roshani, & Rahaman, M. H. (2024). A systematic review for assessing the impact of climate change on landslides: research gaps and directions for future research. Spatial Information Research, 32(2), 165-185. https://doi.org/10.1007/s41324-023-00551-z

Sidle, R.C., Wu,W. 1999. Simulating effects of timber harvesting on the temporal and spatial distribution of shallow landslides. Z. Geomorphol. N.F. 43, 185–201. https://doi.org/10.1127/zfg/43/1999/185

Sidle, R.C., Ochiai, H. 2006. Landslides: processes, prediction and land use. American Geophysical Union (AGU), 2000 Florida Avenue N.W., Washington, D.C. 20009-1277, USA. Water Resources Monograph. 18 (312 pp).

Sidle, R. C., & Bogaard, T. A. 2016. Dynamic earth system and ecological controls of rainfall-initiated landslides. Earth-science reviews, 159, 275-291. https://doi.org/10.1016/j.earscirev.2016.05.013

Simoni, S., Zanotti, F., Bertoldi, G., & Rigon, R. (2008). Modelling the probability of occurrence of shallow landslides and channelized debris flows using GEOtop-FS. Hydrological Processes, 22(4), 532–545. https://doi.org/10.1002/hyp.6886

Sistema Nazionale Protezione Ambiente (SNPA) 2021. Rapporto sugli indicatori di impatto dei cambiamenti climatici – Edizione 2021. Report SNPA 21/2021. ISBN 978-88-448-1058-0 © Report SNPA, 21/2021

Sistema Nazionale Protezione Ambiente (SNPA) 2023. Il clima in Italia nel 2023, Report ambientali SNPA, n. 42/2024 ISBN 978-88-448-1217-1 © Report ambientali SNPA, 42/2024

Soci, C., Hersbach, H., Simmons, A., Poli, P., Bell, B., Berrisford, P., ... & Thépaut, J. N. (2024). The ERA5 global reanalysis from 1940 to 2022. Quarterly Journal of the Royal Meteorological Society, 150(764), 4014-4048. https://doi.org/10.1002/qj.4803

Stanley, T. A., Kirschbaum, D. B., Benz, G., Emberson, R. A., Amatya, P. M., Medwedeff, W., & Clark, M. K. (2021). Data-driven landslide nowcasting at the global scale. Front Earth Sci (Lausanne) 9. https://doi.org/10.3389/feart.2021.640043

Stoffel, M., Mendlik, T., Schneuwly-Bollschweiler, M., & Gobiet, A. (2014). Possible impacts of climate change on debris-flow activity in the Swiss Alps. Climatic Change, 122(1–2), 141–155. https://doi.org/10.1007/s10584-013-0993-z

Stokes, A., Atger, C., Bengough, A.G., Fourcaud, T., Sidle, R.C. 2009. Desirable plant root traits for protecting natural and engineered slopes against landslides. Plant Soil 324, 1–30. https://doi.org/10.1007/s11104-009-0159-y

Struglia, M. V., Anav, A., Antonelli, M., Calmanti, S., Catalano, F., Dell'Aquila, A., Pichelli, E., and Pisacane, G.: Impact of spatial resolution on multi-scenario WRF-ARW simulations driven by the CMIP6 MPI-ESM1-2-HR global model: a focus on precipitation distribution over Italy, Geosci. Model Dev., 18, 6095–6116, https://doi.org/10.5194/gmd-18-6095-2025, 2025.

Tang, H., McGuire, L. A., Rengers, F. K., Kean, J. W., Staley, D. M., and Smith, J. B., 2019. Evolution of Debris-Flow Initiation Mechanisms and Sediment Sources During a Sequence of

Postwildfire Rainstorms. Journal of Geophysical Research: Earth Surface, 124(6), 1572–1595. https://doi.org/10.1029/2018JF004837

Tehrani, F. S., Calvello, M., Liu, Z., Zhang, L., & Lacasse, S. (2022). Machine learning and landslide studies: recent advances and applications. Nat Hazards. https://doi.org/10.1007/s11069-022-05423-7

Terlien, M. T. J. (1998). The determination of statistical and deterministic hydrological landslide triggering thresholds. Environmental Geology, 35(2–3), 124–130. https://doi.org/10.1007/s002540050299

Terzaghi, K. (1950) Mechanism of Landslides. In Application of Geology to Engineering Practice. Geological Society of America: Boulder, CO. https://doi.org/10.1130/Berkey.1950.83

Thomas, M. A., Mirus, B. B., & Collins, B. D. (2018). Identifying physics-based thresholds for rainfall-induced landsliding. Geophysical Research Letters, 45(18), 9651–9661. https://doi.org/10.1029/2018GL079662

Thomas, M.A., Rengers, F.K., Kean, J.W., McGuire, L.A., Staley, D.M., Barnhart, K.R. and Ebel, B.A. (2021). Postwildfire soil-hydraulic recovery and the persistence of debris flow hazards. Journal of Geophysical Research: Earth Surface, 126(6). https://doi.org/10.1029/2021JF006091

Tien Bui, D., Pradhan, B., Lofman, O., Revhaug, I., & Dick, Ø. B. (2013). Regional prediction of landslide hazard using probability analysis of intense rainfall in the Hoa Binh province, Vietnam. Nat Hazards 66(2):707–730. https://doi.org/10.1007/s11069-012-0510-0

Titti, G., Sarretta, A., Lombardo, L., Crema, S., Pasuto, A., & Borgatti, L. (2022). Mapping susceptibility with open-source tools: a new plugin for QGIS. Frontiers in Earth Science, 10, 842425. https://doi.org/10.3389/feart.2022.842425

Titti, G., Hu, L., Festi, P., Elia, L., Borgatti, L., & Lombardo, L. (2025). An updated version of the SZ-plugin: from space to space-time data-driven modeling in QGIS. International Journal of Applied Earth Observation and Geoinformation. https://doi.org/10.1016/j.jag.2025.104679

Treppiedi, D., Cipolla, G., Francipane, A., Noto, L.V., 2021. Detecting precipitation trend using a multiscale approach based on quantile regression over a Mediterranean area. Int. J. Clim. 41, 5938–5955. https://doi.org/10.1002/joc.7161.

Trigo, I. F., T. D. Davies, and G. R. Bigg, 1999. Objective climatology of cyclones in the Mediterranean region. J. Climate, 12, 1685–1696, https://doi.org/10.1175/1520-0442(1999)012<1685:OCOCIT>2.0.CO;2

Trigo, R. M., Lorenzo, M. N., Trigo, I. F., & DaCamara, C. C. (2005). The influence of the North Atlantic Oscillation on rainfall triggering of landslides near Lisbon. Natural Hazards, 36, 331–354. https://doi.org/10.1007/s11069-004-4548-x

Tufano, R., Formetta, G., Calcaterra, D., & De Vita, P. (2021). Hydrological control of soil thickness spatial variability on the initiation of rainfall-induced shallow landslides using a three-dimensional model. Landslides, 18(10), 3367–3380. https://doi.org/10.1007/s10346-021-01723-5

Tungol, N. M., & Regalado, M. T. M. (1996). Rainfall, acoustic flow monitor records, and observed lahars of the Sacobia River in 1992. In: Fire and mud: eruptions and lahars of Mount Pinatubo (Newhall CG, Punongbayan RS, eds). Philippine Institute of Volcanology and Seismology, Quezon City and University of Washington Press, Seattle, 1126 pp

Uchida, T., Kosugi, K., Mizuyama, T. (2001). Effects of pipeflow on hydrological process and its relation to landslide: a review of pipeflow studies in forested headwater catchments. Hydrol. Process. 15, 2151–2174. https://doi.org/10.1002/hyp.281

Urgilez Vinueza, A., Robles, J., Bakker, M., Guzman, P., & Bogaard, T. (2020). Characterization and hydrological analysis of the guarumales deep-seated landslide in the tropical ecuadorian andes. Geosciences, 10(7), 267. https://doi.org/10.3390/geosciences10070267

Vahedifard, F., Abdollahi, M., Leshchinsky, B.A., Stark, T.D., Sadegh, M. and AghaKouchak, A., 2024. Interdependencies between wildfire-induced alterations in soil properties, near-surface processes, and geohazards. Earth and Space Science, 11(2). https://doi.org/10.1029/2023EA003498

Valiante, M., Bozzano, F., & Guida, D. (2016). The Sant'Andrea-Molinello landslide system (Mt. Pruno, Roscigno, Italy). Rendiconti Online della Società Geologica Italiana, 41, 214–217. https://doi.org/10.3301/ROL.2016.132

Vallet, A., Varron, D., Bertrand, C., Fabbri, O., & Mudry, J. (2016). A multi-dimensional statistical rainfall threshold for deep landslides based on groundwater recharge and support vector machines. Natural Hazards, 84(2), 821–849. https://doi.org/10.1007/s11069-016-2453-3

Van Asch, T. W. J., van Beek, L. P. H., & van Balen, R. T. (1999). A view on some hydrological triggering systems in landslides. Geomorphology, 30(1–2), 25–32. https://doi.org/10.1016/S0169-555X(99)00055-0

Vassallo, R., Grimaldi, G. M., & Di Maio, C. (2015). Pore water pressures induced by historical rain series in a clayey landslide: 3D modeling. Landslides, 12, 731-744. https://doi.org/10.1007/s10346-014-0508-7

Vaughan, P. R. (1994). Assumption, prediction and reality in geotechnical engineering. Géotechnique, 44(4), 573-609.

Vergani, C., Giadrossich, F., Buckley, P., Conedera, M., Pividori, M., Salbitano, F., ... & Schwarz, M. (2017). Root reinforcement dynamics of European coppice woodlands and their effect on shallow landslides: A review. Earth-science reviews, 167, 88-102. https://doi.org/10.1016/j.earscirev.2017.02.002

Vertessy, R., O'Loughlin, E., Beverly, E., & Butt, T. (1994). Australian experiences with the CSIRO Topog model in land and water resources management. In Water resources planning in a changing world: Proceedings of the UNESCO International Symposium (pp. 135–144).

Vicente-Serrano, S.M., Tramblay, Y., Reig, F. et al. (2025). High temporal variability not trend dominates Mediterranean precipitation. Nature 639, 658–666. https://doi.org/10.1038/s41586-024-08576-6

Vianello, D., Vagnon, F., Bonetto, S. et al. (2023).Debris flow susceptibility mapping using the Rock Engineering System (RES) method: a case study. Landslides 20, 735–756. https://doi.org/10.1007/s10346-022-01985-6

Vieira, B. C., & Fernandes, N. F. (2004). Landslides in Rio de Janeiro: the role played by variations in soil hydraulic conductivity. Hydrological Processes, 18(4), 791-805. https://doi.org/10.1002/hyp.1363

Viterbo, F., Sperati, S., Vitali, B., D'Amico, F., Cavalleri, F., Bonanno, R., Lacavalla, M. (2024). M ERIDA HRES: A new high-resolution reanalysis dataset for Italy. Meteorological Applications, 31(6), e70011. https://doi.org/10.1002/met.70011

Wahl, S., Bollmeyer, C., Crewell, S., Figura, C., Friederichs, P., Hense, A., ... & Ohlwein, C. (2017). A novel convective-scale regional reanalysis COSMO-REA2: Improving the representation of precipitation. Meteorologische Zeitschrift, 26(4), 345-361. https://doi.org/10.1127/metz/2017/0824.

Waliser, D., Gleckler, P. J., Ferraro, R., Taylor, K. E., Ames, S., Biard, J., ... & Tuma, M. (2020). Observations for model Intercomparison project (Obs4MIPs): Status for CMIP6. Geoscientific Model Development, 13(7), 2945-2958. https://doi.org/10.5194/gmd-13-2945-2020

Watson, A., Phillips, C., Marden, M. 1999. Roost strength, growth, and rates of decay: root reinforcement changes of two three species and their contribution to slope stability. Plant Soil 217, 39–47. https://doi.org/10.1023/A:1004682509514

Wicki, A., Lehmann, P., Hauck, C., Seneviratne, S. I., Waldner, P., & Stähli, M. (2020). Assessing the potential of soil moisture measurements for regional landslide early warning. Landslides, 17(8), 1881-1896. https://doi.org/10.1007/s10346-020-01400-y

Wieczorek, G. F. (1987). Effect of rainfall intensity and duration on debris flows in central Santa Cruz Mountains, California. In: Debris flow=avalanches: process, recognition, and mitigation (Costa JE, Wieczorek GF, eds). Geological Society of America, Reviews in Engineering Geology 7: 93–104. https://doi.org/10.1130/REG7-p93

Wieczorek, G. F., Morgan, B. A., & Campbell, R. H. (2000). Debris-flow hazards in the Blue Ridge of central Virginia. Environmental & Engineering Geoscience, 6(1), 3-23. https://doi.org/10.2113/gseegeosci.6.1.3

Wieczorek GF, Glade T (2005) Climatic factors influencing occurrence of debris flows. In: Jakob M, Hungr O (eds) Debris flow hazards and related phenomena. Springer, Berlin Heidelberg, pp 325–362

Wong, J.L., Lee, M.L., Teo, F.Y., Liew, K.W. (2022). A Review of Impacts of Climate Change on Slope Stability. In: Kolathayar, S., Mondal, A., Chian, S.C. (eds) Climate Change and Water Security. Lecture Notes in Civil Engineering, vol 178. Springer, Singapore. https://doi.org/10.1007/978-981-16-5501-2_13

Wu, W., & Sidle, R. C. (1995). A distributed slope stability model for steep forested hillslopes. Water Resources Research, 31(8), 2097–2110. https://doi.org/10.1029/95WR01136

Wu, Y., Lan, H., Gao, X., Li, L., & Yang, Z. (2015). A simplified physically based coupled rainfall threshold model for triggering landslides. Engineering Geology, 195, 63–69. https://doi.org/10.1016/j.enggeo.2015.05.022

Zêzere, J. L., Trigo, R. M., & Trigo, I. F. (2005). Shallow and deep landslides induced by rainfall in the Lisbon region (Portugal): Assessment of relationships with the North Atlantic Oscillation. Natural Hazards and Earth System Sciences, 5(3), 331–344. https://doi.org/10.5194/nhess-5-331-2005

Zêzere, J.L., Vaz, T., Pereira, S. et al. (2015). Rainfall thresholds for landslide activity in Portugal: a state of the art. Environ Earth Sci 73, 2917–2936 (2015). https://doi.org/10.1007/s12665-014-3672-0

Zhao, L., Liu, M., Song, Z., Wang, S., Zhao, Z., & Zuo, S. (2022). Regional-scale modeling of rainfall-induced landslides under random rainfall patterns. Environmental Modelling & Software, 155, 105454. https://doi.org/10.1016/j.envsoft.2022.105454

Zhou, W., & Tang, C. (2014). Rainfall thresholds for debris flow initiation in the Wenchuan earthquake-stricken area, southwestern China. Landslides, 11(5), 877-887. https://doi.org/10.1007/s10346-013-0421-5

Zhu, Y., & Newell, R. E. (1998). A proposed algorithm for moisture fluxes from atmospheric rivers. Monthly weather review, 126(3), 725-735. https://doi.org/10.1175/1520-0493(1998)126%3C0725:APAFMF%3E2.0.CO;2

Zimmermann, M., Mani, P., Gamma, P., Gsteiger, P., Heiniger, O., Hunziker, G. (1997). Murganggefahr und Klimänderungein GIS-basierter Ansatz. In: Schlussbericht des Nationalen Forschungsprogrammes, NFP 31. Zürich: vdf Hochschulverlag AG, 161 pp